Application of Ultra-thin Polymer Coating on Metallic Wires

by

Juan Yu B. Eng.

This thesis is submitted as the fulfilment of the requirement for the award of Master Degree of Engineering by research to the

Dublin City University

School of Mechanical & Manufacturing Engineering,
Dublin City University.

August 1992

Dedicated to My Parents

CONTENTS

Declaration

I declare that all work described in this thesis is entirely of my own, except where references have been made. The author further declares that no part of the work contained in this thesis has been submitted in support of any other degree or qualification of this or any other institution of learning.

signed 

Juan Yu

August 1992

Acknowledgements

The author wishes to express her sincere thanks to Professor M. S. J. Hashmi for his elaborate supervision and valuable guidance during the period of this research.

The author would like to take this opportunity to express her deep appreciation to Ms. Lesley Lawlor, Mr. Tommy Walsh, Mr. Ian Hooper, Mr. Liam Domican and all the others for their kind assistance and valuable support at various stages of this work.

Finally, thanks to her husband for his support and encouragement during the period of completion of her work.

ABSTRACT

Application of Ultra-thin Polymer Coating on Metallic Wires

Juan Yu B. Eng.

In this study, the coating of fine wires using hydrodynamic pressure technique has been investigated theoretically and experimentally. One of the principal aims of the project is to establish the minimum possible coating thickness on fine wires which can be applied by means of hydrodynamic technique. Models based on steady, uniform and laminar flow of Newtonian as well as non-Newtonian fluid for polymer coating for the process of plasto-hydrodynamic wire coating in a stepped bore unit have been developed. The closed form analytical solution is established in cylindrical coordinate since the practical case is a mathematical axisymmetric problem. The comparison of theoretical results between Newtonian and non-Newtonian fluid, and Cartesian and cylindrical coordinate systems has been made.

The experimental procedures and methods have been outlined, a melt chamber and a die unit have been designed and used, and investigations into a wide range of coating and drawing conditions have been carried out. The experimental work includes by the polymer of low density polyethylene (Escoren) coating on stainless steel wires with three diameters ranging from 0.1 - 0.4mm, varying the temperature of the polymer melt between 120 - 155°C, converting the different diameters of dies ranging from 0.2 - 0.5mm, and shifting the drawing speed between 0.08 - 1.31m/s. The experimental data have been processed and presented graphically. Some significant conclusions have been made.

Nomenclature

R_1, R_2	Radii of parts 1 and 2 in the unit;
D_0, R_0	Diameter and Radius of the wire;
L_1, L_2	Length of parts 1 and 2 of the unit;
u_0	Speed of drawing wire;
u_1, u_2	Velocity of fluid in part 1 and 2;
Q_1, Q_2	Flow of fluid in part 1 and 2;
μ	Viscosity of polymer;
p_1,p_2	Pressure in part 1 and 2;
P_m	Pressure at the step;
P_{m1},P_{m2}	Pressure at step from part 1 and 2;
τ_1, τ_2	Shear stress of fluid in part 1 and 2;
σ_e	Equivalent stress;
σ_x	Stress along x-axis;
τ_{10}	Shear stress on surface of wire in part 1;
τ_{20}	Shear stress on surface of wire in part 2;
k	Non-linear factor.

Chapter 1 Introduction

1.1 Development of Wire Drawing & Coating

Wire drawing is one of the earliest crafts in metal forming, but no significant development of the process took place until the beginning of this century and only single-die machines were used. Later on multi-die machines and tungsten-carbide dies were introduced, but the operating principle remained the same, namely, the wire is pulled through a tapered reduction die and the material deforms plastically whilst passing through the die. The purpose of the wire drawing process is to reduce the wire to a specified size and to obtain the required metallurgical properties, including surface finish and a high degree of repeatability.

When the wire is drawn, metal to metal contact takes place causing friction which leads to a reduction in die life due to wear, and a very high drawing load is required. Due to this reason, lubrication is essential. There are two main types of lubrication used: "wet drawing" and "dry drawing". In wet drawing, the wire and drawing apparatus are submerged in a bath of lubricant. This method produces a high surface finish and it is usually used drawing fine wires of less than

0.5 (mm) diameter. In dry drawing, the wire pass through a soap powder container before entering the die. This method is used for when the finish is unimportant or when the presence of lubricant is desirable for further processing.

In both "wet" and "dry" drawing, friction between the wire and die is of the boundary type, this occurs even though there is a lubricant present. From the device to reduce the die wear and to obtain the good surface finish, hydrodynamic lubrication method is developed. Hydrostatic Lubrication refers to a high pressure which is produced by viscous action between the wire and the lubricant in a tube through which the wire passes. In this case, no metal to metal contact takes place as there is a continuous lubricant film present which separates two metal surfaces and hence reduces the die wear significantly. Prior to hydrodynamic lubrication action boundary lubrication was the dominant regime. The film thickness produced in dry lubrication is greater than that in boundary lubrication but less than that in hydrodynamic lubrication[1][2]. The conventional wire drawing processes are at a very advanced level and there is not likely to be any further significant breakthrough. This leaves the way open for investigation into hydrodynamic wire lubrication.

1.2 Hydrodynamic Lubrication

Hydrodynamic lubrication method has been used in drawing processes in recent years. One of the first investigations

in this respect was carried out by Christopherson and Naylor.[3] They used a long tube having a length up to 500 times the diameter of the wire, with a narrow gap between the tube and the wire, which was firmly attached at the entrance side of the die as shown in Figure 1. Oil was used for lubrication because a good deal of rheological data was known about oil. The lubricant adhered to the wire and was dragged into the clearance between the tube and wire, high pressures were generated in the lubricant by viscous action. The pressurised lubricant then completely separates the wire from the die, preventing metal to metal contact. Experimental results showed that hydrodynamic conditions were achieved under the designed conditions and the wire started deforming before it entered the die. Along with these encouraging results there were practical difficulties which prevented it being taken up by industry. Some of these difficulties were that the tube had to be in a vertical plane and it needed a leader wire, and since hydrodynamic lubrication did not begin at start up, there was still some die wear.

Wistreich[4] used dry soap for lubrication as it is a very good boundary lubricant so that the drawing tube could be shortened to about 2 inch in length. Wistreich carried out experiments with this die. The experimental results showed that drawing speed, temperature, and tube gap had a direct effect on the property of the film thickness developed. He also noted that oil produced a thicker film thickness than soap. Sturgen and Tattersal[5] designed the (B.I.S.R.A.) dry

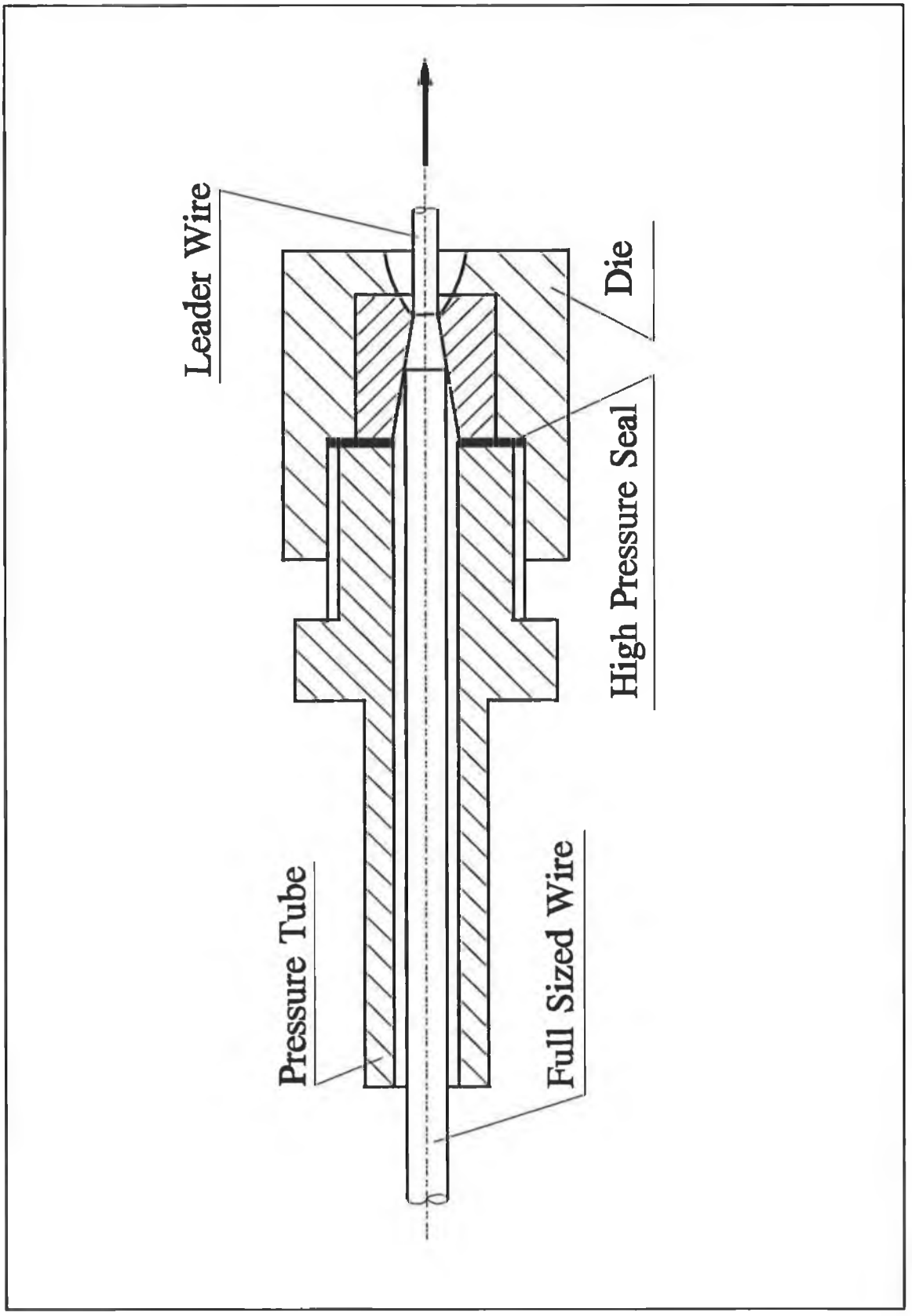

Figure 1 Typical Christopherson tube assembly.

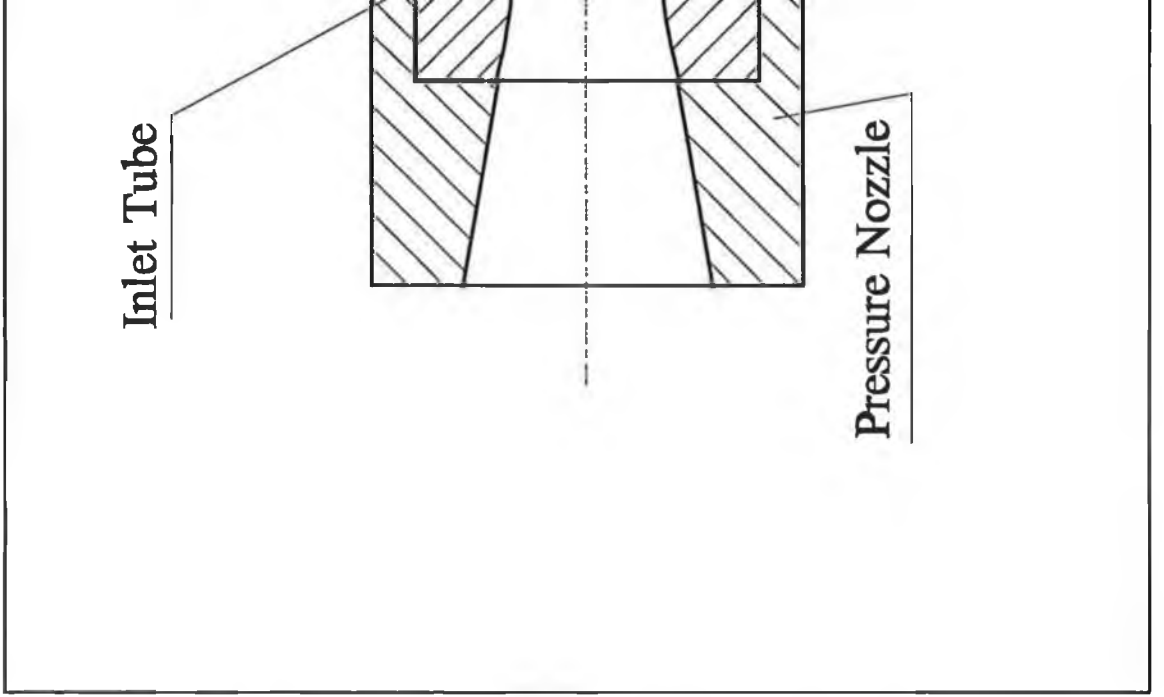

Figure 2 Nozzle - Die unit (BIRSA).

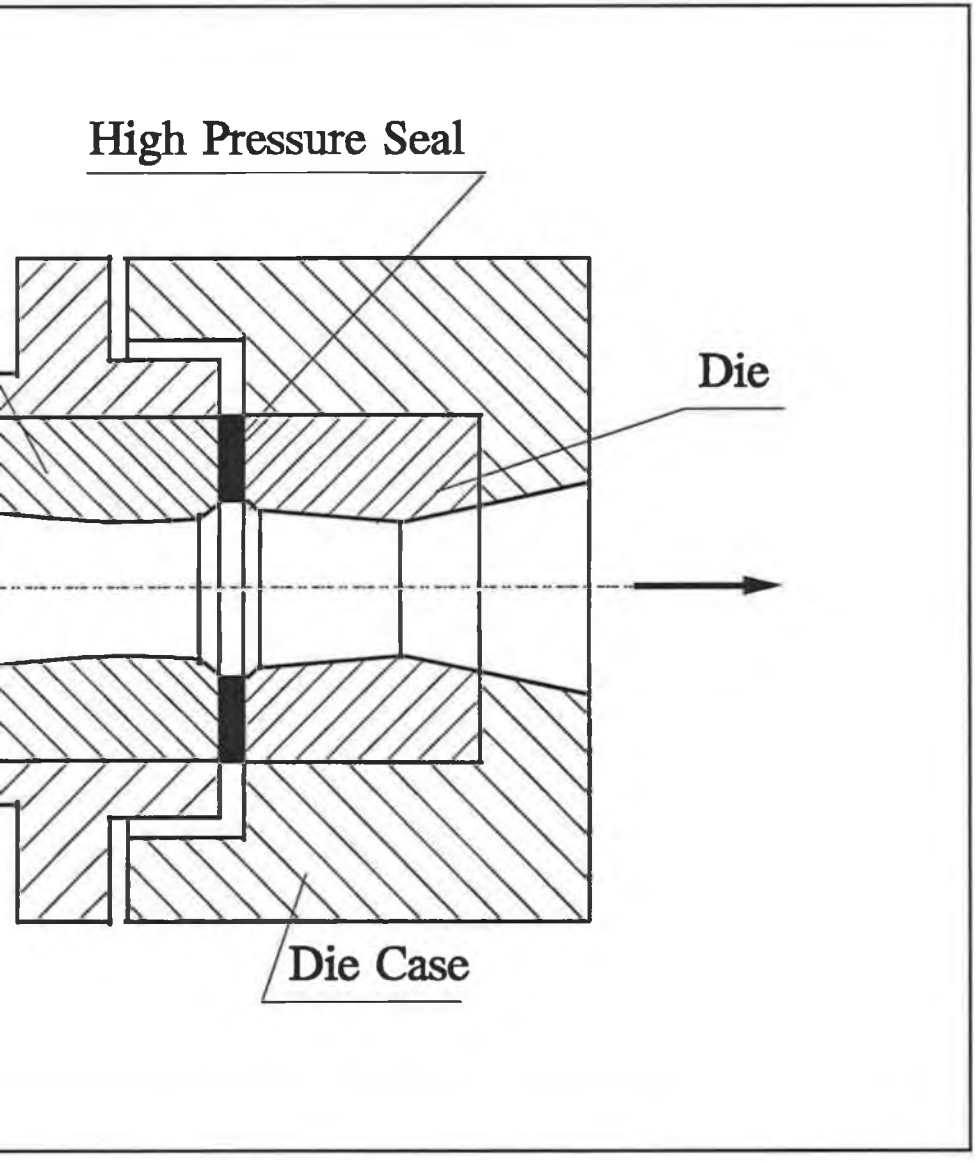
High Pressure Seal
Die
Die Case

soap nozzles. (see Figure 2), and then Tattersal[6] presented a detailed analysis of plasto-hydrodynamic lubrication action in wire drawing taking some rheological and metallurgical properties of the process into account. Consequently Middlemiss[7] developed a double die system(see Figure 3). The system had an "ironing" die which acted as a seal and reduced the wire by about 5%: it used externally pressurised oil. This type of die had one major drawback; it needs a high pressure pump to produce the required oil pressure between the dies.

The double die system was developed further by Orlov, et al[8] as a viable whole system using an approach die equal to the nominal diameter of the wire (see Figure 4). The exit cone from the pressure die and the entry cone to the drawing die produced the pressure, so a high pressure pump was unnecessary. The pressure was great enough to produce hydrodynamic lubrication.

Kolmogorov *et al* [9]produced experimental work on tube sinking under hydrodynamic action. They used soda-soap powder as the lubricant: as the lubrication process in tube sinking was much lower, there was no seal between the nozzle and the die.

Bloor et al[10] produced a theoretical analysis for elasto-plasto-hydrodynamic lubrication for strip drawing through wedge shaped dies taking account of the elastic

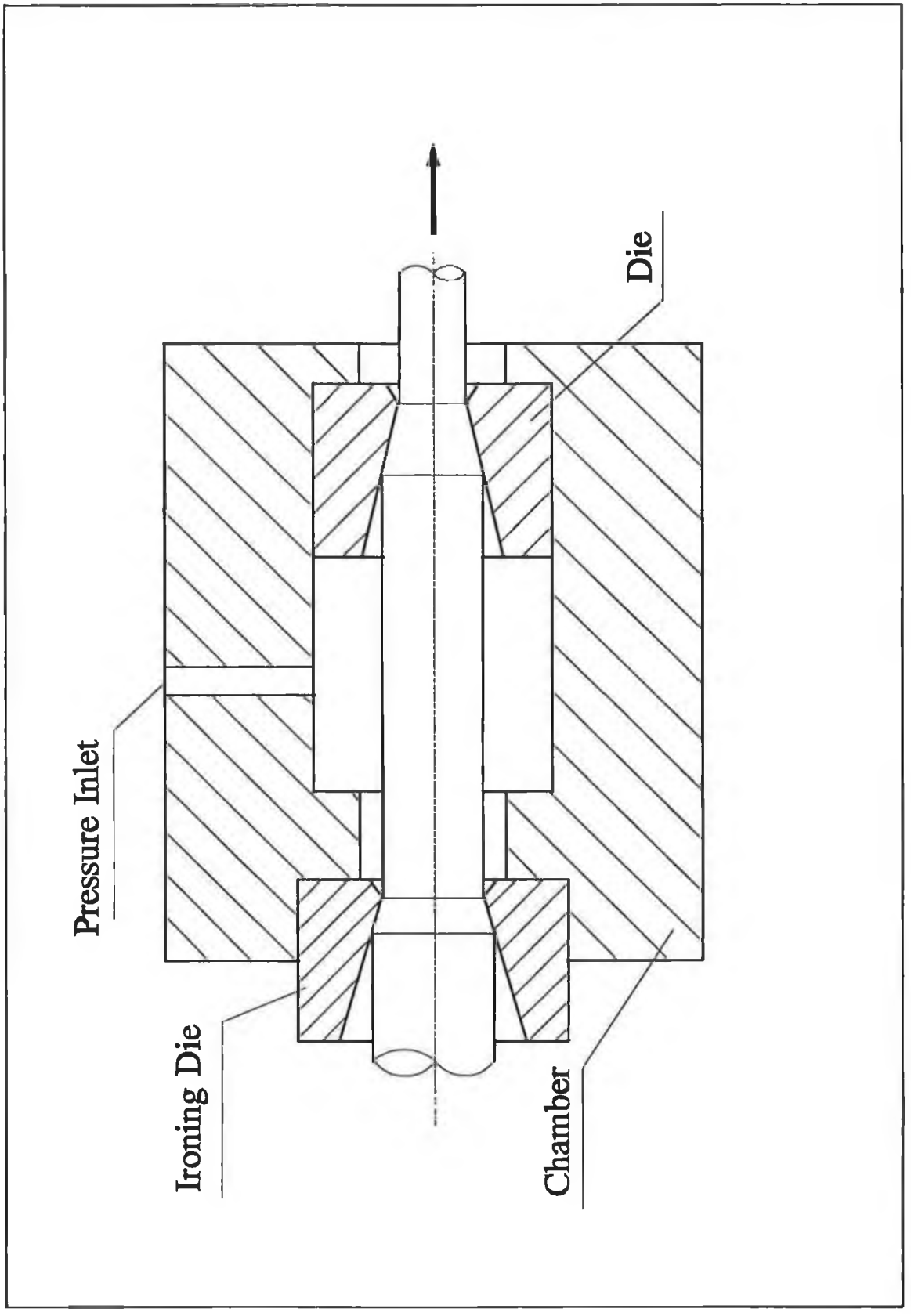

Figure 3 Pressurized chamber.

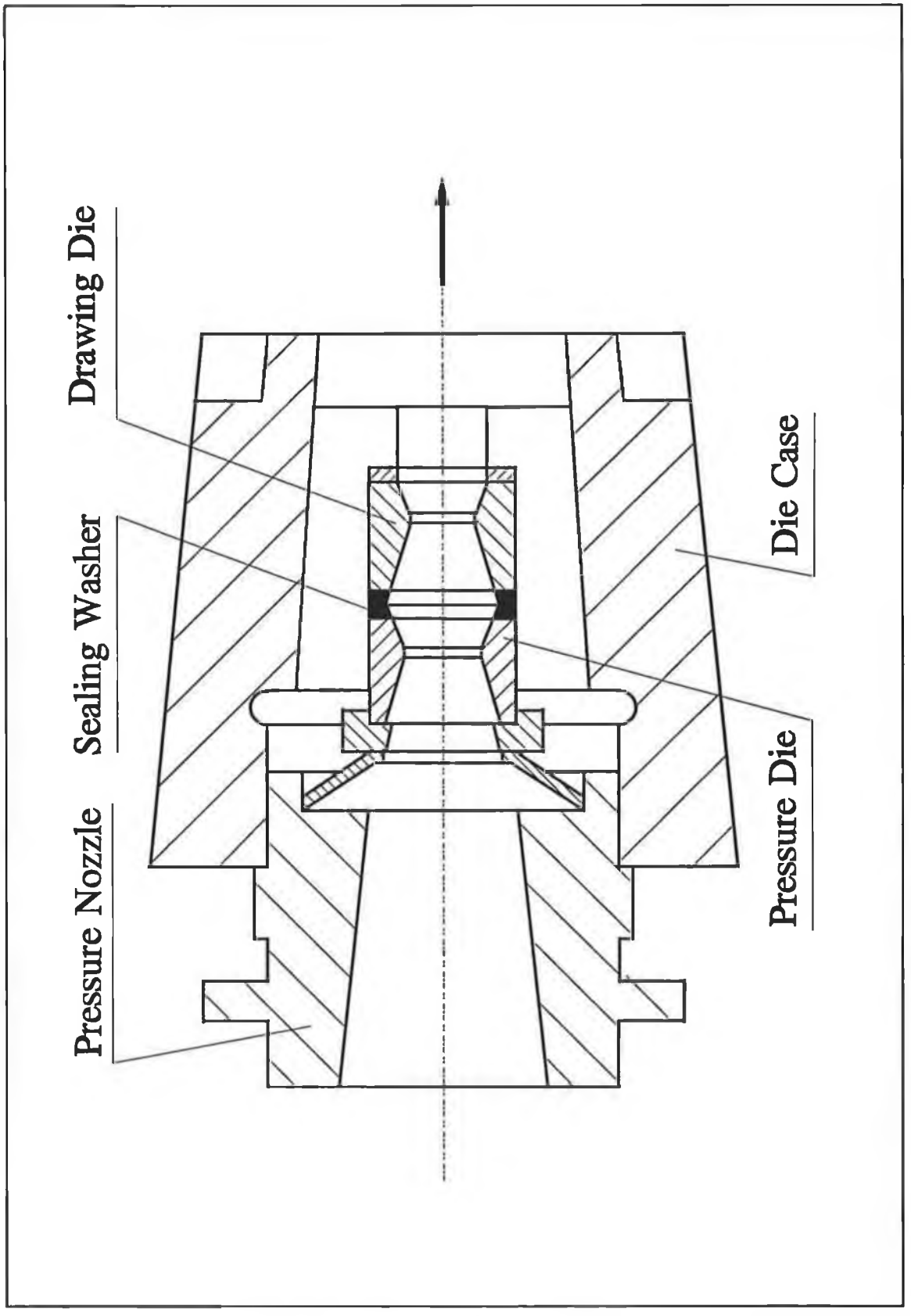

Figure 4 Double die unit.

component in the strip at entry and exit to the die.

An experimental study with cold sheet drawing through wedge shaped dies was carried out by Kudo et al[11] to investigate plasto-hydrodynamic lubrication in metal forming processes.

1.3 Background of Polymer Melt as a Lubricant in Wire Drawing

Recently polymers have been used as lubricants in drawing process. They were chosen because of the differing characteristics from the conventional lubricants either soap or oil.

The use of a polymer melt as a lubricant in wire drawing was first suggested by Symmons and Thompson[12]. They investigated the adherence of a polymer coat onto the wire. There was some hydrodynamic lubrication action of polymer on the wire achieved. Stevens[13] conducted experimental work which showed that polymer coating of wire was possible. Crampton[14] carried out an study of the wire drawing using a unit similar to the one adopted by Stevens. The apparatus they used consisted of a pressure tube connected to the forward end of a conventional die. The polymer melt was dragged into the tube by the motion of the wire generating high pressures which resulted in hydrodynamic lubrication and coating of wire. The experiments they conducted reduced the cross-sectional area of the wire. Both of them noted that

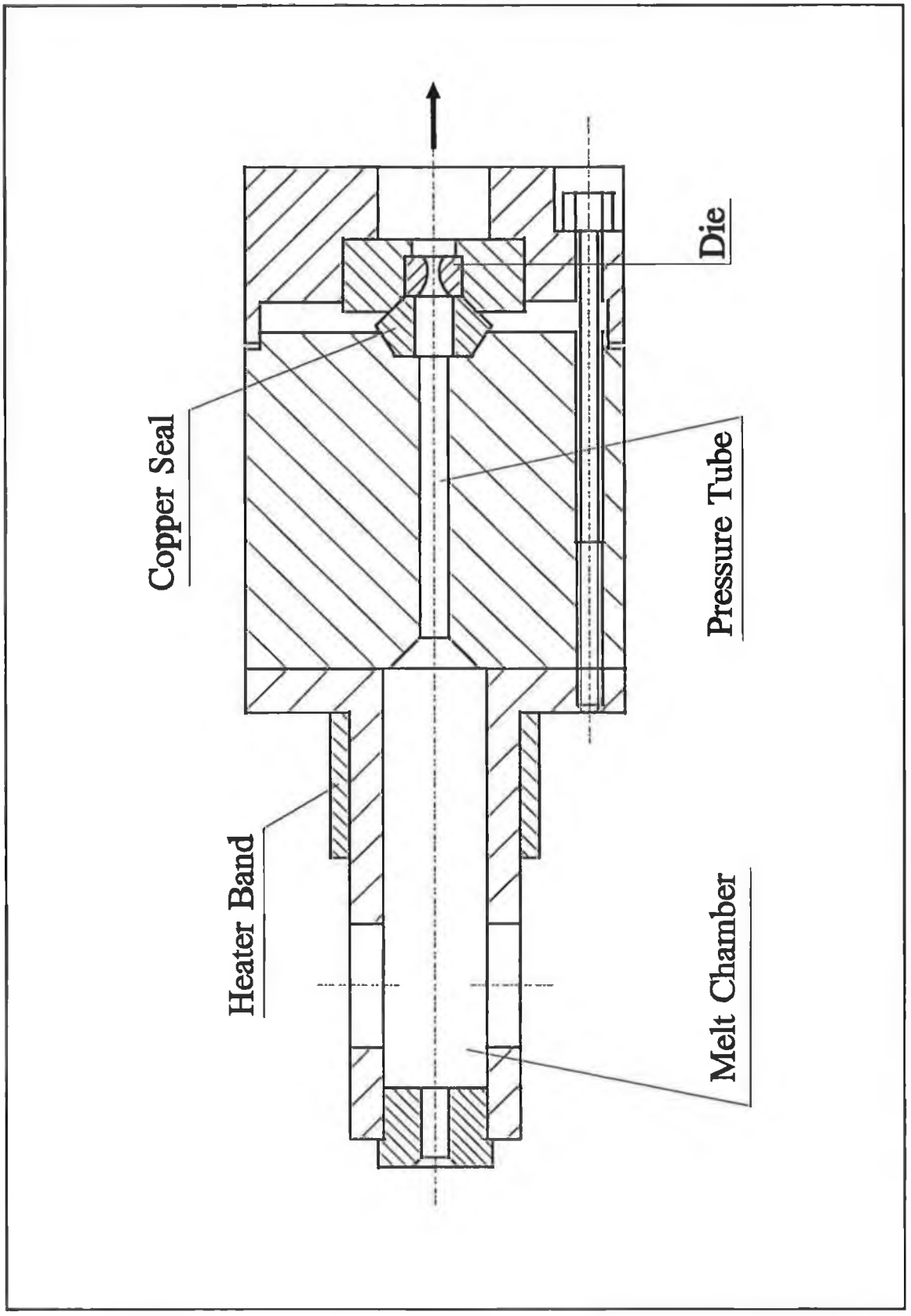

Figure 5 Pressure tube - Die arrangement.

the polymer coating of wire is affected by the temperature of polymer melt, viscosity of the polymer and drawing speed of the wire and the polymer coat thickness on the wire decreased as the drawing speed is increased. The section view of the unit is shown in Figure 5. On the basis of the experimental evidence it is apparent that the deformation of the wire commences within the tube itself before reaching the reduction die, which effectively acted only as a seal. Under these conditions the die geometry becomes of secondary importance and deformation actually takes place as if an effective die of continuously changing die angle is being used. Furthermore, work carried out by Hashmi[15], Symmons[16] and Parvinmehr[17] showed that reduction of the wire diameter should be possible using a polymer melt in conjunction with a stepped bore tubular unit only, thus eliminating the need for a conventional reduction die, the least diameter of the stepped bore reduction unit being greater than the nominal wire diameter. Thus a new concept in drawing was investigated and patented as "Plasto-hydrodynamic Die-less drawing". In this novel technique, the wire is pulled through a melt chamber filled with polymer melt and then through a stepped or tapered gap bore reduction unit. The motion of the wire causes the gap between the wire surface and the inner surface of the unit to be filled with polymer melt which results in hydrodynamic lubrication and permanent deformation in the wire can be achieved.

1.4 Present Work

This experimental research is the continuation and development of the work of Lamb[18]. The test for diameters of the wire below 0.2mm were used in his work. Actually, there are many factors affecting the quality of coating of wires. In this investigation more parameters have been considered besides the variation of the diameters of wires ranging from 0.1-0.4 mm.

The objectives of the present project are:

(1) to design the experimental drawing unit to facilitate plasto-hydrodynamic drawing and coating of fine wires.

(2) to develop a mathematical model for the prediction of various parameters involved in the process such as pressure distribution, the equivalent stress of the wire and the pulling force, coating thickness etc.

(3) to investigate the polymer coating thickness, uniformity, continuity and quality on the wires altering the following variables:
    (a) variation of the drawing speed;
    (b) temperature of the polymer;
    (c) variation of the gap between the wire and the die,
    (d) wire diameter.

Chapter 2 Models and Analytical Solutions

2.1 Introduction

There are many factors which affect the coating qualities such as drawing speed, the size of the die, the gap between the die and the wire and the properties of the polymer coating materials, *etc.* In order to control the coating qualities it is necessary to study and verify hydrodynamical properties of pressure developed within the unit. The analysis of a coating unit requires, the idealization of the system into a form that can be analyzed, the formulation of governing equilibrium equations, and the interpretation of the results. Therefore, in this chapter the mechanical model is first simplified, secondly the systematic equilibrium equation is derived, finally the analytical solutions of the equations are given.

2.2 The Governing Equilibrium Equation

The present analysis is established in cylindrical coordinate since the practical case is a mathematical axisymmetric problem. The geometrical configuration of the

pressure unit and the wire being drawn are shown in Figure 6, where u_0 is the drawing velocity of the wire, D_0 is the diameter of the wire, R_1 and R_2 are the inlet and outlet radii respectively. A stepped pressure unit is used and there is a gap between the drawn wire and the die, and the unit is completely filled with the polymer melt. An external force by a drive system pulls the wire through the unit at a constant velocity and the relative motion between the wire and the polymer causes a pressure that acts on the wire. It is this pressure which assists in developing a thin coating of the polymer adhered to the wire that is passing through the unit.

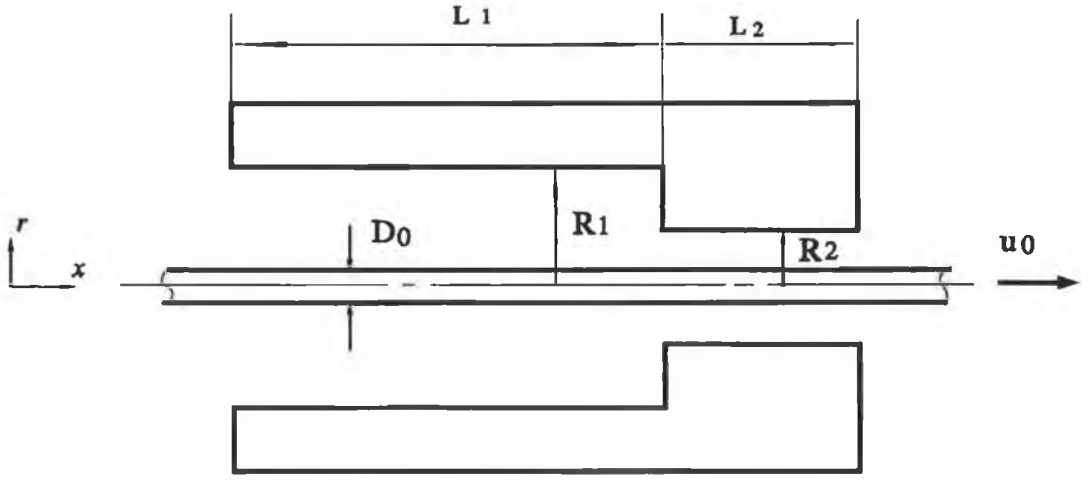

Figure 6 *The geometrical configuration of pressure unit and the wire.*

The unit is divided into two parts (step 1 and step 2) to be analyzed, whose lengths are L_1 and L_2 respectively. Each part is considered as a pipe through which a wire is passing

and the solutions in the two parts are coupled by the continuities of pressure and flow volume at the junction. To formulate the analysis, the following reasonable assumptions are made:

(1) The flow of the fluid is incompressible, steady and uniform;
(2) The flow of the polymer is laminar;
(3) The material of the wire is rigid.

Consider the case of steady laminar flow between a stationary circular cross-section pipe and a core wire, which is moving at a velocity u_0 in the flow direction. The flow condition may be analyzed by application of the momentum equation to an annular element of the flow - *ABCD* in Figure 7. The momentum equation may be stated as:

$$\sum F=\Delta M, \tag{1}$$

where ΣF is the resultant force in flow direction and ΔM is the rate of change of momentum in flow direction. For an element of fixed mass m, the equation may be written as

$$\sum F = m\frac{dv}{dt}, \tag{2}$$

and the acceleration of the flow is described by the equation

$$\frac{dv}{dt} = \frac{\partial v}{\partial t} + v\frac{\partial v}{\partial x}. \tag{3}$$

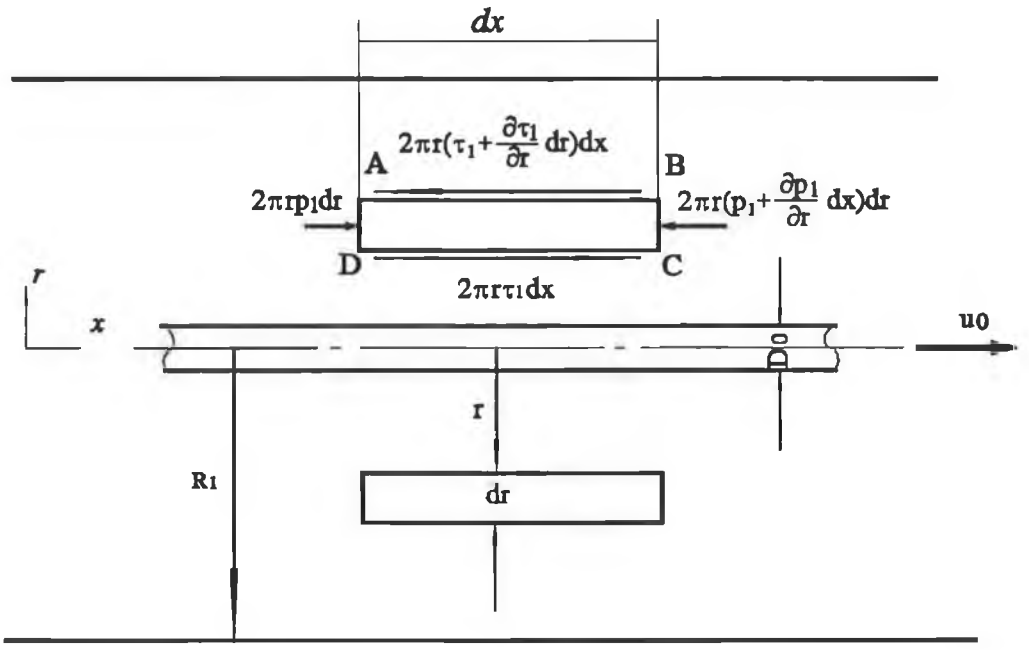

Figure 7 *The force acting on an annular element in the first step of the pressure unit.*

The convective acceleration $v(\partial v/\partial x)$ due to the movement of the particle from one point to another point at which the velocity at the given instant is different; while the local or temporal acceleration $(\partial v/\partial t)$ due to the change of velocity at every point with time.

For steady flow $\partial v/\partial t=0$, while for uniform flow $\partial v/\partial x=0$, hence $dv/dt=0$, *i.e.* the resultant force acting on the fluid element *ABCD* is zero and the flow is in a state of equilibrium under the action of the forces illustrated.

Consider an annular element in the flow of internal radius r and radial thickness dr, as shown in Figure 7, in the unit of radius R_1 carrying a fluid under laminar flow conditions. Applying the equation of equilibrium to the annular element *ABCD* illustrated in Figure 7, yields an expression

$$2\pi r p_1 - 2\pi r\left(p_1 + \frac{\partial p_1}{\partial x}dx\right)dr - 2\pi r\left(\tau_1 + \frac{\partial \tau_1}{\partial r}dr\right)dx + 2\pi r\tau_1 = 0, \qquad (4)$$

where p_1 is the flow static pressure in the first part of the unit, τ_1 is the shear stress at radius r in the first part. Simplifying the expression (4),

$$\frac{\partial \tau_1}{\partial r}drdx + \frac{\partial p_1}{\partial x}drdx = 0, \qquad (5)$$

and by dividing by $drdx$, a simple relationship between shear stress τ and pressure p results

$$\frac{\partial p_1}{\partial x} = -\frac{\partial \tau_1}{\partial r}. \qquad (6)$$

Actually, the shear stress is only dependent on the coordinate r normal to the wall of the die, which has already been established in connection with the discussion of the flow law. The pressure, or more accurately the negative normal stress in the r-direction, is only dependent on x. The left-hand side of equation (6) can accordingly be a function only of r; the right-hand side a function only of x. Equality of the two expressions can only exist under these conditions

if both sides are constant. We can therefore state that the pressure gradient $(\partial p/\partial x)$ is spatially constant, and therefore the pressure itself increases or decreases linearly with x. The shear stress correspondingly varies linearly with the coordinate r.

Since p_1 and τ_1 are dependent of x and r, equation (6) may be written as follows

$$\frac{dp_1}{dx} = -\frac{d\tau_1}{dr}. \qquad (7)$$

2.3 Analyses Model Based on Newtonian Fluid Characteristics

For Newtonian fluid, the shear stress-velocity gradient expression of equation $\tau = \mu(du_1/dy)$ may be employed in a modified form to take note of the direction of measurement of distance r from the centre of the unit rather than use of y measured from its inner wall, where μ is the viscosity of the fluid and u_1 is the velocity at a radius r. Hence the following equation can be obtained

$$\tau_1 = \mu\frac{du_1}{dy} = -\mu\frac{du_1}{dr}. \qquad (8)$$

Integrating equation (7) with respect to r and noting the pressure gradient (dp/dx) is spatially constant, we have

$$\tau_1 = -\frac{dp_1}{dx}r + C_1, \qquad (9)$$

and combining equations (8) with (9), yields

$$-\mu \frac{du_1}{dr} = -\frac{dp_1}{dx} + C_1 \qquad (10)$$

and

$$du_1 = \frac{1}{\mu}\left(\frac{dp_1}{dx} r dr - C_1 dr\right). \qquad (11)$$

Integrating with respect to r, the following equation can be found

$$u_1 = \frac{r^2}{2\mu}\frac{dp_1}{dx} - \frac{C_1}{\mu} r + C_2, \qquad (12)$$

where values of C_1 and C_2 may be evaluated from boundary conditions: at $r = R_0$ *i.e.* at the wire surface, $u_1 = u_0$; at $r = R_1$, *i.e.* at the inner wall of the unit, $u_1 = 0$. Hence, we have

$$u_0 = \frac{R_0^2}{2\mu}\frac{dp_1}{dx} - \frac{C_1}{\mu} R_0 + C_2 \qquad (13)$$

and

$$0 = \frac{R_1^2}{2\mu}\frac{dp_1}{dx} - \frac{C_1}{\mu} R_1 + C_2, \qquad (14)$$

further

$$C_1 = \frac{1}{2}\frac{dp_1}{dx}(R_0+R_1) + \frac{\mu u_0}{R_1-R_0} \qquad (15)$$

and

$$C_2 = \frac{R_1 u_0}{R_1-R_0} + \frac{R_0 R_1}{2\mu}\frac{dp_1}{dx}. \qquad (16)$$

Finally, the following equations are obtained

$$u_1 = \frac{1}{2\mu}\left[r^2-(R_0+R_1)\,r+R_0R_1\right]\frac{dp_1}{dx} + u_0\frac{R_1-r}{R_1-R_0} \qquad (17)$$

and

$$\tau_1 = \frac{1}{2}(R_0+R_1-2r)\frac{dp_1}{dx} + \frac{\mu u_0}{R_1-R_0}. \qquad (18)$$

The volume flow rate of the pressure medium in the first part of the unit under these flow conditions may be calculated by integrating the incremental flow dQ through an annulus of radial width dr at radius r across the flow from $r = R_0$, to $r = R_1$ (see Figure 7),

$$dQ = u_1 2\pi r dr, \qquad (19)$$

or

$$Q_1 = \int_{R_0}^{R_1} 2\pi u_1 r dr. \qquad (20)$$

Substituting for u_1 at general radius r, yields an expression

$$Q_1=\int_{R_0}^{R_1}\left[\frac{1}{2\mu}(r^2-(R_0+R_1)\,r+R_0R_1)\frac{dp_1}{dx}+u_0\frac{R_1-r}{R_1-R_0}\right]2\pi r\,dr. \tag{21}$$

For two-dimensional continuity flow we have

$$\frac{\partial Q_1}{\partial r}+\frac{\partial Q_1}{\partial x}=0, \tag{22}$$

while

$$\frac{\partial Q_1}{\partial r}=0. \tag{23}$$

Integrating the equation (21) and combining the result of equation (21) with equations (22) and (23), the following equation is obtained,

$$\frac{\partial}{\partial x}\left[-\frac{\pi}{12\mu}(R_1^2-R_0^2)\,(R_1-R_0)^2\frac{dp_1}{dx}+\frac{\pi u_0}{3}(R_1-R_0)\,(R_1+R_0)\right]=0, \tag{24}$$

from which it follows that

$$\frac{d^2p_1}{dx^2}=0. \tag{25}$$

Therefore, for given R_1, R_0, μ and u_0,

$$\frac{dp_1}{dx}=\frac{P_{m1}}{L_1}=Constant, \tag{26}$$

where P_{m1} is the pressure at the step and L_1 is the length of the first part of the unit. Equation (26) further confirms

the conclusion that the pressure gradient *dp/dx* is a constant.

At the second step(see Figure 8), the analysis may be treated in the same way as described at the first step. Thus,

$$\frac{d\tau_2}{dr} = -\frac{dp_2}{dx}, \tag{27}$$

where p_2 is the flow static pressure in the second part of the unit, τ_2 is the shear stress at radius r in the second part. The flow velocity and volume equations are

$$u_2 = \frac{1}{2\mu}\left[r^2 - (R_0+R_2)\,r + R_0R_2\right]\frac{dp_2}{dx} + u_0\frac{R_2-r}{R_2-R_0}, \tag{28}$$

$$\tau_2 = \frac{1}{2}\,(R_0+R_2-2\,r)\,\frac{dp_2}{dx} + \frac{\mu u_0}{R_2-R_0} \tag{29}$$

and

$$\begin{aligned} Q_2 &= \int_{R_0}^{R_2}\left[\frac{1}{2\mu}\left(r^2-(R_0+R_2)\,r+R_0R_2\right)\frac{dp_2}{dx} + u_0\frac{R_2-r}{R_2-R_0}\right]2\pi r\,dr \\ &= \frac{\pi}{12\mu}\,(R_2^2-R_0^2)\,(R_2-R_0)^2\frac{dp_2}{dx} - \frac{\pi u_0}{3}\,(R_2-R_0)\,(R_2+2R_0)\,. \end{aligned} \tag{30}$$

For two-dimensional continuity of flow the following equation is given

$$\frac{\partial Q_2}{\partial r}+\frac{\partial Q_2}{\partial x}=0. \tag{31}$$

Since

$$\frac{\partial Q_2}{\partial r}=0, \tag{32}$$

the following equation can be obtained

$$\frac{\partial Q_2}{\partial x}=0. \tag{33}$$

Therefore, for given R_2, R_0, μ and u_0,

$$\frac{dp_2}{dx}=-\frac{P_{m2}}{L_1}=Constant, \tag{34}$$

where P_{m2} is the pressure at the step and L_2 is the length of the second part of the unit. The continuity of flow gives

$$Q_1=Q_2. \tag{35}$$

Substituting Equations (21) and (30) into above equation, we have

$$\begin{aligned}&-\frac{\pi}{12\mu}(R_1^2-R_0^2)(R_1-R_0)^2\frac{dp_1}{dx}-\frac{\pi u_0}{3}(R_1-R_0)(R_1+2R_0)\\&=\frac{\pi}{12\mu}(R_2^2-R_0^2)(R_2-R_0)^2\frac{dp_2}{dx}-\frac{\pi u_0}{3}(R_2-R_0)(R_2+2R_0).\end{aligned} \tag{36}$$

The pressure at the junction of the two parts is equal, therefore, we have $P_{m1}=P_{m2}=P_m$, *i.e.*

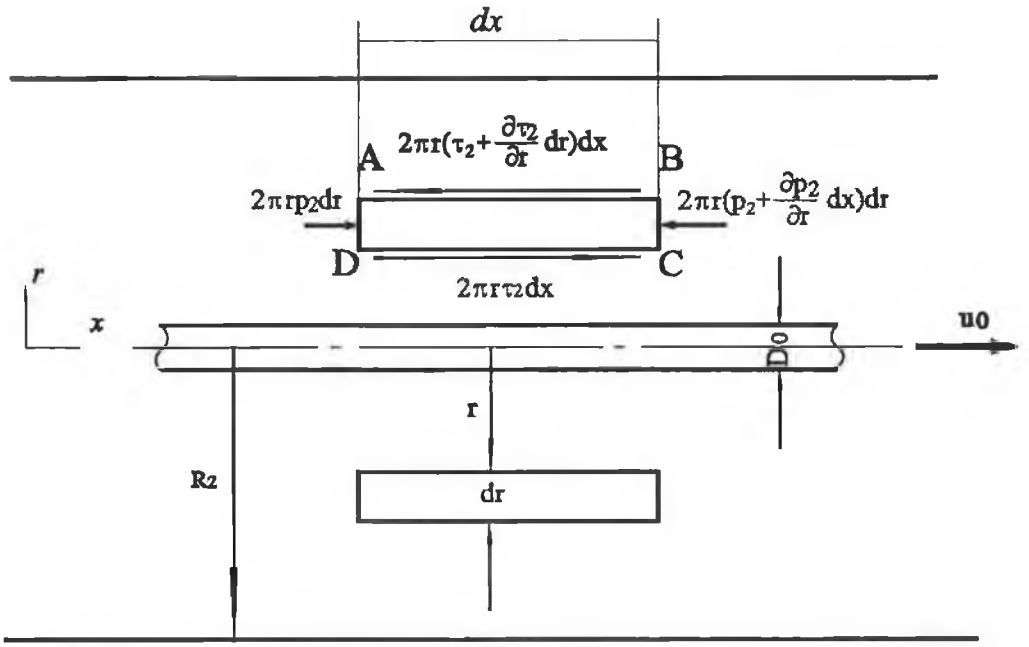

Figure 8 *The force acting on an annular element in the second step of the pressure unit.*

$$-\frac{\pi}{12\mu}(R_1^2-R_0^2)(R_1-R_0)^2\frac{P_m}{L_1}-\frac{\pi u_0}{3}(R_1-R_0)(R_1+2R_0)$$

$$=\frac{\pi}{12\mu}(R_2^2-R_0^2)(R_2-R_0)^2\frac{P_m}{L_2}-\frac{\pi u_0}{3}(R_2-R_0)(R_2+2R_0)\,. \tag{37}$$

Hence

$$\frac{\pi P_m}{12\mu}\left[\frac{(R_1^2-R_0^2)(R_1-R_0)^2}{L_1}+\frac{(R_2^2-R_0^2)(R_2-R_0)^2}{L_2}\right]$$

$$=\frac{\pi u_0}{3}(R_1-R_2)(R_1+R_2+R_0) \tag{38}$$

or

$$P_m = \frac{4\mu u_0 (R_1 - R_2)(R_1 + R_2 + R_0)}{\frac{(R_1^2 - R_0^2)(R_1 - R_0)^2}{L_1} + \frac{(R_2^2 - R_0^2)(R_2 - R_0)^2}{L_2}} \qquad (39)$$

The shear stresses at $r=R_0$ from Equation (18) and Equation (29) are respectively

$$\tau_{10} = \frac{1}{2}(R_1 - R_0)\frac{dp_1}{dx} + \frac{\mu u_0}{R_1 - R_0} = \frac{1}{2}(R_1 - R_0)\frac{P_m}{L_1} + \frac{\mu u_0}{R_1 - R_0} \qquad (40)$$

and

$$\tau_{20} = \frac{1}{2}(R_2 - R_0)\frac{dp_2}{dx} + \frac{\mu u_0}{R_2 - R_0} = -\frac{1}{2}(R_2 - R_0)\frac{P_m}{L_2} + \frac{\mu u_0}{R_2 - R_0}. \qquad (41)$$

The axial force on the wire at any point distance x from the entry can be obtained by considering the shear force action on the surface of the wire. Thus

$$F = \int_0^{L_1} 2\pi R_0 \tau_{10}\, dx + \int_0^{L_2} 2\pi R_0 \tau_{20}\, dx = 2\pi R_0 (\tau_{10} L_1 + \tau_{20} L_2). \qquad (42)$$

By substituting for τ_{10} and τ_{20} above, we have

$$F = \pi R_0 (R_1 - R_2) P_m + 2\pi\mu u_0 R_0 \left(\frac{R_1 + R_2 - 2R_0}{(R_1 - R_0)(R_2 - R_0)} \right). \qquad (43)$$

In cylindrical coordinate system, the general differential equations of equilibrium are as follows

$$\left.\begin{aligned} &\frac{\partial \sigma_r}{\partial r}+\frac{1}{r}\frac{\partial \tau_{\theta r}}{\partial \theta}+\frac{\partial \tau_{xr}}{\partial x}+\frac{\sigma_r-\sigma_\theta}{r}+F_r=0 \\ &\frac{1}{r}\frac{\partial \sigma_\theta}{\partial \theta}+\frac{\partial \tau_{r\theta}}{\partial r}+\frac{\partial \tau_{x\theta}}{\partial x}+\frac{2\tau_{r\theta}}{r}+F_\theta=0 \\ &\frac{\partial \sigma_x}{\partial x}+\frac{\partial \tau_{rx}}{\partial r}+\frac{1}{r}\frac{\partial \tau_{\theta x}}{\partial \theta}+\frac{\tau_{rx}}{r}+F_x=0 \end{aligned}\right\} \qquad (44)$$

where F_x, F_r and F_θ are the components of body forces along axial, radial and tangential directions respectively, and we can find the following expressions for the strain components

$$\left.\begin{aligned} &\varepsilon_r=\frac{\partial u_r}{\partial r}, \qquad \varepsilon_\theta=\frac{u_r}{r}+\frac{1}{r}\frac{\partial u_\theta}{\partial \theta}, \qquad \varepsilon_x=\frac{\partial u_x}{\partial x} \\ &\gamma_{xr}=\frac{\partial u_r}{\partial x}+\frac{\partial u_x}{\partial r}, \quad \gamma_{r\theta}=\frac{1}{r}\frac{\partial u_r}{\partial \theta}+\frac{\partial u_\theta}{\partial r}-\frac{u_\theta}{r}, \quad \gamma_{\theta x}=\frac{\partial u_\theta}{\partial x}+\frac{1}{r}\frac{\partial u_x}{\partial \theta}. \end{aligned}\right\} \qquad (45)$$

In the case of wire drawing in which the wire is deformed by loads symmetrical about the r, θ, x, with corresponding displacement components u_r, u_θ, u_x, the component u_θ vanishes and u_r and u_x are independent of θ. Then the stress components are also independent of θ, two of them, $\tau_{r\theta}$ and $\tau_{x\theta}$, being zero. Therefore, Equation (44) for the equilibrium of an element reduces to

$$\left.\begin{aligned} &\frac{\partial \sigma_r}{\partial r}+\frac{\partial \tau_{xr}}{\partial x}+\frac{\sigma_r-\sigma_\theta}{r}=0 \\ &\frac{\partial \sigma_x}{\partial x}+\frac{\partial \tau_{rx}}{\partial r}+\frac{\tau_{rx}}{r}=0 \end{aligned}\right\} \qquad (46)$$

For the present Newtonian model, the corresponding strain-displacement relations reduce to

$$\varepsilon_r=\frac{\partial u_r}{\partial r}\ ,\quad \varepsilon_\theta=\frac{u_r}{r}\ ,\quad \varepsilon_x=\frac{\partial u_x}{\partial x},\quad \gamma_{xr}=\frac{\partial u_r}{\partial x}+\frac{\partial u_x}{\partial r}. \tag{47}$$

The boundary condition are

$$\sigma_r|_{r=R_0,\ x=L_1}=-p_m\ , \tag{48}$$

in the first step

$$\tau_{rx}|_{r=R_0}=-\tau_{10}, \tag{49}$$

and in the second step

$$\tau_{rx}|_{r=R_0}=-\tau_{20}\ . \tag{50}$$

Assuming that the tension force acted on the wire is equally distributed on its cross-section, we have

$$\sigma_x=\frac{F}{\pi R_0^2}\ . \tag{51}$$

To evaluate the stresses σ_r and σ_θ, we consider the stress distribution in a hollow cylinder submitted to uniform pressure on the inner and outer surfaces shown in Figure 9. Letting a and b denote the inner and outer radii of the cylinder, and p_i and p_o the uniform internal and external pressures, we have

$$\sigma_r=\frac{a^2b^2(p_0-p_i)}{b^2-a^2}\frac{1}{r^2}+\frac{p_ia^2-p_0b^2}{b^2-a^2} \tag{52}$$

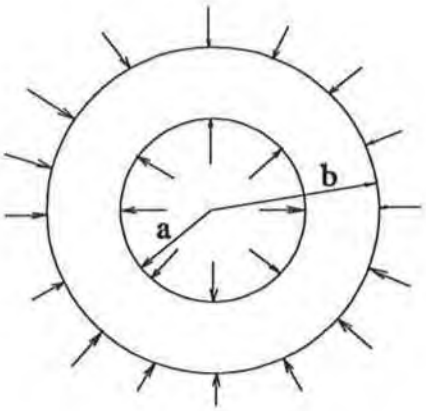

Figure 9 *The stress distribution in a hollow cylinder submitted to uniform pressure on the inner and outer surfaces.*

and

$$\sigma_\theta = -\frac{a^2 b^2 (p_0 - p_i)}{b^2 - a^2}\frac{1}{r^2} + \frac{p_i a^2 - p_0 b^2}{b^2 - a^2}. \qquad (53)$$

Let $a=0$ and $p_i=0$, the following equation can be obtained

$$\sigma_r = -p_o , \qquad \sigma_\theta = -p_o. \qquad (54)$$

The equivalent stress can be obtained as follows according to the yield theory of von Mises

$$\sigma_e = \sqrt{\frac{1}{2}\left[(\sigma_x-\sigma_r)^2+(\sigma_x-\sigma_\theta)^2+(\sigma_r-\sigma_\theta)^2+\tau_{rx}^2+\tau_{r\theta}^2+\tau_{x\theta}^2\right]} \qquad (55)$$

Letting $\sigma_r=\sigma_\theta=-P_m$, $\sigma_x=F/\pi R_0^2$, $\tau_{x\theta}=\tau_{r\theta}=0$ and $\tau_{rx}=\tau_{10}$, we have

$$\sigma_e=\sqrt{(\sigma_x+p_m)^2+\frac{1}{2}\tau_{10}^2}. \tag{56}$$

The yielding condition is

$$\sigma_e\leq\sigma_s, \tag{57}$$

where σ_s is the yielding limit of drawn material.

All the experimental parameters are chosen as such requirements that the deformation of a drawn wire is within the elastic range. However, it can be done to deform plastically the drawn wire by means of the adjustment of the corresponding parameters.

2.4 Analyses based on Non-Newtonian fluid Characteristics

For non-Newtonian fluid, an equation relating the shear stress and shear rate of polymer melts was suggested by Rabinowitsch [19] in the form

$$\tau+k\tau^3=\mu\frac{du}{dy}. \tag{58}$$

This equation may be employed in a modified form to take note of the direction of measurement of distance r from the centre of the unit rather than use of y measured from its inner wall. Hence,

$$\tau + k\tau^3 = \mu \frac{du}{dy} = -\mu \frac{du}{dr} . \qquad (59)$$

Substituting τ_1 in Equation (9) for τ, we have

$$-\mu \frac{du_1}{dr} = -\frac{dp_1}{dx} r + C_1 + k\left(-\frac{dp_1}{dx} r + C_1\right)^3 \qquad (60)$$

$$\mu \frac{du_1}{dr} = \frac{dp_1}{dx} r - C_1 + k\left[\left(\frac{dp_1}{dx} r\right)^3 - 3\left(\frac{dp_1}{dx} r\right)^2 C_1 + 3\frac{dp_1}{dx} C_1^2 - C_1^3\right] \qquad (61)$$

Integration with respect to r gives:

$$\mu u_1 = \frac{dp_1}{dx}\frac{r^2}{2} - C_1 r + k\left[\left(\frac{dp_1}{dx}\right)^3 \frac{r^4}{4} - \left(\frac{dp_1}{dx}\right)^2 r^3 C_1 + \frac{3}{2}\frac{dp_1}{dx} r^2 C_1^2 - C_1^3 r\right] + C_2 \qquad (62)$$

$$u_1 = \frac{r^2}{4\mu}\left(\frac{dp_1}{dx}\right)\left[2 + k\left(\frac{dp_1}{dx} r\right)^2\right] - \frac{r}{\mu}\left[1 + k\left(\frac{dp_1}{dx} r\right)^2\right] C_1$$

$$+ \frac{3k}{2\mu}\frac{dp_1}{dx} r^2 C_1^2 - \frac{kr}{\mu} C^3 + \frac{C_2}{\mu} \qquad (63)$$

Values of C_1 and C_2 may be evaluated from boundary conditions at $r = R_0$ and $r = R_1$. Therefore, at $r = R_0$, $u = u_0$; at $r = R_1$, *i.e.* at the inner wall of the unit, the local flow velocity is zero, $u_1 = 0$. Hence,

$$\mu u_0 = \frac{R_0^2}{4}\left(\frac{dp_1}{dx}\right)\left[2 + k\left(\frac{dp_1}{dx} R_0\right)^2\right] - R_0\left[1 + k\left(\frac{dp_1}{dx} R_0\right)^2\right] C_1 \qquad (64)$$

$$+ \frac{3k}{2}\frac{dp_1}{dx} R_0^2 C_1^3 - k R_0 C_1^3 + C_2$$

$$0=\frac{R_1^2}{4}\left(\frac{dp_1}{dx}\right)\left[2+k\left(\frac{dp_1}{dx}R_1\right)^2\right]-R_1\left[1+k\left(\frac{dp_1}{dx}R_1\right)^2\right]C_1 \tag{65}$$

$$+\frac{3k}{2}\frac{dp_1}{dx}R_1^2C_1^2-kR_1C_1^3+C_2$$

and substituting Equation (65) from Equation (64), we have

$$\mu u_1=\frac{R_0^2-R_1^2}{4}\left(\frac{dp_1}{dx}\right)\left[2+k\left(\frac{dp_1}{dx}\right)^2(R_0^2+R_1^2)\right]-(R_0-R_1)\left[1+\right. \tag{66}$$

$$\left.+k(R_0^2+R_0R_1+R_1^2)\left(\frac{dp_1}{dx}\right)^2\right]C_1+\frac{3k}{2}\frac{dp_1}{dx}(R_0^2-R_1^2)C_1^2-k(R_0-R_1)C_1^3.$$

Hence,

$$kC_1^3-\frac{3}{2}\frac{dp_1}{dx}(R_0+R_1)kC_1^2+\left[1+k\left(\frac{dp_1}{dx}\right)^2(R_0^2+R_0R_1+R_1^2)\right]C_1 \tag{67}$$

$$-\frac{R_0+R_1}{4}\frac{dp_1}{dx}\left[2+k\left(\frac{dp_1}{dx}\right)^2(R_0^2+R_1^2)\right]+\frac{u_0\mu}{(R_0-R_1)}=0.$$

Setting $\xi_1 = R_0/R_1$ yields the following equation

$$C_1^3-\frac{3R_1}{2}(1+\xi_1)\frac{dp_1}{dx}C_1^2+\left[\frac{1}{k}+\left(\frac{dp_1}{dx}R_1\right)^2(1+\xi+\xi^2)\right]C_1 \tag{68}$$

$$-\frac{R_1}{4}(1+\xi_1)\left(\frac{dp_1}{dx}\right)\left[\frac{2}{k}+\left(\frac{dp_1}{dx}R_1\right)^2(1+\xi^2)\right]-\frac{u_0\mu}{kR_1(1-\xi_1)}=0.$$

Selecting the following parameters

$$J_1=-\frac{3}{2}\frac{dp_1}{dx}R_1(1+\xi_1), \tag{69}$$

$$M_1=\left(\frac{dp_1}{dx}\right)^2(1+\xi_1+\xi^2)R_1^2+\frac{1}{k} \tag{70}$$

and

$$N_1=-\frac{R_1}{4}(1+\xi_1)\left(\frac{dp_1}{dx}\right)\left[\frac{2}{k}+R_1^2(1+\xi_1^2)\left(\frac{dp_1}{dx}\right)^2\right]-\frac{u_0\mu}{kR_1(1-\xi_1)}, \tag{71}$$

we obtain

$$C_1^3+J_1C_1^2+M_1C_1+N_1=0. \tag{72}$$

Also letting

$$C_1=\Phi_1-\frac{J_1}{3}, \tag{73}$$

we have

$$(\Phi_1-\frac{J_1}{3})^3+J_1(\Phi_1-\frac{J_1}{3})^2+M_1(\Phi_1-\frac{J_1}{3})+N_1=0 \tag{74}$$

and

$$\Phi_1^3+(-\frac{1}{3}J_1^2+M_1)\Phi_1+\frac{2}{27}J_1^3-\frac{M_1J_1}{3}+N_1=0. \tag{75}$$

Letting

$$\lambda_1=-\frac{1}{3}J_1^2+M_1=\frac{R_1^2}{4}(\frac{dP_1}{dx})^2(1-\xi_1)^2+\frac{1}{k} \tag{76}$$

and

$$\zeta_1=\frac{2}{27}J_1^3+N_1-\frac{M_1J_1}{3}=\frac{u_0\mu}{kR_1(1-\xi_1)}, \tag{77}$$

the following expression can be obtained

$$\Phi_1^3+\lambda_1\Phi_1+\zeta_1=0. \tag{78}$$

This equation has a definite solution with two imaginary roots and one real root, the real root being;

$$\Phi_1=\left\{-\frac{\zeta_1}{2}+\left[(\frac{\zeta_1}{2})^2+\frac{(\lambda_1)^3}{3}\right]^{\frac{1}{2}}\right\}^{\frac{1}{3}}+\left\{-\frac{\xi_1}{2}-\left[(\frac{\xi_1}{4})^2+(\frac{\lambda_1}{3})^3\right]^{\frac{1}{2}}\right\}^{\frac{1}{3}} \tag{79}$$

Substituting for λ_1 and ζ_1 into above equation and combining with equation (73) gives

$$C_1=\left\{-\frac{\zeta_1}{2}+\left[\left(\frac{\zeta_1}{2}\right)^2+\left(\frac{\lambda_1}{3}\right)^3\right]^{\frac{1}{2}}\right\}^{\frac{1}{3}}$$

$$+\left\{-\frac{\zeta_1}{2}-\left[\left(\frac{\zeta_1}{2}\right)^2+\left(\frac{\lambda_1}{3}\right)^3\right]^{\frac{1}{2}}\right\}^{\frac{1}{3}}+\frac{1}{2}\frac{dp_1}{dx}R_1(1+\xi_1) \qquad (80)$$

or

$$C_1=\left\{-\frac{\mu u_0}{2kR_1(1-\xi_1)}+\left[\left(\frac{\mu u_0}{2kR_1(1-\xi_1)}\right)^2+\frac{1}{27}\left(\frac{1}{4}\left(\frac{dp_1}{dx}R_1\right)^2(1-\xi_1^2)+\frac{1}{k}\right)^3\right]^{\frac{1}{2}}\right\}^{\frac{1}{3}}$$

$$+\left\{-\frac{\mu u_0}{2kR_1(1-\xi_1)}-\left[\left(\frac{\mu u_0}{2kR_1(1-\xi_1)}\right)^2+\frac{1}{27}\left(\frac{R_1}{4}\left(\frac{dp_1}{dx}\right)^2(1-\xi_1)+\frac{1}{k}\right)^3\right]^{\frac{1}{2}}\right\}^{\frac{1}{3}}$$

$$+\frac{R_1}{2}\left(\frac{dp_1}{dx}\right)(1+\xi_1)\,. \qquad (81)$$

If the pressure gradient (dp_1/dx) can be determined, the constant C_1 can be calculated from Equation (81). Then from equation (64), we have

$$C_2=-\frac{1}{2}\frac{dp_1}{dx}R_1^2+C_1R_1$$

$$+k\left[\left(-\frac{dp_1}{dx}\right)^3\frac{R_1^4}{4}+\left(\frac{dp_1}{dx}\right)^2R_1^3C_1-\frac{3}{2}\frac{dp_1}{dx}R_1^2C_1^2+C_1^3R_1\right]. \qquad (82)$$

The volume flow rate of the polymer through the first part of the unit under these flow conditions may be

calculated by integrating the incremental flow dQ through an annulus of radial width dr at radius r across the flow from $r = R_0$ to $r = R_1$ (see Figure 6),

$$dQ_1 = 2\pi u_1 r dr \tag{83}$$

or

$$Q_1 = \int_{R_0}^{R_1} 2\pi u_1 r dr . \tag{84}$$

Substituting Equation (63), yields the following expression

$$Q_1 = \frac{\pi}{4\mu}\frac{dp_1}{dx}(R_1^4 - R_0^4) - \frac{2\pi}{3\mu}(R_1^3 - R_0^3)C_1 + \frac{k\pi}{12\mu}\left(\frac{dp_1}{dx}\right)^3 (R_1^6 - R_0^6)$$

$$- \frac{2\pi k C_1}{5\mu}\left(\frac{dp_1}{dx}\right)^2 (R_1^5 - R_0^5) C_1 + \frac{3\pi k C_1^2}{4\mu}\frac{dp_1}{dx}(R_1^4 - R_0^4) \tag{85}$$

$$- \frac{2k\pi}{3\mu}(R_1^3 - R_0^3) C_1^3 + \frac{C_2\pi}{\mu}(R_1^2 - R_0^2)$$

or

$$Q_1 = \frac{\pi k}{12\mu}\left(\frac{dp_1}{dx}\right)^3 R_1^6 (1 - \xi_1^6) - \frac{2\pi k C_1}{5\mu}\left(\frac{dp_1}{dx}\right)^2 R_1^5 (1 - \xi_1^5)$$

$$+ \frac{\pi R_1^4}{4\mu}(1 - \xi_1^4)(1 + 3kC_1^2)\frac{dp_1}{dx} - \frac{2\pi}{3\mu} R_1^3 C_1 (1 - \xi_1^3)(1 + kC_1^2) \tag{86}$$

$$+ \frac{C_2\pi}{\mu} R_1^2 (1 - \xi_1^2) .$$

For two-dimensional continuity flow gives

$$\frac{\partial Q_1}{\partial r} + \frac{\partial Q_1}{\partial x} = 0 , \tag{87}$$

while

$$\frac{\partial Q_1}{\partial r}=0, \tag{88}$$

hence

$$\frac{\partial Q_1}{\partial x}=0. \tag{89}$$

Substituting equations (81) and (82) into (86) and differentiating gives

$$\frac{\partial^2 p_1}{\partial x^2}=0. \tag{90}$$

Hence

$$\frac{\partial p_1}{\partial x}=\frac{P_m}{L_1}=constant \tag{91}$$

where P_m is the maximum pressure in the unit and L_1 is the length of the first part of the unit.

At the second step, the analysis may be treated in the same manner as described at the first step. Hence

$$\frac{dp_2}{dx}+\frac{d\tau_2}{dr}=0. \tag{92}$$

Integration gives

$$\tau_2=-\frac{dp_2}{dx}r+C_3, \tag{93}$$

substituting τ_2 into Equation (59) gives

$$u_2=\frac{dp_2}{dx}\frac{r^2}{2\mu}-\frac{C_3}{\mu}r$$

$$+\frac{k}{\mu}\left[(\frac{dp_2}{dx})^3\frac{r^4}{4}-(\frac{dp_2}{dx})^2r^3C_3+\frac{3}{2}\frac{dp_2}{dx}r^2C_3^2-C_3^3r\right]+\frac{C_4}{\mu}, \tag{94}$$

and when $r = R_2$, $u_2 = 0$ and $r = R_0$, $u_2 = u_0$, setting $\xi_2=R_0/R_2$ rearranging gives

$$C_3^3-\frac{3}{2}\frac{dp_2}{dx}R_2(1+\xi_2)C_3^2+\left(\frac{1}{k}+(\frac{dp_2}{dx})^2R_2^2(1+\xi_2+\xi_2^2)\right)C_3$$

$$-\frac{1}{4}(\frac{dp_2}{dx})^3R_2^3(1+\xi_2^2)(1+\xi_2)-\frac{1}{2k}\frac{dp_2}{dx}R_2(1+\xi_2)-\frac{u_0\mu}{kR_2(1-\xi_2)}=0. \tag{95}$$

Letting

$$J_2=-\frac{3}{2}\frac{dp_2}{dx}R_2(1+\xi_2) \tag{96}$$

$$M_2=(\frac{dp_2}{dx})^2(1+\xi_2+\xi_2^2)R_2^2+\frac{1}{k} \tag{97}$$

$$N_2=-\frac{R_2}{4}(1+\xi_2)(\frac{dp_2}{dx})[\frac{2}{k}+R_2^2(1+\xi_2^2)(\frac{dp_2}{dx})^2]-\frac{u_0\mu}{kR_2(1-\xi_2)} \tag{98}$$

we have

$$C_3^3+J_2C_3^2+M_2C_3+N_2=0 \tag{99}$$

If

$$C_3=\Phi_2-\frac{J_2}{3} \tag{100}$$

we have

$$(\Phi_2-\frac{J_2}{3})^3+J_2(\Phi_2-\frac{J_2}{3})^2+M_1(\Phi_2-\frac{J_1}{3})+N_2=0 \qquad (101)$$

and

$$\Phi_2^3+(-\frac{1}{3}J_2^2+M_2)\Phi_2+\frac{2}{27}J_2^3-\frac{M_2J_2}{3}+N_2=0. \qquad (102)$$

Letting

$$\lambda_2=-\frac{1}{3}J_2^2+M_2, \qquad (103)$$

we have

$$\Phi_2^3+\lambda_2\Phi_2+\zeta_2=0. \qquad (104)$$

Actually, we can find

$$\lambda_2=\frac{R_2^2}{4}(\frac{dp_2}{dx})^2(1-\xi_2)^2+\frac{1}{k} \qquad (105)$$

and

$$\zeta_2=\frac{u_0\mu}{kR_1(1-\xi_2)}. \qquad (106)$$

Equation (104) has two imaginary roots and one real root, the real root being

$$\Phi_2=\left[-\frac{\zeta_2}{2}+(\frac{\zeta_2^2}{4}+\frac{\lambda_2^3}{27})^{\frac{1}{2}}\right]^{\frac{1}{3}}+\left[-\frac{\zeta_2}{2}-(\frac{\zeta_2^2}{4}+\frac{\lambda_2^3}{27})^{\frac{1}{2}}\right]^{\frac{1}{3}}. \qquad (107)$$

Substituting for λ_2 and ζ_2 into above equation and for Φ_2 into equation (100) gives

$$C_3=\left\{-\frac{\mu u_0}{2kR_2(1-\xi_2)}+\left[\left(\frac{\mu u_0}{2kR_1(1-\xi_2)}\right)^2+\frac{1}{27}\left(\frac{1}{4}\left(\frac{dp_2}{dx}R_2\right)^2(1-\xi_2^2)+\frac{1}{k}\right)^3\right]^{\frac{1}{2}}\right\}^{\frac{1}{3}}$$

$$+\left\{-\frac{\mu u_0}{2kR_2(1-\xi_2)}-\left[\left(\frac{\mu u_0}{2kR_2(1-\xi_2)}\right)^2+\frac{1}{27}\left(\frac{R_2}{4}\left(\frac{dp_2}{dx}\right)^2(1-\xi_2)+\frac{1}{k}\right)^3\right]^{\frac{1}{2}}\right\}^{\frac{1}{3}}$$

$$+\frac{R_2}{2}\left(\frac{dp_2}{dx}\right)(1+\xi_2)\,. \qquad (108)$$

The constant C_3 can be calculated by Equation (108), if (dp_2/dx) has been determined.

From Equation (94), we can obtain

$$C_4=-\frac{1}{2}\frac{dp_2}{dx}R_2^2$$

$$+C_2R_2+k\left(\left(-\frac{dp_2}{dx}\right)^3\frac{R_2^4}{4}+\left(\frac{dp_2}{dx}\right)^2R_2^3C_3-\frac{3}{2}\frac{dp_2}{dx}R_2^2C_3^2+C_3^3R_2\right). \qquad (109)$$

The volume flow rate in the second part is given by

$$dQ_2=2\pi u_2 r\,dr \qquad (110)$$

or

$$Q_2=\int_{R_0}^{R_1}2\pi u_2 r\,dr\,. \qquad (111)$$

Substituting Equation (94) into above and integrating gives

$$Q_2=\frac{\pi k}{12\mu}\left(\frac{dp_2}{dx}\right)^3 R_2^6(1-\xi_2^6)-\frac{2\pi kC_3}{5\mu}\left(\frac{dp_2}{dx}\right)^2 R_2^5(1-\xi_2^5)$$

$$+\frac{\pi}{4\mu}\frac{dp_2}{dx}R_2^4(1-\xi_2^4)(1+3kC_3^2)-\frac{2\pi}{3\mu}R_1^3C_1(1-\xi_1^3)(1+kC_1^2) \qquad (112)$$

$$-\frac{C_4\pi R_2^2}{\mu}(1-\xi_2^2)\,.$$

For two-dimensional continuity flow we can obtain

$$\frac{\partial Q_2}{\partial r}+\frac{\partial Q_2}{\partial x}=0, \qquad (113)$$

while

$$\frac{\partial Q_2}{\partial r}=0. \qquad (114)$$

Hence,

$$\frac{\partial Q_2}{\partial x}=0. \qquad (115)$$

Substituting equations (108) and (109) into (112) and differentiating gives

$$\frac{\partial^2 p_2}{\partial x^2}=0, \qquad (116)$$

Hence

$$\frac{\partial p_2}{\partial x}=-\frac{P_m}{L_2}, \qquad (117)$$

where P_m is the pressure in the unit and L_2 is the length of the second part of the unit. The distribution of the pressure

along the axial direction within the unit is shown in Figure 10.

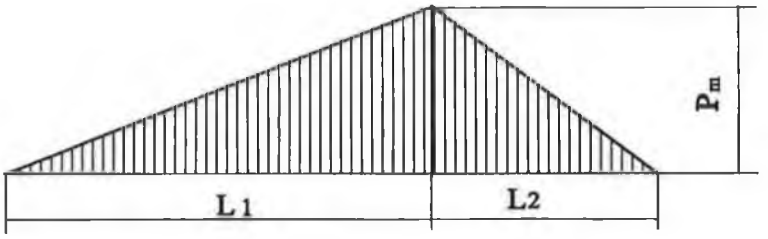

Figure 10 *The distribution of the pressure within the unit.*

The volumetric flow rate and pressure at the connective cross section between the two steps should be continuous. Therefore, the unknown variables C_1, C_2, C_3, C_4, $(\partial p_1/\partial x)$ and $y(\partial p_2/dx)$ in the Equations (81), (82), (108), (109) may be solved simultaneously together with the flow rate continuous condition Equations (86) and (112), and the pressure continuous condition Equations (91) and (117).

Chapter 3

Calculations and the Analyses of Results

3.1 Introduction

The methods of the analytical solutions have been outlined in Chapter 2 for the theoretical models based on Newtonian and non-Newtonian fluids characteristics. For the former model the calculation is relatively easier to be carried out, that can be done directly by substituting the initial input data into the corresponding equations given in Section 2.2. Because of the various input parameters, it is still necessary to use a computer program to solve them. While in the latter model, the determination of the solutions is more complicated because although five independent equations have been obtained for five unknown variables, there are a group of high order non-linear equations, therefore it is very difficult or impossible to find their solutions by analytical methods. In this chapter, the programs and their explanations of the numerical solutions used for both Newtonian and non-Newtonian fluid models will be given, the results calculated will be presented, and the comparison between models based on Newtonian and non-

Newtonian fluids, and also between Cartesian and cylindrical coordinate systems will be made.

3.2 Newtonian Fluid

3.2.1 Solution Procedure

The calculations have been made for different magnitudes of inlet length L_1 and outlet length L_2, the radius of outlet R_2 and the viscosity of the polymer μ. The chosen values of these parameters are shown in Table 1.

Table 1 *The initial input variables for Newtonian fluid.*

L_1 (mm)	10, 20, 25, 30
L_2 (mm)	1, 2, 5
μ (Nsm^{-2})	50, 100, 140
R_2 (mm)	0.21, 0.22, 0.23, 0.25

The typical program for Newtonian fluid model is given in Appendix I, which contains the initial input data file and a general output file, and also pressure-speed, force-speed and stress-speed output files for each L_1. The inlet length L_1 is varied for four values so that in total thirteen data files are generated for each calculation to inspect or to draw the corresponding figures. Similarly, the programs shown

in Appendix II-IV with respect to the variations of parameters L_2, R_2 and μ have also been set up.

3.2.2 Results of Newtonian Fluid Model

The relationship of the maximum pressure P_m at the step with drawing speed of the wire under the variation of inlet length L_1 and for the viscosity of the polymer $\mu=50\ Nsm^{-2}$ other geometrical parameters being constant, is shown in Figure 11. The corresponding geometrical constants are given in the Figure. It can be seen that the maximum pressure P_m increases linearly with the drawing speed. P_m also increases significantly with L_1.

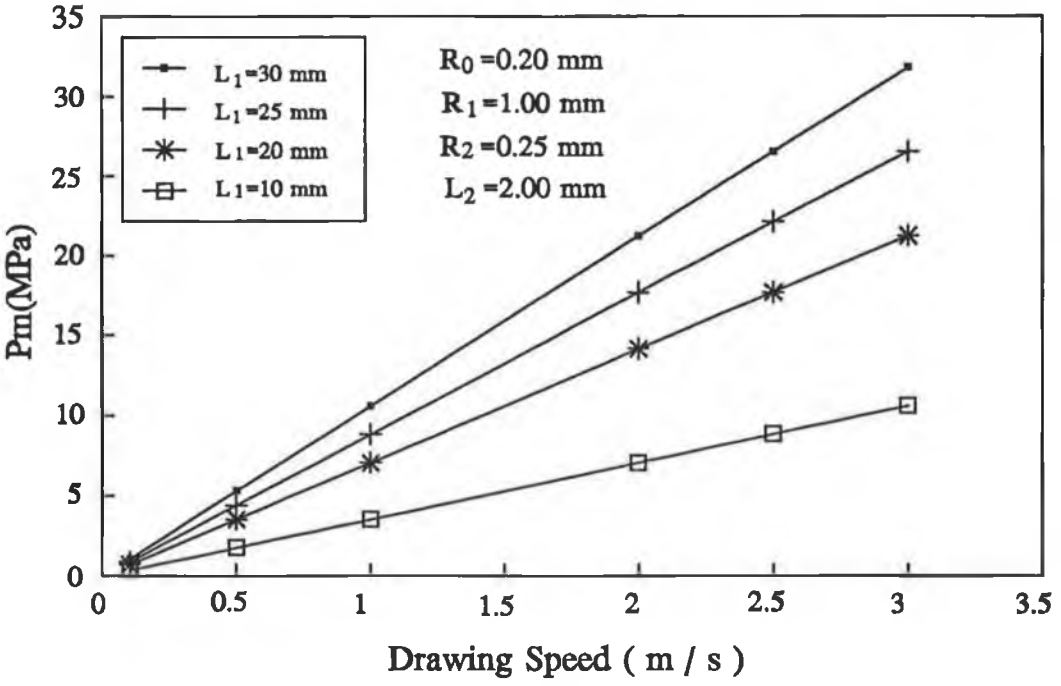

Figure 11 *The relationship of the maximum pressure with drawing speed under the variation of L_1.*

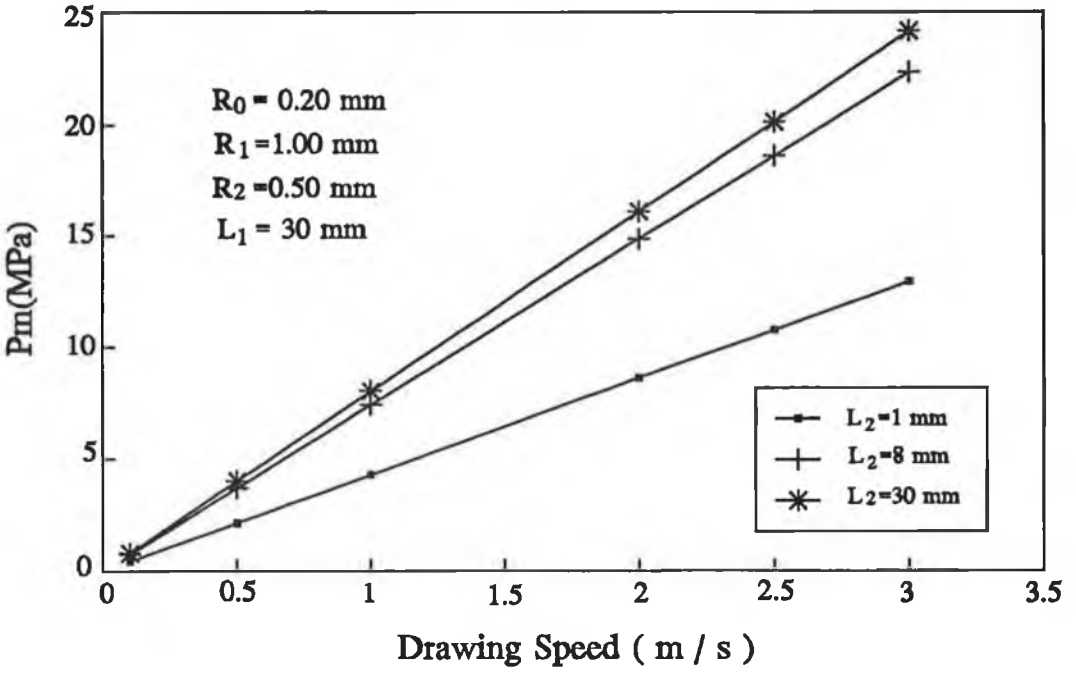

Figure 12 *The relationship of the maximum pressure with drawing speed under the variation of L_2.*

The relationship of the maximum pressure P_m at the step with drawing speed of the wire for the variation of the outlet length L_2, and for the viscosity of the polymer μ=*50* Nsm^{-2} is shown in Figure 12. The corresponding geometrical constants are given in the Figure. It can be seen that the pressure P_m increases linearly with the drawing speed u. The variation of L_2 affects the pressure at the step P_m and as L_2 increases, the pressure at the step increases.

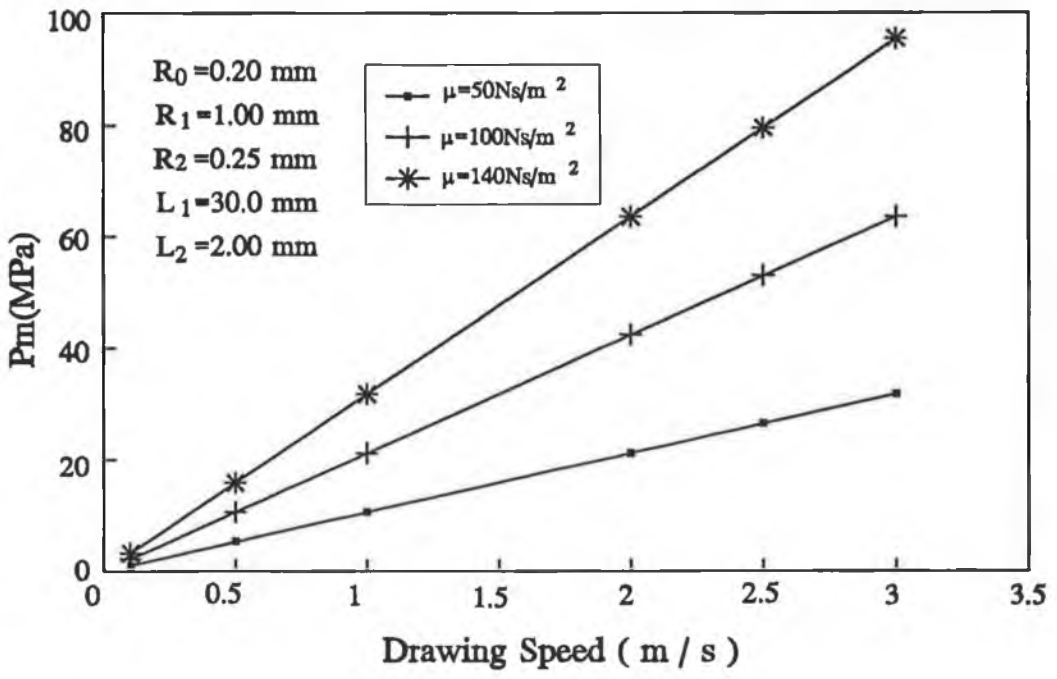

Figure 13 *The relationship of the maximum pressure with drawing speed under the variation of* μ.

The relationship of the maximum pressure P_m at the step with drawing speed of the wire u under the variation of the viscosity of the polymer μ for Newtonian fluid is shown in Figure 13. It can be seen that the pressure P_m at the step shows a linear relationship with the drawing speed u and that P_m also increases with μ significantly. This shows the type and property of the polymers used affects the pressure at the step. Therefore, if the temperature of the polymer is changed, the pressure at the step, *i.e.* the maximum pressure in the unit will also vary.

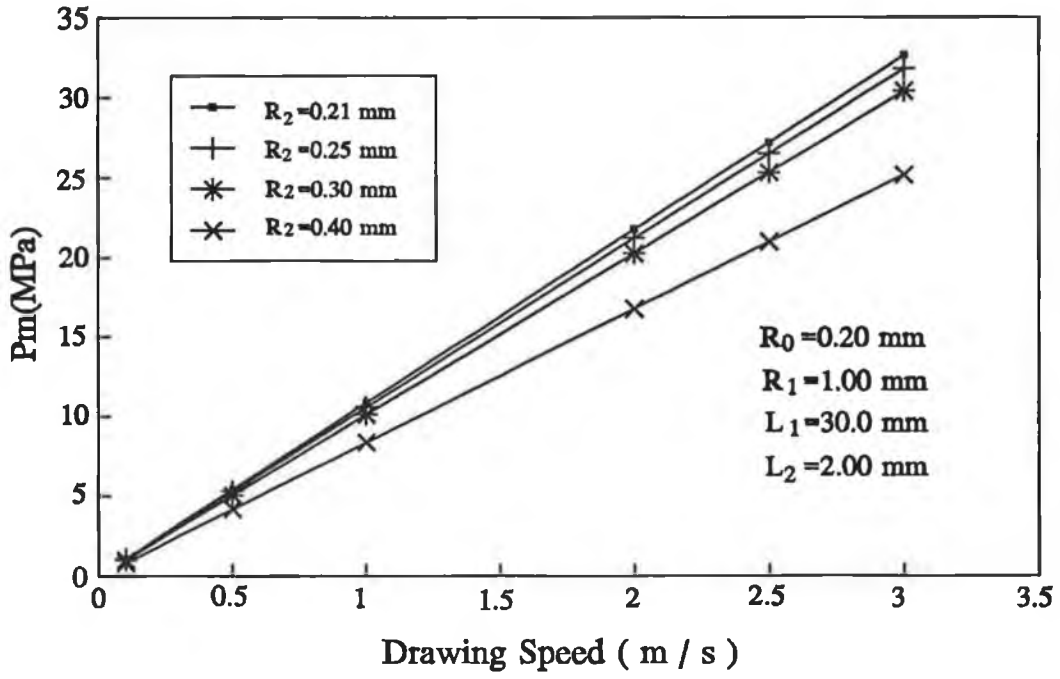

Figure 14 *The relationship of the maximum pressure with drawing speed under the variation of R_2.*

The relationship of the maximum pressure P_m at the step with drawing speed of the wire u under the variation of outlet radius R_2 and in the condition of the viscosity of the polymer $\mu=50Nsm^{-2}$ is shown in Figure 14. Obviously the maximum pressure P_m increases linearly with the drawing speed. It can be seen that the effect of the outlet radius R_2 on the pressure at the step is small. Therefore, it may be concluded that the pressure at the step is not affected by small variations in the geometrical parameters at the end of the outlet in the Newtonian model.

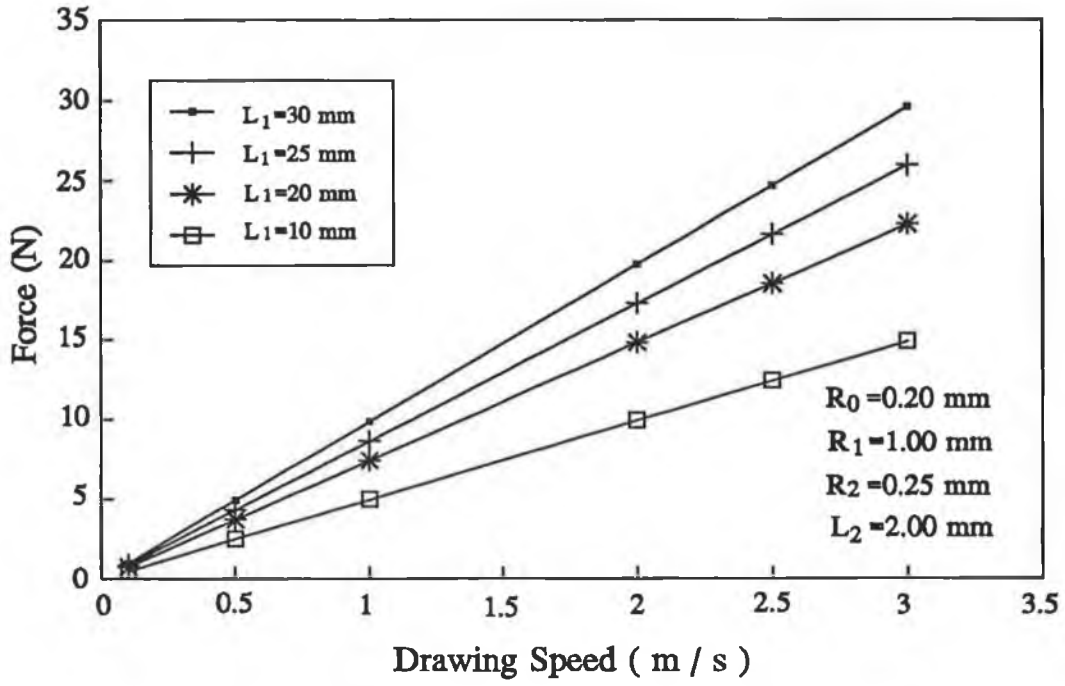

Figure 15 *The relationship of the pulling force with drawing speed under the variation of L_1.*

The relationship of the pulling force F with drawing speed u of the wire under the variation of inlet length L_1 and for the viscosity of the polymer $\mu=50\ Nsm^{-2}$ is shown in Figure 15. It can be seen that the pulling force F linearly increases with the drawing speed u and it also varies with the inlet length L_1 proportionally. It is worth noting that to increase the length of the inlet in order to achieve a higher pressure in the step will generated a larger pulling force on the wire.

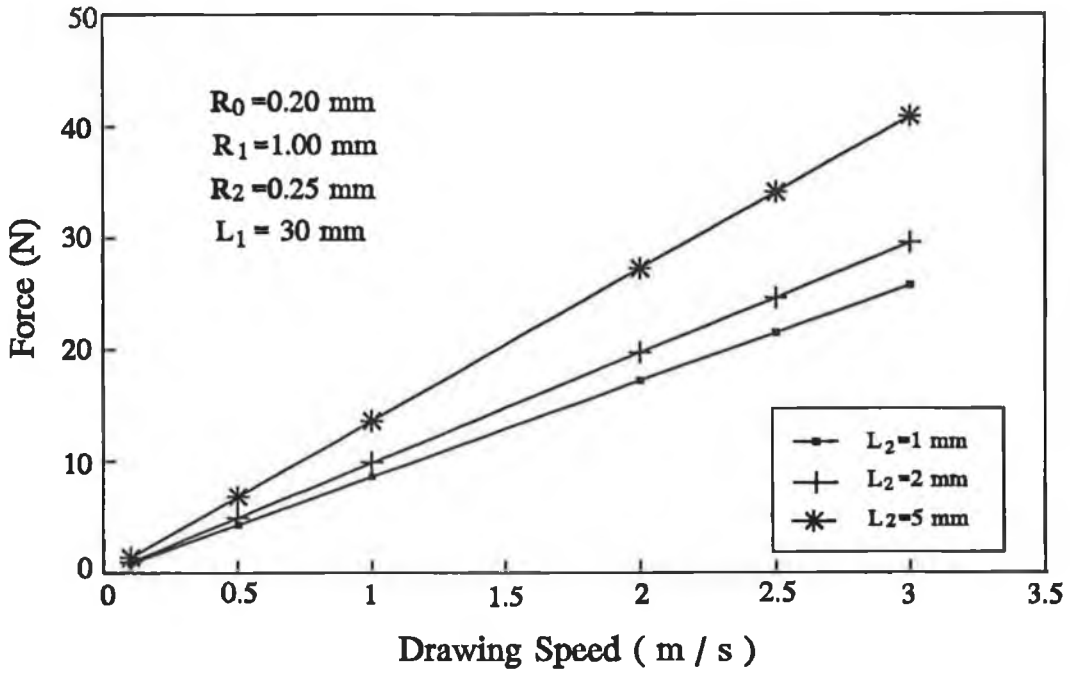

Figure 16 *The relationship of the pulling force with drawing speed under the variation of L_2.*

The relationship of the pulling force F with drawing speed of the wire u under the variation of outlet length L_2 and for the viscosity of the polymer $\mu=50\ Nsm^{-2}$ is shown in Figure 16. It can be seen that the pulling force F increases linearly with drawing speed of wire u. The variation of L_2 apparently affects the pulling force F and as L_2 increases, the pulling force rapidly rises, especially for higher drawing speeds.

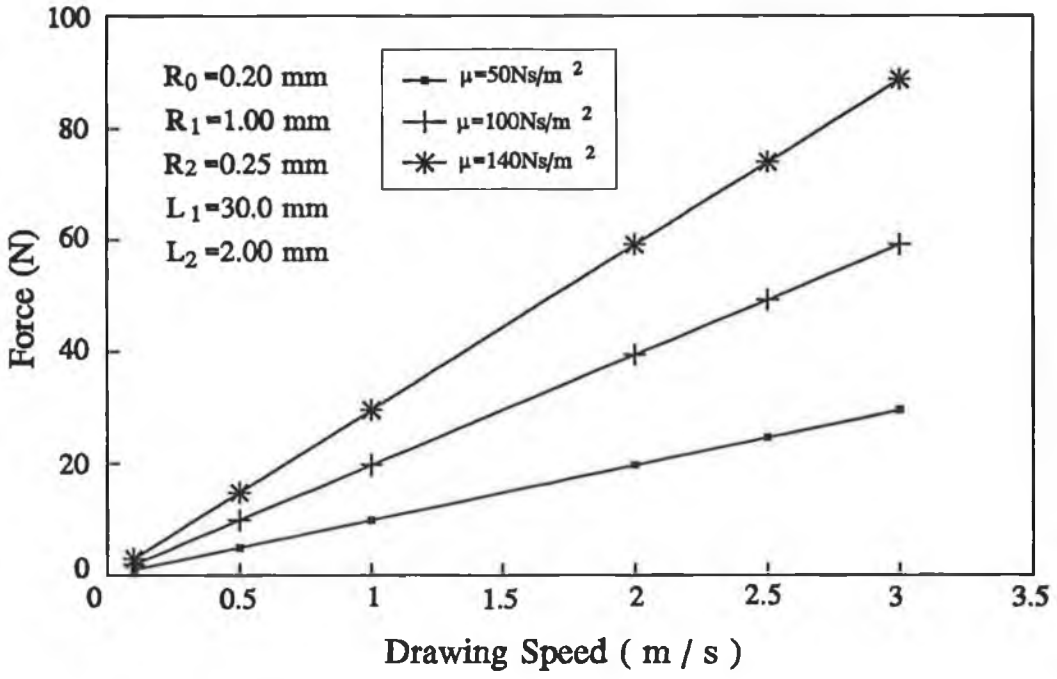

Figure 17 *The relationship of the pulling force with drawing speed under the variation of* μ.

The relationship of the pulling force *F* on the wire with drawing speed of the wire *u* under the variation of the viscosity of the polymer μ is shown in Figure 17. It can be seen that besides the linear relationship with the drawing speed of the wire *u*, the pulling force *F* varies with μ significantly. The higher the viscosity of the polymer, the larger the pulling force. It can be deduced that the working temperature of the polymer used directly affects the external load on the wire.

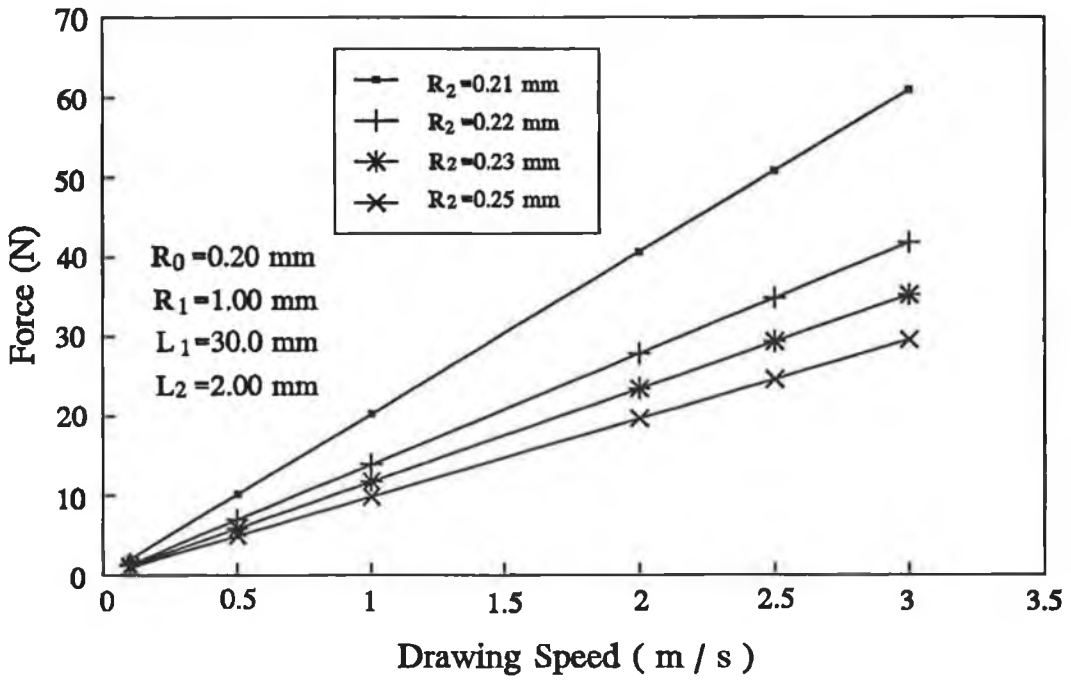

Figure 18 *The relationship of the pulling force with drawing speed under the variation of R_2.*

The relationship of the pulling force on the wire *F* with drawing speed of the wire *u* under the variation of outlet radius R_2 and for the viscosity of the polymer μ=*50 Nsm*$^{-2}$ is shown in Figure 18. The pulling force *F* linearly increases with the drawing speed and as R_2 increases, *F* will reduce apparently. Unlike the effect on the pressure at the step, in the case of thicker coating, the pulling force on the wire will get smaller.

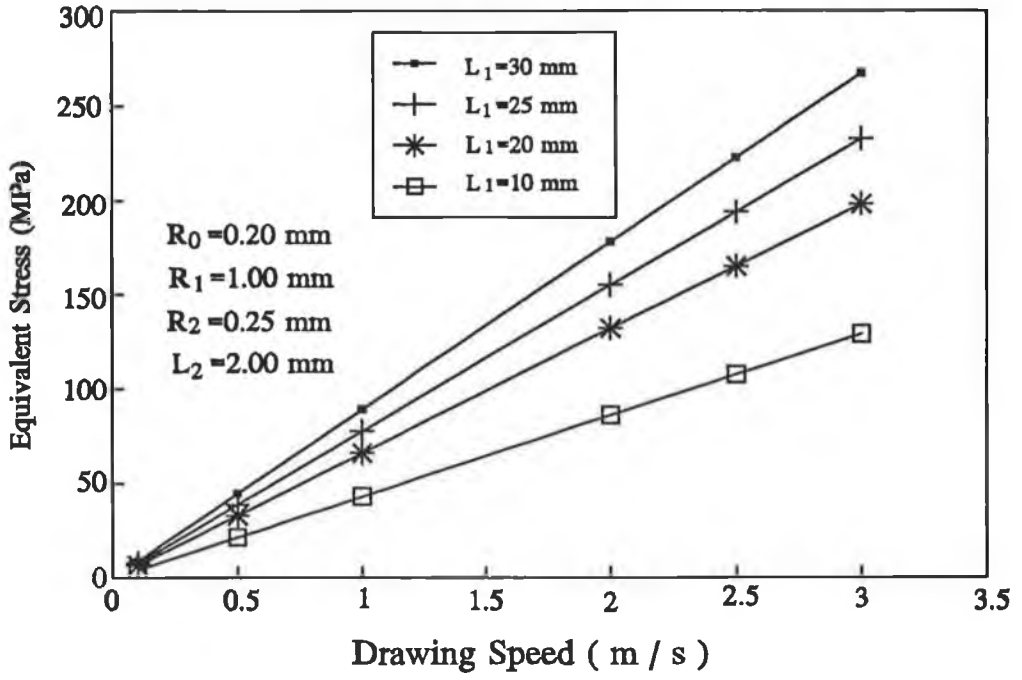

Figure 19 *The relationship of the equivalent stress in the wire with drawing speed under the variation of L_1.*

The relationship of the equivalent stress in the wire at the step point with drawing speed u under the variation of the inlet length L_1 for the viscosity of the polymer μ=*50 Nsm*$^{-2}$ and for Newtonian fluid is shown in Figure 19. It can be seen that the equivalent stress also increases linearly with drawing speed of the wire and the equivalent stress also increases with L_1. Therefore, in the process of the coating of a thin wire, the choice of the inlet length should be noted so that fracture of the wire can be prevented.

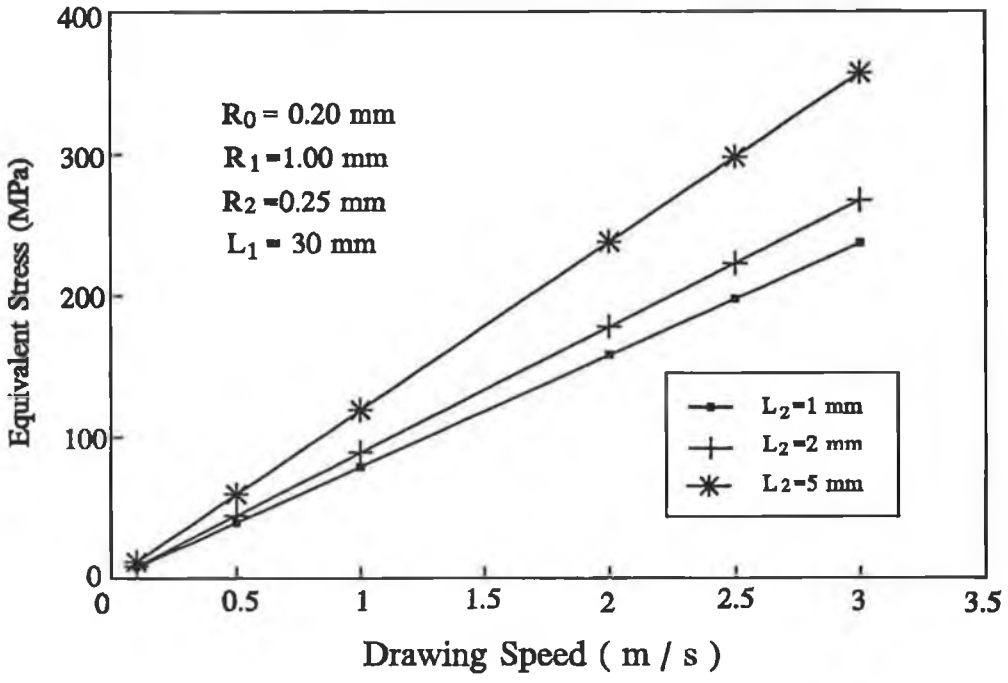

Figure 20 *The relationship of the equivalent stress in the wire with drawing speed under the variation of L_2.*

The relationship of the equivalent stress in the wire at the step point with drawing speed of the wire under the variation of the outlet length L_2, for the viscosity of the polymer $\mu=50\ Nsm^{-2}$ and for Newtonian fluid is shown in Figure 20. It can be seen that the equivalent stress increases with L_2, it can also be seen that equivalent stress increases linearly with drawing speed. Like the inlet length L_1, the length of L_2 should also be properly chosen for the coating of a thin wire.

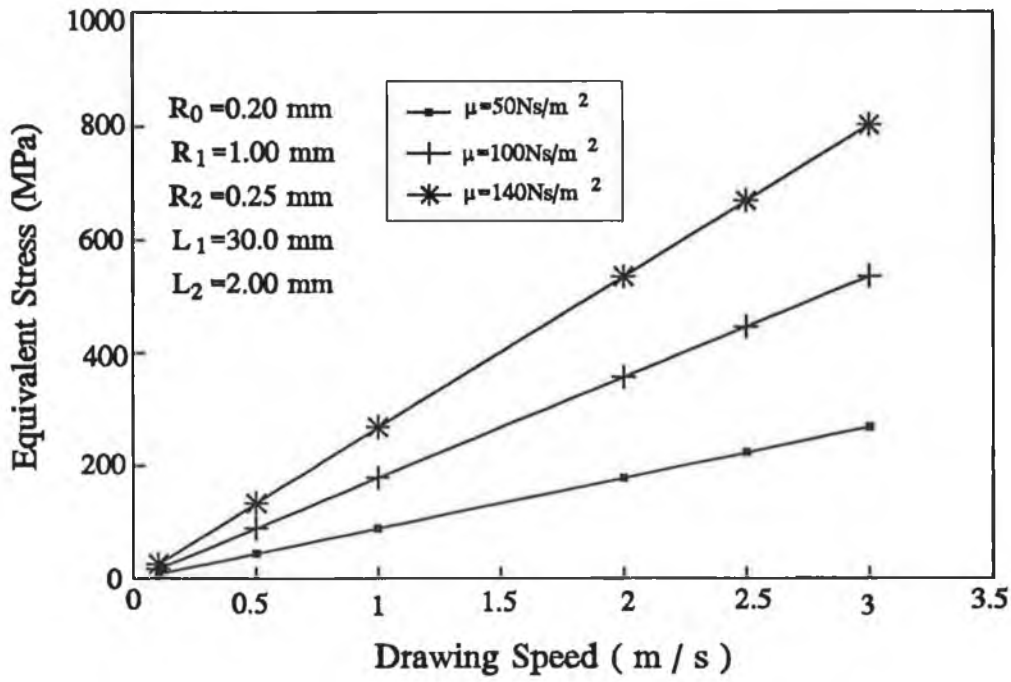

Figure 21 *The relationship of the equivalent stress in the wire with drawing speed under the variation of* μ.

The relationship of the equivalent stress in the wire at the step point with drawing speed *u* under the variation of the viscosity of the polymer μ and for Newtonian fluid is shown in Figure 21. It can be seen that the equivalent stress increases linearly with drawing speed and it also increases with μ significantly. In the range of the high speed, the effect becomes more apparent, *i.e.* the choices of the properties and using condition of the polymer is an important factor.

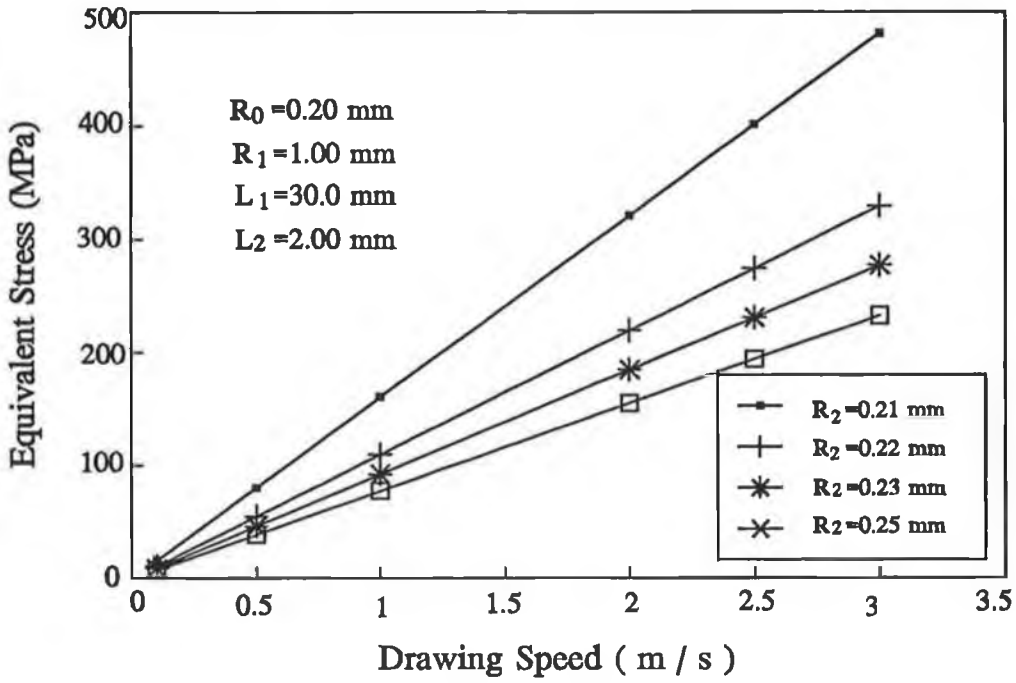

Figure 22 *The relationship of the equivalent stress in the wire with drawing speed under the variation of R_2.*

The relationship of the equivalent stress in the wire at the step point with drawing speed under the variation of outlet radius R_2 and for Newtonian fluid is shown in Figure 22. This graph shows that the equivalent stress increases linearly with drawing speed. It also can be seen that as R_2 increases, the equivalent stress will reduce considerably. Therefore, in general all the four factors L_1, L_2, R_2 and μ have effects on the equivalent stress of the wire.

3.3 Non-Newtonian Fluid

3.3.1 Solution Procedure

The task of developing a theoretical model for non-Newtonian fluid as the coating material leads to determining the roots for a group of non-linear equations.

From equation (67) we have

$$C_{13}C_1^3+C_{12}C_1^2+C_{11}C_1+C_{10}=0 \tag{118}$$

where

$$C_{13}=k(R_0-R_1)$$

$$C_{12}=-\frac{3k}{2}(R_0^2-R_1^2)\left(\frac{dp_1}{dx}\right)$$

$$C_{11}=(R_0-R_1)+k(R_0^3-R_1^3)\left(\frac{dp_1}{dx}\right)^2 \tag{119}$$

$$C_{10}=u_0\mu-\frac{(R_0^2-R_1^2)}{2}\left(\frac{dp_1}{dx}\right)-\frac{k}{4}\left(\frac{dp_1}{dx}\right)^3(R_0^4-R_1^4)$$

Setting an initial value of $dp_1/dx=dp_2/dx=p_m$ and by means of the numerical iterative method, the unknown constant C_1 in equation (118) can be determined. According to equation (82)

$$C_2=\mu u_1+C_1r-kC_1^3r-\frac{r^2}{2}(1+3kC_1^2)\frac{dp_1}{dx}+\left(\frac{dp_1}{dx}\right)^2kr^3C_1-\left(\frac{dp_1}{dx}\right)^3\frac{kr^4}{4} \tag{120}$$

C_2 may be obtained in terms of the initial p_m. From equation (95), we have

$$C_{33}C_3^3+C_{32}C_3^2+C_{31}C_3+C_{30}=0 \qquad (121)$$

where

$$C_{33}=k(R_0-R_2),$$

$$C_{32}=-\frac{3k}{2}(R_0^2-R_2^2)\left(\frac{dp_2}{dx}\right),$$

$$C_{31}=(R_0-R_2)+k(R_0^3-R_2^3)\left(\frac{dp_2}{dx}\right)^2, \qquad (122)$$

$$C_{30}=u_0\mu-\frac{(R_0^2-R_2^2)}{2}\left(\frac{dp_2}{dx}\right)-\frac{k}{4}\left(\frac{dp_2}{dx}\right)^3(R_0^4-R_2^4).$$

In the same way, the value C_3 can be obtained from equation (121) and the unknown constant C_4 may also be obtained from equation (109).

Substituting the known constants C_1, C_2, C_3, C_4 and the initial set p_m into equations (85) and (112), the value of (Q_1-Q_2) can be determined. If (Q_1-Q_2) is equal to zero or less than the allowable error, then the initial set p_m is the solution wanted, else, p_m is set to a new value according to the iterative method until the magnitude of (Q_1-Q_2) comes within the allowable margin of error. In the solution process, the numerical iterative method is used twice for each set p_m, once when determining the constants C_1 and C_3, and then when checking whether (Q_1-Q_2) is equal to zero or less than the allowable error. Furthermore, using different

values of k in each calculation, the pressure at the step with respect to k can be obtained. The pulling force and equivalent stresses are also determined at the same time. The program for non-Newtonian fluid model is shown in Appendix V.

3.3.2 Results of Non-Newtonian Fluid Model

The relationship of the maximum pressure at the step P_m with drawing speed of the wire under the variation of inlet length L_1 and for non-Newtonian fluid is shown in Figure 23. It can be seen that the maximum pressure P_m increases with drawing speed and P_m also increases significantly with L_1 .

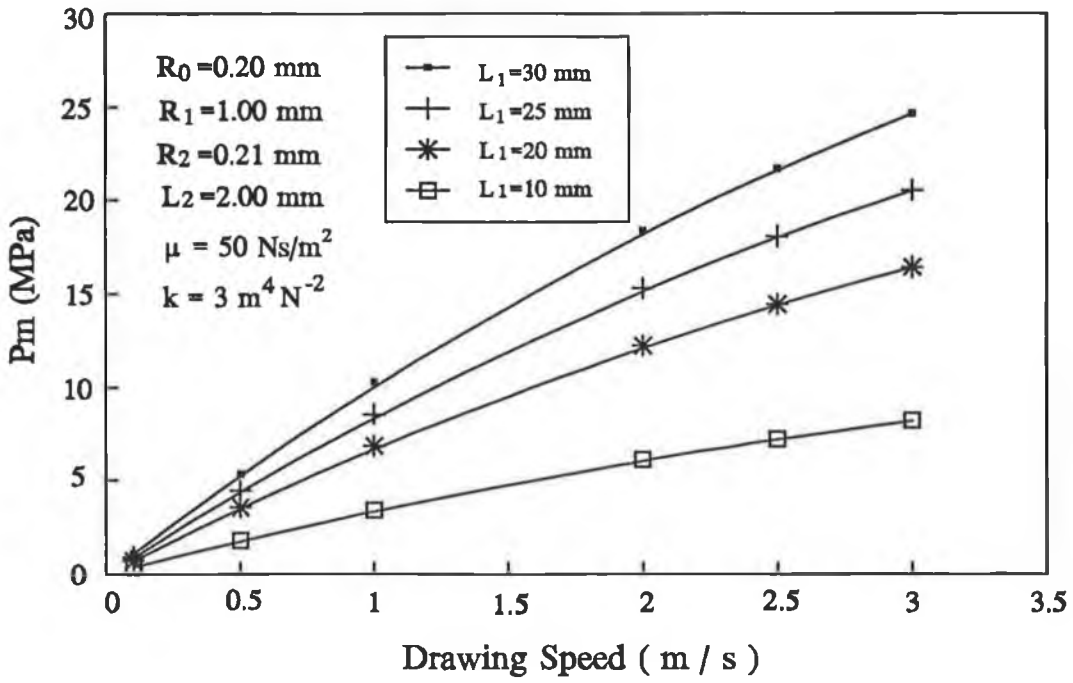

Figure 23 *The relationship of the maximum pressure with drawing speed under the variation of L_1.*

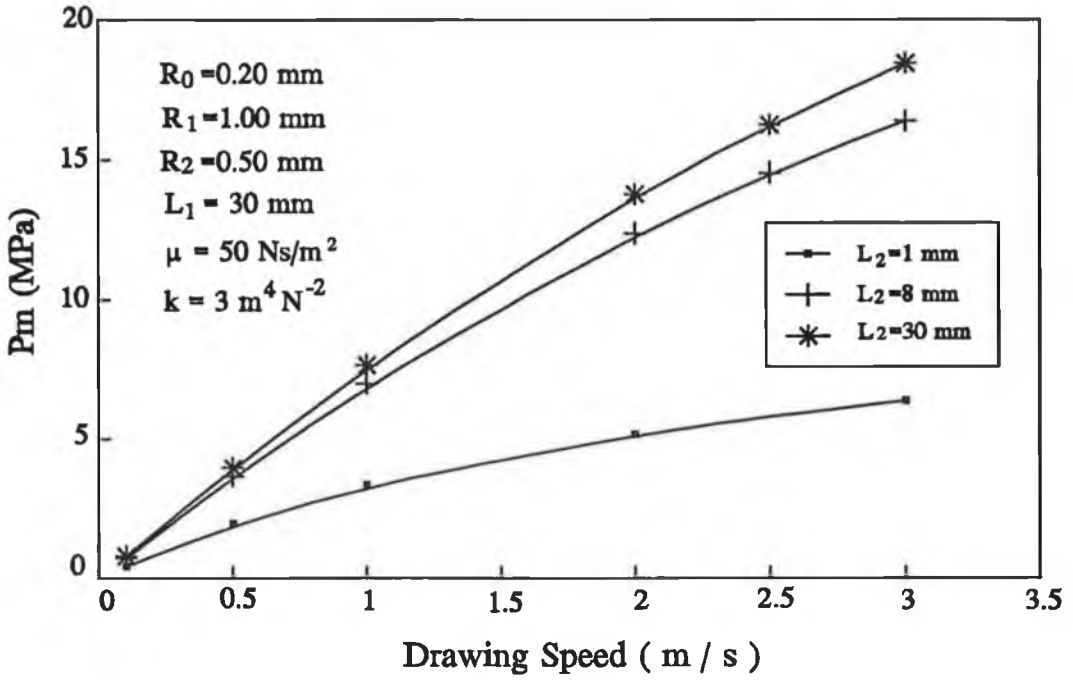

Figure 24 *The relationship of the maximum pressure with drawing speed under the variation of L_2.*

The relationship of the maximum pressure at the step P_m with drawing speed of the wire under the variation of outlet length L_2 and for non-Newtonian fluid is shown in Figure 24. The corresponding geometrical constants are given in the Figure. It can be seen that the maximum pressure P_m increases with drawing speed. Like Newtonian fluid, the variation of L_2 affects the pressure at the step P_m and as L_2 increases, the pressure at the step increases.

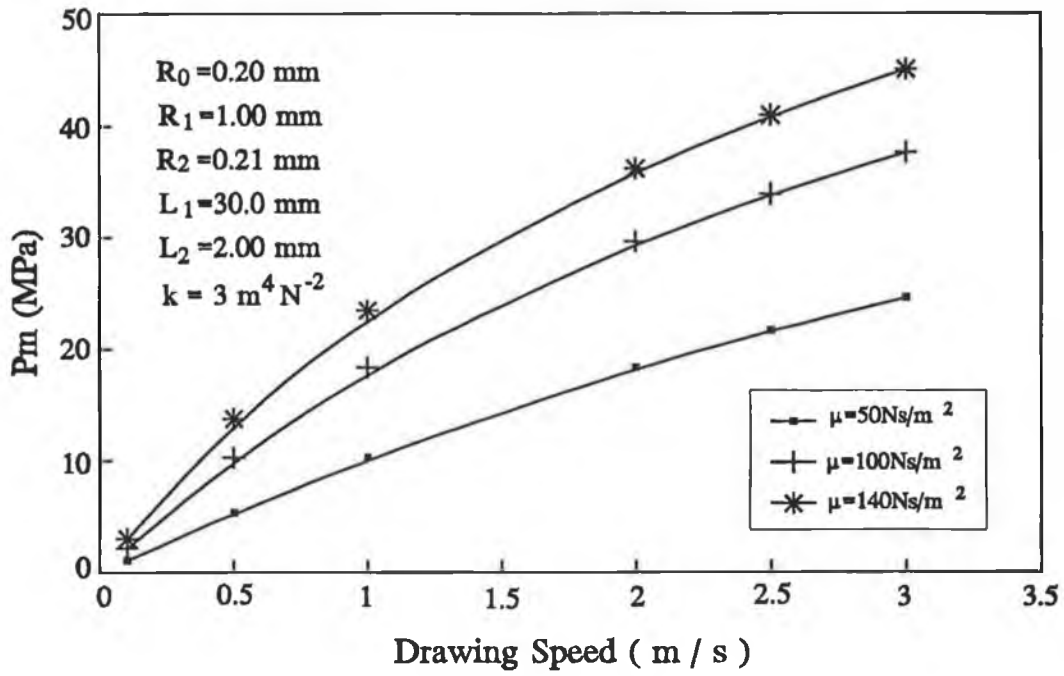

Figure 25 *The relationship of the maximum pressure with drawing speed under the variation of* μ.

The relationship of the maximum pressure at the step P_m with drawing speed of the wire u under the variation of the viscosity of the polymer μ and for non-Newtonian fluid is shown in Figure 25. It can be seen that the pressure P_m at the step increases non-linearly with drawing speed u and P_m also increases with μ significantly. This shows that the type and property of the polymers used play great roles in the variation of the pressure at the step. Therefore, if the temperature of the polymer is changed, the pressure at the step, *i.e.* the maximum pressure in the unit will also vary.

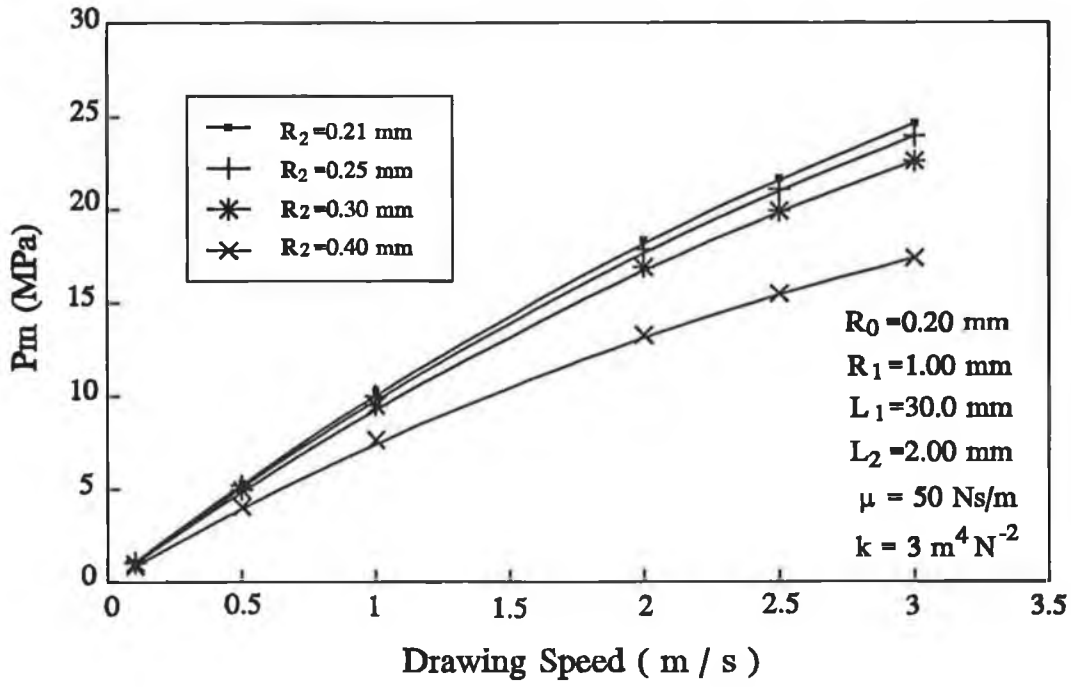

Figure 26 *The relationship of the maximum pressure with drawing speed under the variation of R_2.*

The relationship of the maximum pressure P_m at the step with drawing speed of the wire u under the variation of outlet radius R_2 and for non-Newtonian fluid is shown in Figure 26. It can be seen that the maximum pressure P_m increases with drawing speed. It can also be seen that as R_2 increases, P_m increases only slightly unless R_2 is increased by 50 percent or more. Therefore, it can be concluded that the pressure at the step is less affected by the variation of geometrical parameters at the end of the outlet for both Newtonian and non-Newtonian models.

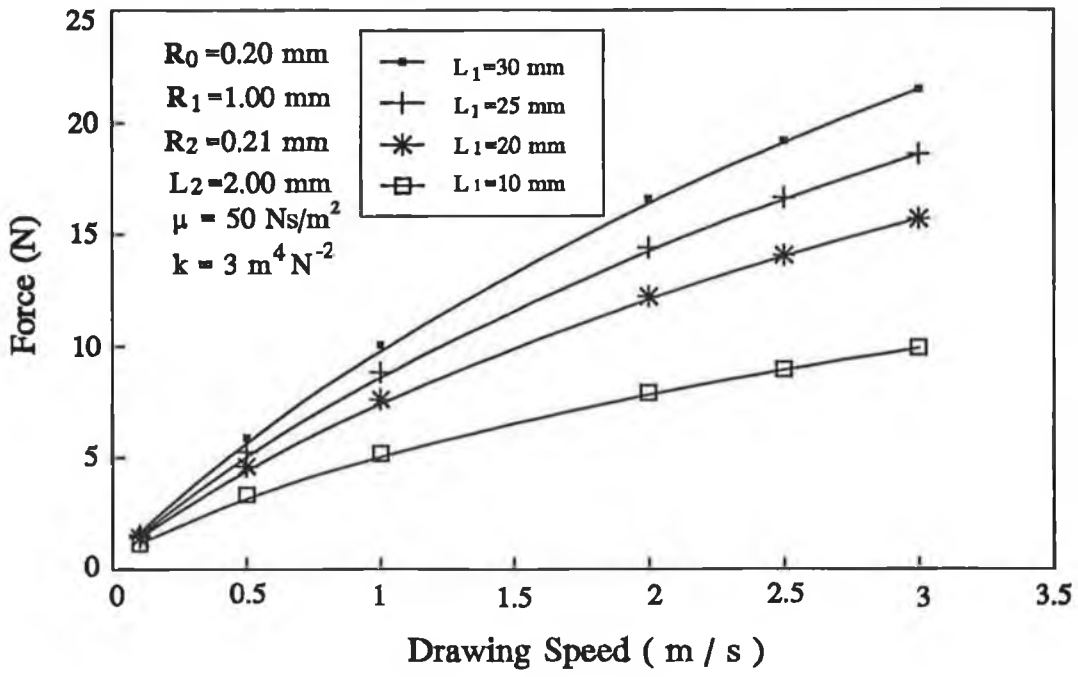

Figure 27 *The relationship of the pulling force with drawing speed under the variation of L_1.*

The relationship of the pulling force F with drawing speed of the wire under the variation of inlet length L_1 and for non-Newtonian fluid is shown in Figure 27. It can be seen that the pulling force F increases non-linearly with the drawing speed and F also increases appreciably with L_1 apparently. It is worth noting that to increase the length of the inlet in order to achieve a higher pressure in the step will lead a larger pulling force on the wire.

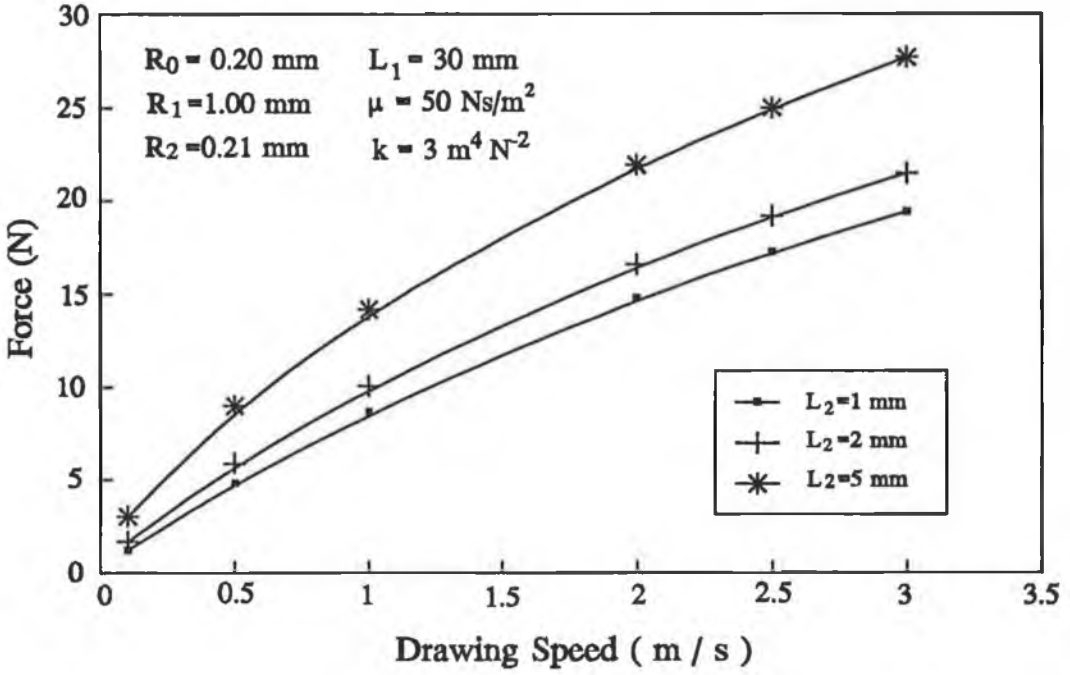

Figure 28 *The relationship of the pulling force with drawing speed under the variation of L_2.*

The relationship of the pulling force F with drawing speed of the wire u under the variation of outlet length L_2 and for non-Newtonian fluid is shown in Figure 28. It can be seen that pulling force F increases non-linearly with the drawing speed of wire u. The variation of L_2 affects the pulling force F significantly and as L_2 increases, the pulling force rapidly rises, especially in the range of the high drawing speed.

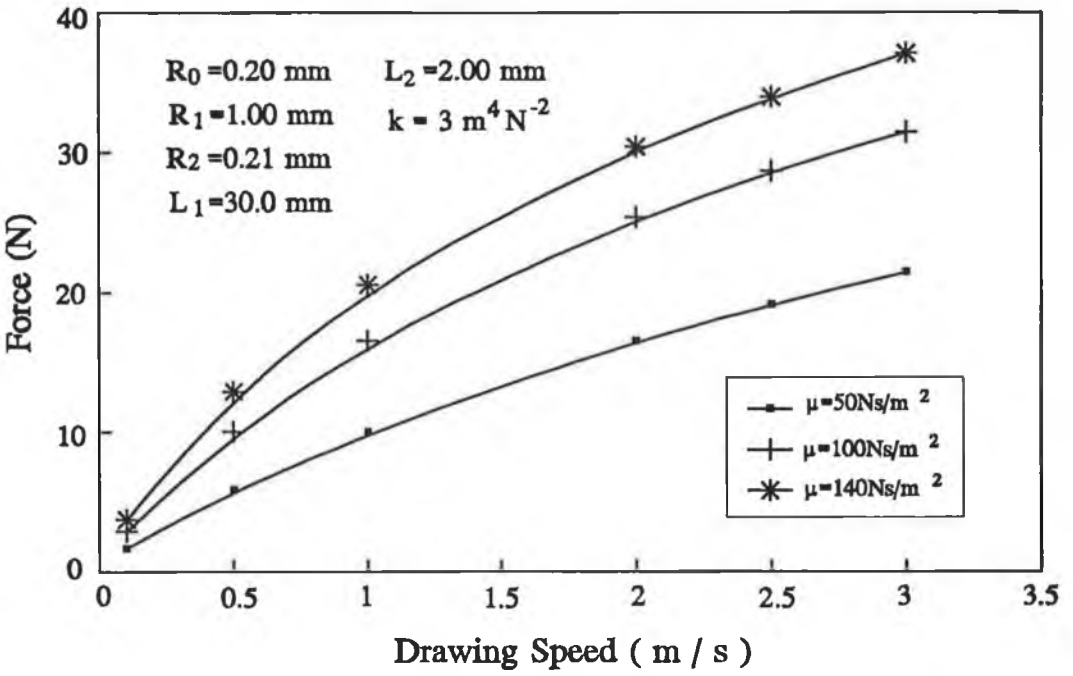

Figure 29 *The relationship of the fulling force with drawing speed under the variation of* μ.

The relationship of the pulling force *F* with drawing speed of the wire under the variation of the viscosity of the polymer μ and for non-Newtonian fluid is shown in Figure 29. It can be seen that besides the non-linear relationship with the drawing speed of the wire *u*, the pulling force *F* varies with μ significantly. The higher the viscosity of the polymer, the larger the pulling force. It can be deduced that the working temperature of the polymer used will directly affect the pulling load acted on the wire.

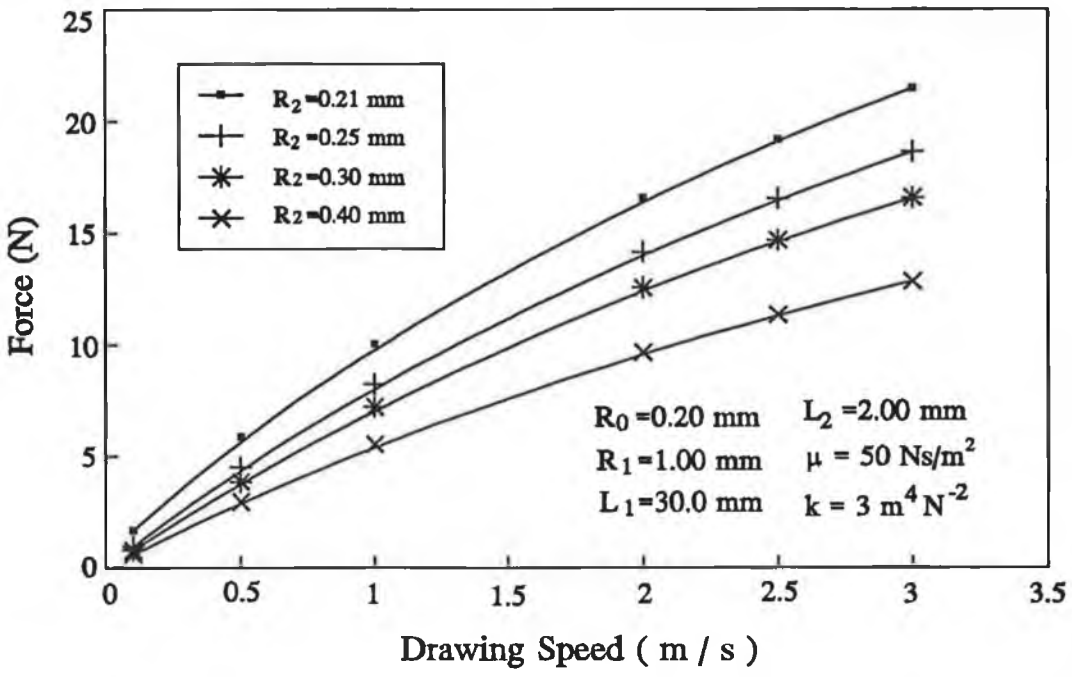

Figure 30 *The relationship of the pulling force with drawing speed under the variation of R_2.*

The relationship of the pulling force F with drawing speed of the wire under the variation of outlet radius R_2 and for non-Newtonian fluid is shown in Figure 30. The pulling force F increases non-linearly with drawing speed and as R_2 increases, F will reduce a little, but the scope is not as obvious as for Newtonian fluid in which the external force F decreases appreciably as the outlet radius R_2 increases.

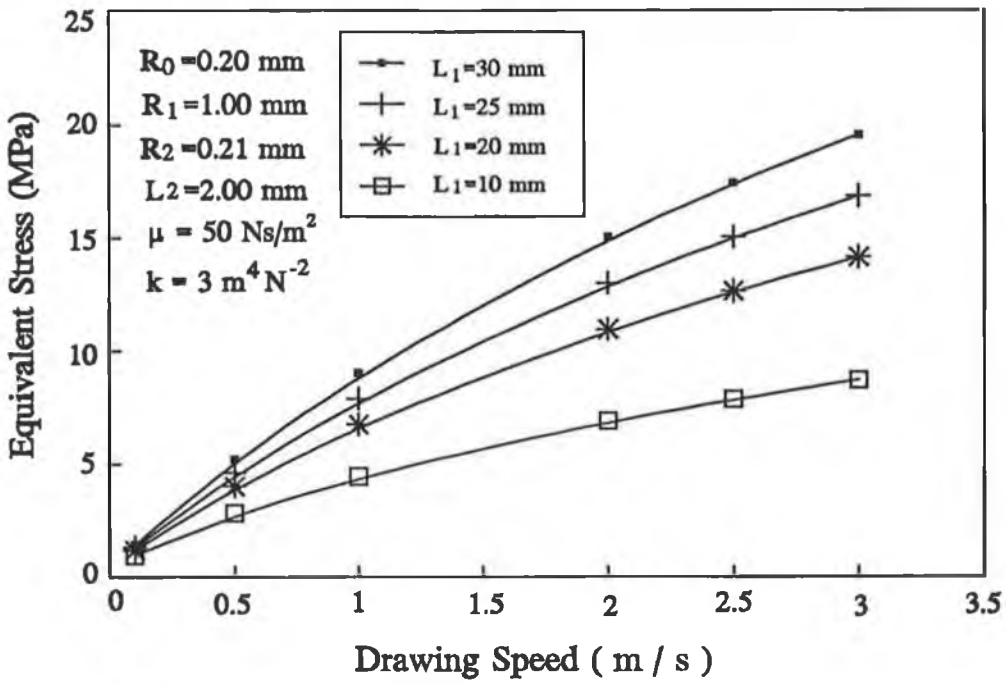

Figure 31 *The relationship of the equivalent stress with drawing speed under the variation of L_1.*

The relationship of the equivalent stress in the wire at the step point with drawing speed under the variation of inlet length L_1 and for non-Newtonian fluid is shown in Figure 31. It can be seen that the equivalent stress increases with drawing speed and also with L_1 appreciably. Therefore, in the process of the coating a thin wire, the choice of the inlet length should be made carefully.

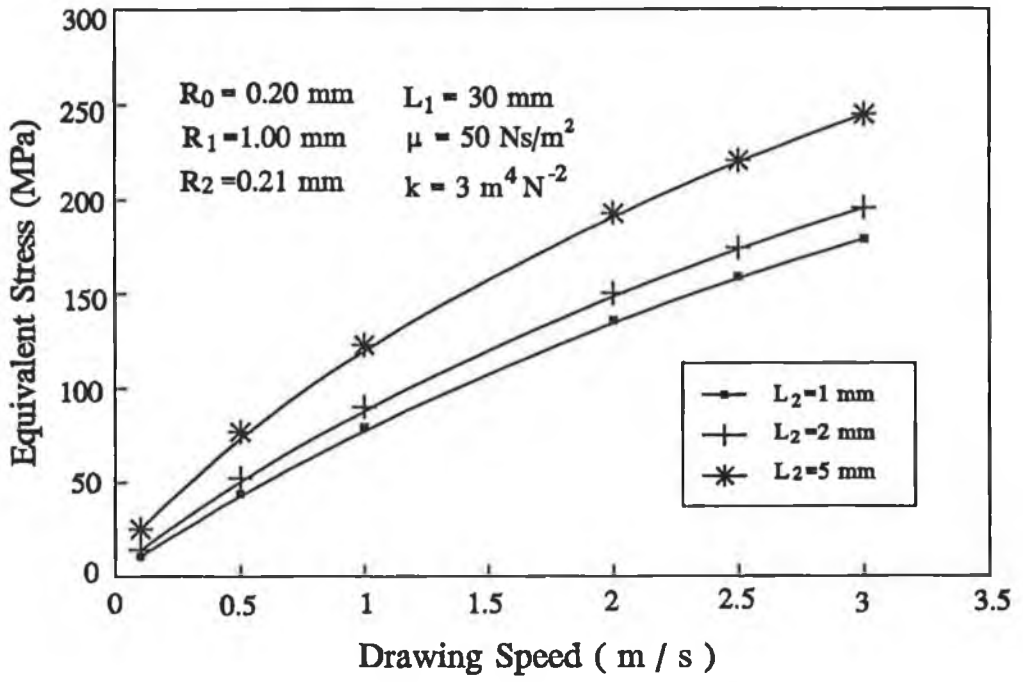

Figure 32 *The relationship of the equivalent stress with drawing speed under the variation of L_2.*

The relationship of the equivalent stress in the wire at the step point with drawing speed of the wire under the variation of outlet length L_2 and for non-Newtonian fluid is shown in Figure 32. It can be seen that the equivalent stress increases with L_2 considerably, it also can be seen that the equivalent stress increases non-linearly with the drawing speed. Like the inlet length L_1, the length of L_2 should also be properly chosen for the coating of a thin wire.

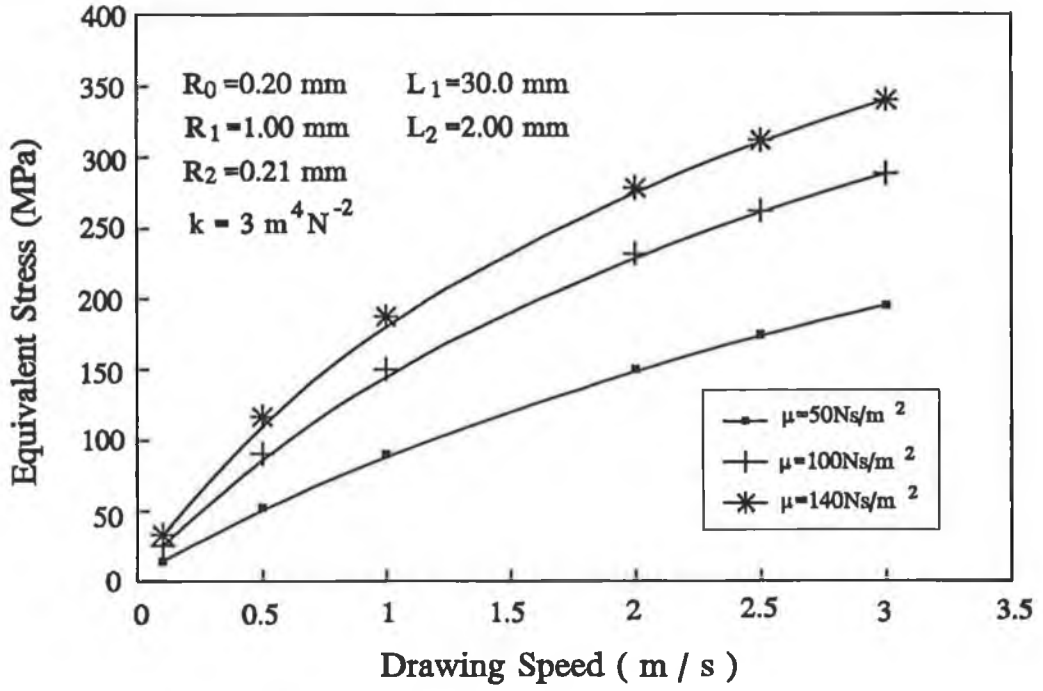

Figure 33 *The relationship of the equivalent stress with drawing speed under the variation of* μ.

The relationship of the equivalent stress in the wire at the step point with drawing speed of the wire *u* under the variation of the viscosity of the polymer μ and for non-Newtonian fluid is shown in Figure 33. It can be seen that the equivalent stress increases non-linearly with the drawing speed and it also increases with μ significantly. In the range of the high speed, the effect becomes more apparent, *i.e.* the choices of the properties the polymer is an important factor.

The relationship of the equivalent stress in the wire at the step point with drawing speed of the wire *u* under the

variation of outlet radius R_2 and for non-Newtonian fluid is shown in Figure 34. This graph shows that the equivalent stress increases with the drawing speed. It also can be seen that as R_2 increases, equivalent stress will reduce, but not significantly unless for higher drawing speeds. In general all the four factors L_1, L_2, R_2 and μ have effects on the equivalent stress of the wire.

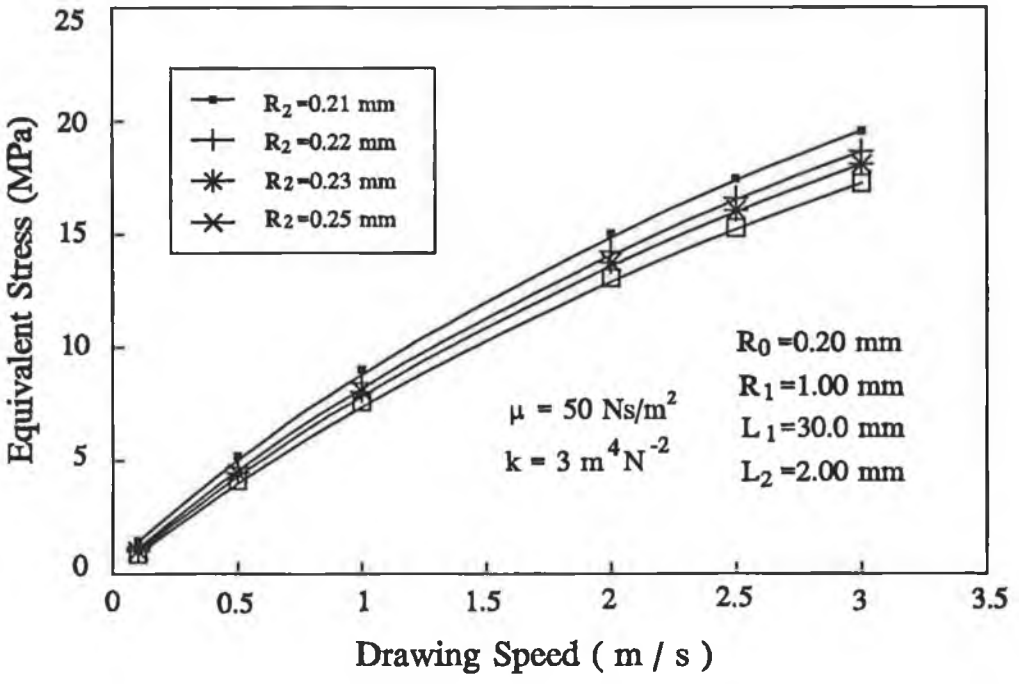

Figure 34 *The relationship of the equivalent stress with drawing speed under the variation of R_2.*

3.4 Results Discussions

The relationships of the maximum pressure, pulling force and equivalent stress with respect to the non-linear factor k are shown in Figure 35, Figure 36 and Figure 37

respectively. It can be seen that P_m, F and σ_e rapidly decrease with the increase of the non-linear factor k. When $k = 0$, the results of non-Newtonian fluid model become those of Newtonian fluid model. Therefore, the calculation in Newtonian fluid model can be considered as a specific case of non-Newtonian fluid model. The results also show that the force and equivalent stress according to the two models differ rapidly with the drawing speed, while the predicted pressure at the step for drawing speeds of less than 1 *m/s* show very little difference. As the speed increases, the difference of the pressure becomes rather obvious.

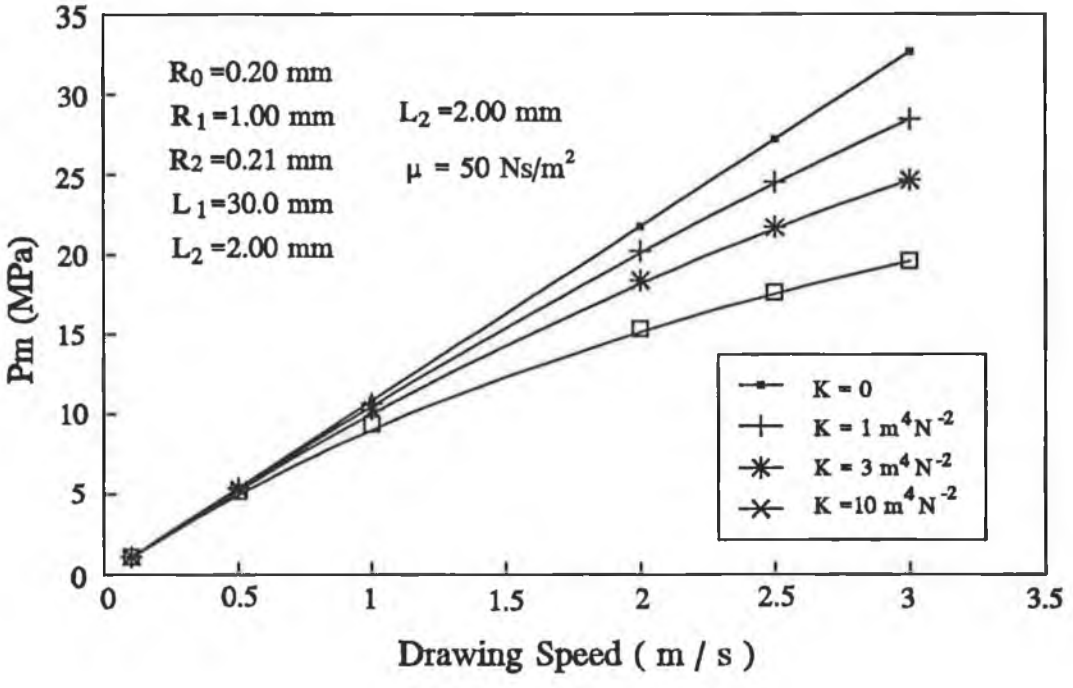

Figure 35 *The relationship of the maximum pressure with drawing speed under the variation of k.*

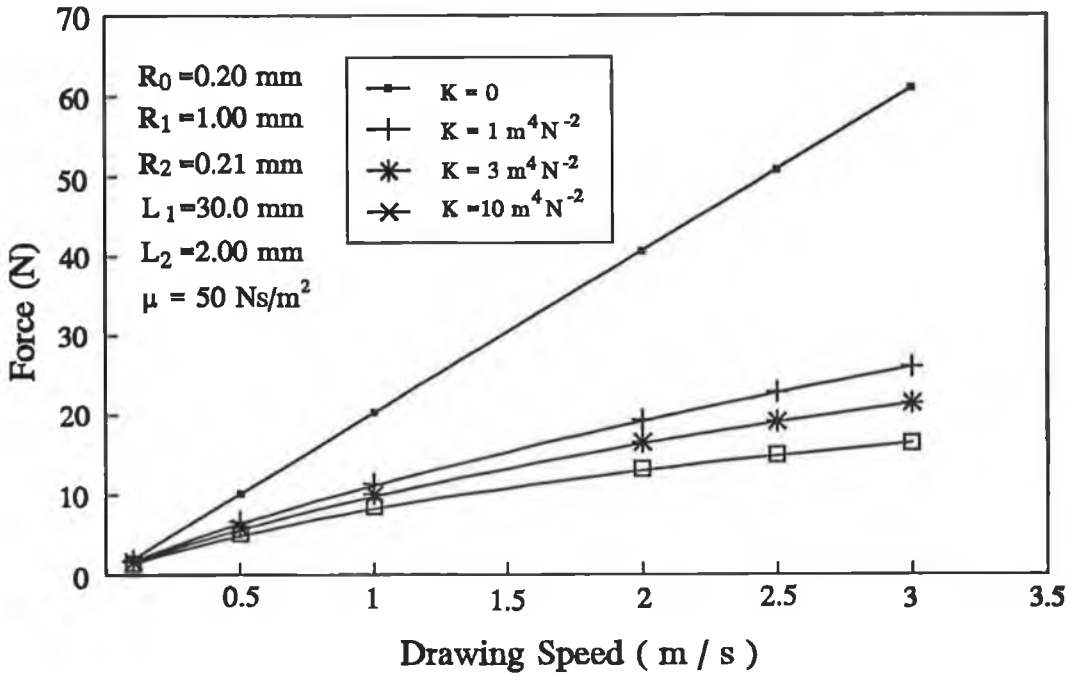

Figure 36 *The relationship of the pulling force with drawing speed under the variation of k.*

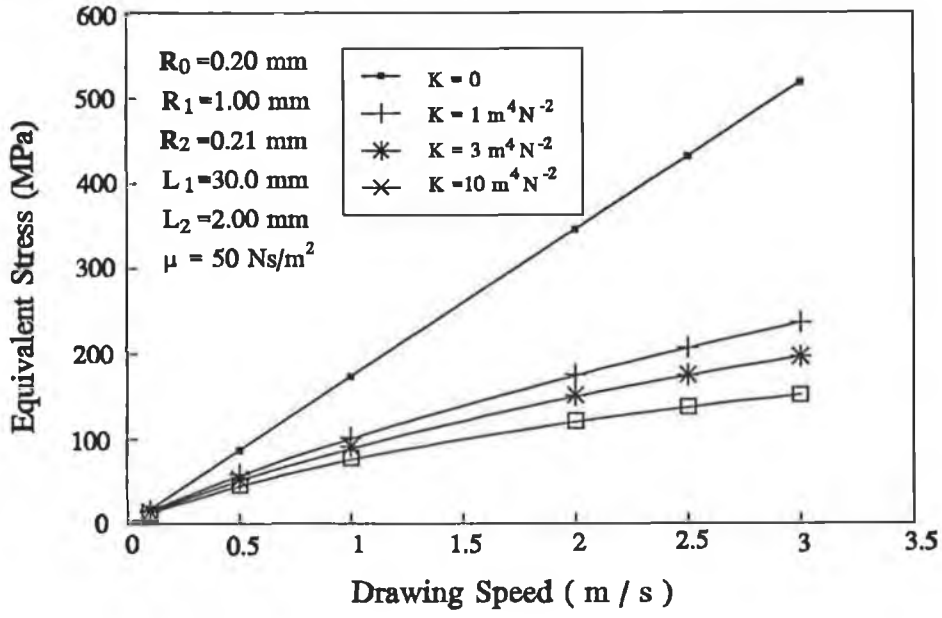

Figure 37 *The relationship of the equivalent stress with drawing speed under the variation of k.*

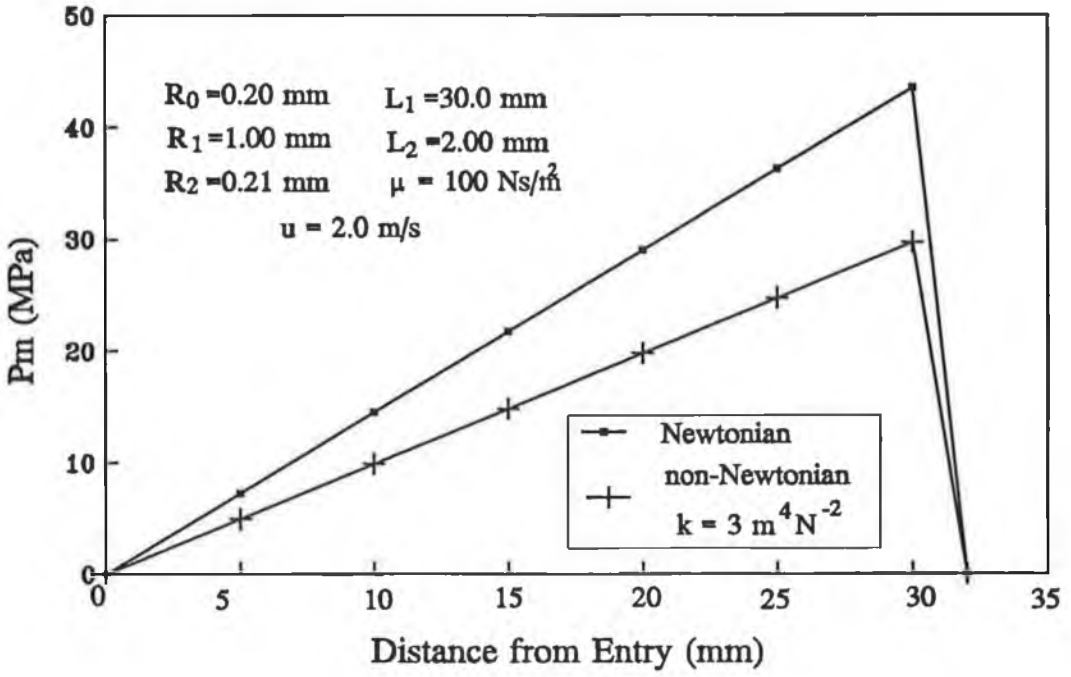

Figure 38 *The pressure distribution in the unit according to Newtonian and non-Newtonian fluid models.*

Figure 38 shows the pressure distribution in the unit according to Newtonian and non-Newtonian fluid model for drawing speed of *2 m/s*. It can be seen that in all the positions within the unit, the pressures based on Newtonian fluid is greater than those based on non-Newtonian fluid model.

Figure 39, Figure 40 and Figure 41 respectively shows the comparisons of P_m, F and σ_e with respect to the drawing speed of the wire under Newtonian and non-Newtonian fluid models. One can see that all the results obtained according to non-Newtonian fluid model are smaller than those according to Newtonian fluid model.

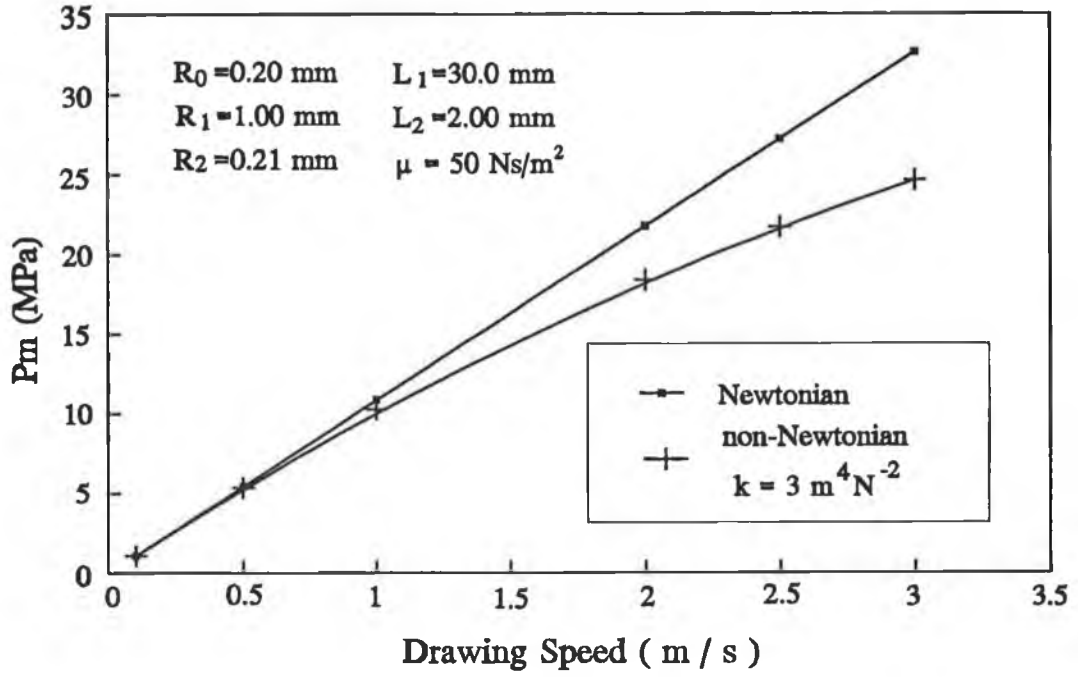

Figure 39 *The comparison of the pressure at the step according to Newtonian and non-Newtonian fluid models.*

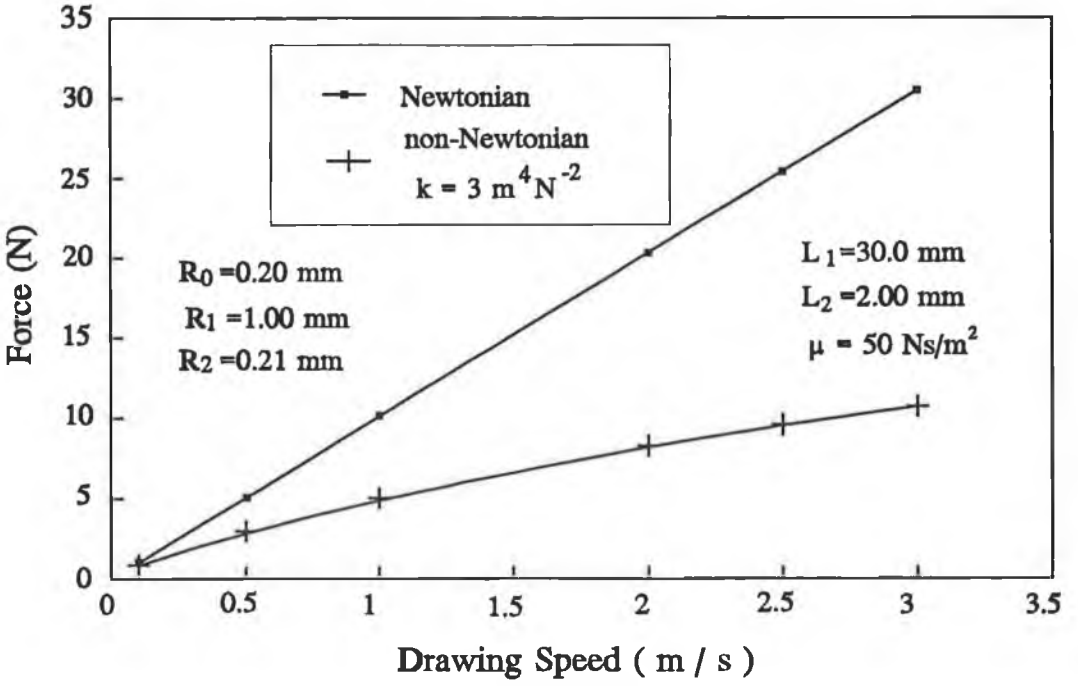

Figure 40 *The comparison of the pulling force according to Newtonian and non-Newtonian fluid models.*

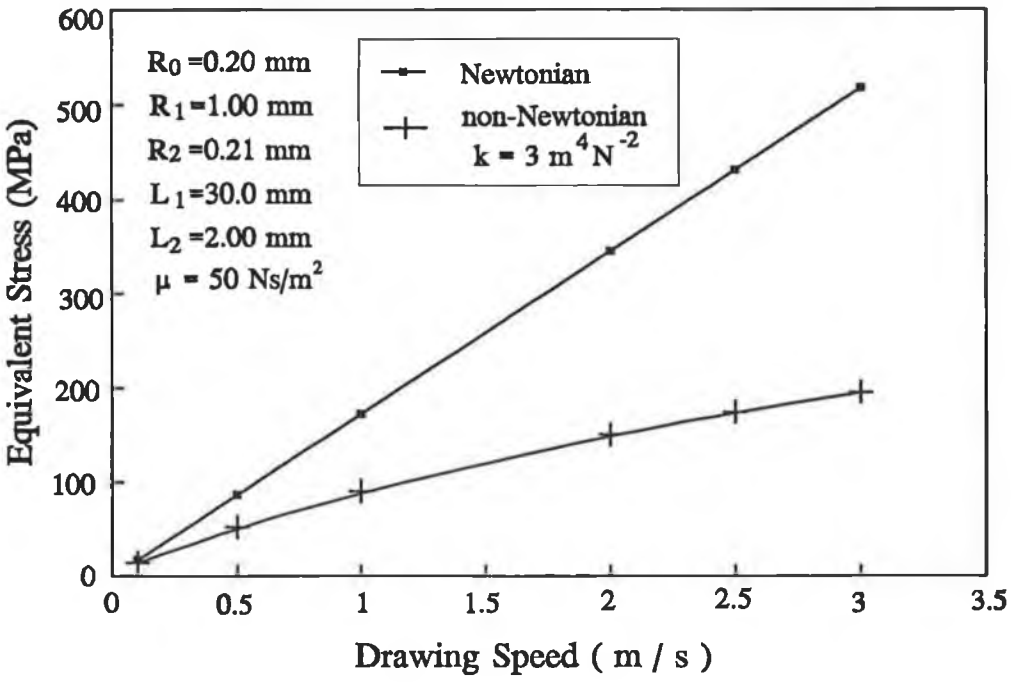

Figure 41 *The comparison of the equivalent stress according to Newtonian and non-Newtonian fluid models.*

The comparisons of the pressure distribution in the unit and the maximum pressure under Cartesian and cylindrical coordinate systems are shown in Figure 42 and Figure 43 respectively. From these results, it is evident that the pressure at the step obtained under the Cartesian coordinate system is higher than that obtained under the cylindrical coordinate system and the difference between them becomes more at higher drawing speed. The distribution of the pressure under the former system is also larger than that in the latter system, especially within the inlet length of the unit.

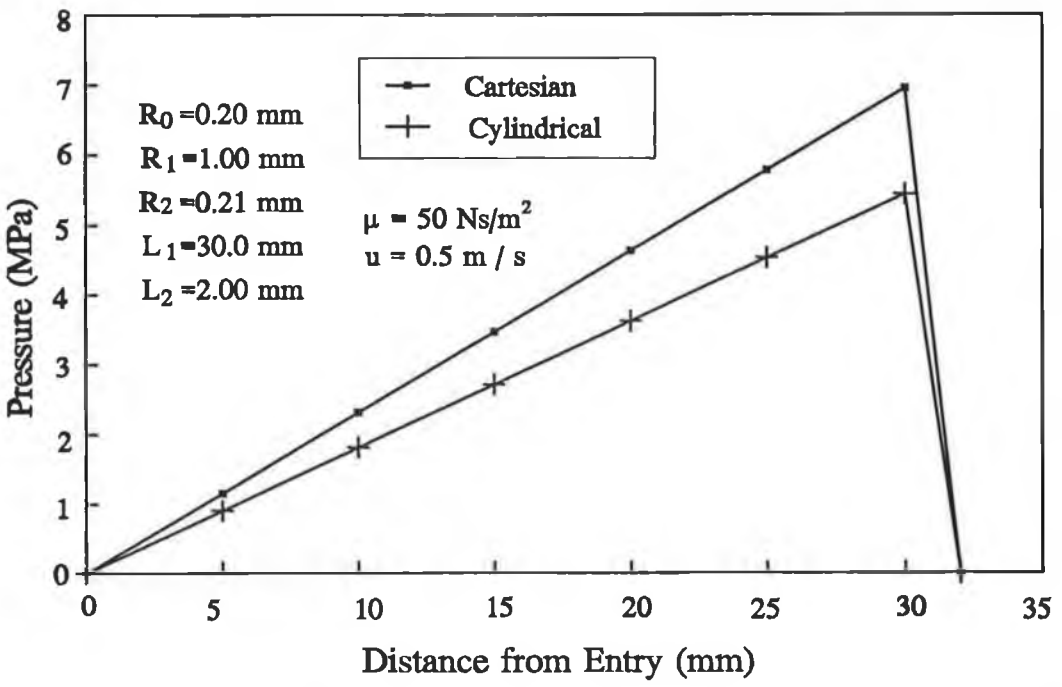

Figure 42 *The pressure distribution in the unit according to Cartesian and cylindrical coordinate systems.*

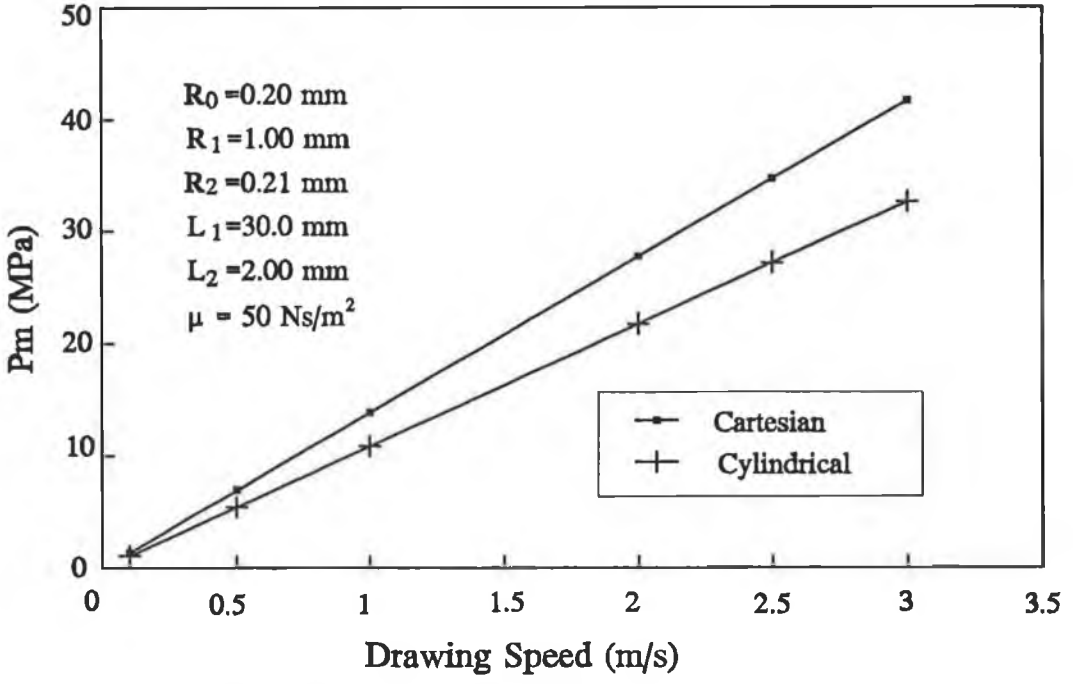

Figure 43 *Comparison of the pressure at the step according to Cartesian and cylindrical coordinate systems.*

From the theoretical results it can be said that as the inlet length L_1 increases, the maximum pressure, pulling force and equivalent stress increases appreciably. As the outlet length L_2 increases, the maximum pressure changes only marginally but the pulling force and equivalent stress increase significantly. As the viscosity of polymer μ increases, the pressure, pulling force and stress all increase appreciably. As the outlet radius increases, the force and stress reduce slightly, and the pressure reduces negligibly. From the above results, it can also be stated that for Newtonian fluid, maximum pressure P_m, pulling force F and equivalent stress σ_e change linearly with drawing speed. However, for non-Newtonian fluid, P_m, F and σ_e change non-linearly with drawing speed. The results based on non-Newtonian model are smaller than those based on Newtonian model. For Newtonian fluid, the results under cylindrical are smaller than those under Cartesian system. The model established according to cylindrical system should be most appropriate since the real unit is axisymmetrical.

Chapter 4 Experimental Equipment

The equipment for the experiment consists of five components. These are the drive train, the pressure die unit, the wire feed mechanism, the electrical installation and the drawing bench.

4.1 Drive Train

The drive train is composed of an electric motor, a gearbox, couplings and a bull block. An electrical stepless speed regulating system enables the wire to be drawn at an arbitrary speed between 0.05 to 20 m/s. The maximum drawing load for the system is 500 N at a drawing speed of 4 m/s, the wire stemming from two separate drawing chambers can be drawn onto the same bull block (at different times) with minimal alterations to the system. Only one of the two drawing chambers is utilised in the experiment, which can be used for drawing fine wires and is located vertically over the bull block. The motor is a standard 3 phase, 4 pole squirrel cage motor, 3kW, and the associated variac is a KEB Combivert 56. The frequency inverter has a number of facilities which allow one to vary the operating parameters of the motor. These include being able to adjust the minimum/maximum speed of the

motor, its acceleration/deceleration times along with being able to increase the maximum torque of the motor above its design torque for short periods of time. It also provides fail safes for the motor so that if the motor overheats or a phase fails, the inverter will shut the motor down. The frequency inverter is normally operated from the remote control unit which is mounted on the bench. From this remote control unit one can run the motor forward or reverse, start or stop the motor, adjust the speed of the motor and also monitor the frequency at which the motor is being run. The gearbox is a David Brown CA237 10:1 handling position gearbox with an exact gear ratio of 9.67:1. Its maximum input power rating at 1450 RPM is 2.55 kW. According to the manufacturers literature, this rating can be exceeded by 100% on occasions without damaging the gearbox. The various parts of the drive train are connected together using Fenner RM112 rigid couplings. The motor speed is determined using a remote sensing tachometer, Shimpo DT205, which records rotating motion of the motor's coupling by means of a piece of reflective tape. It has a recording time of a few seconds. From this non-contact rotary measurement one can determine the rotary speed of the bull block and hence its drawing speed. The bull block's operating range of drawing speeds is shown in Table 2.

With these configurations it is possible to obtain the whole speed range for the bull block with good overlap

between configurations. The view of the drive train can be seen in Photo 1.

Table 2 *The operating range of drawing speeds of the bull block.*

	Min. Speed (m/s)	Max. Speed (m/s)
Motor/Gearbox/Small Bull Block	0.03	0.01
Motor/Gearbox/Large Bull Block	0.08	2.00
Motor/Small Bull Block	0.3	8.00
Motor/Large Bull Block	0.8	20.0

4.2 Pressure Die Unit and Modifications

4.2.1 Description of the Previous Pressure Die Unit

The pressure die chamber is capable of being heated to 400°C, using heater bands. There are two of these heater bands; one for the pressure die chamber and the other for the melt chamber. Since the pressure die chamber and melt chamber are capable of heating up to temperatures of 400°C, there is an insulated housing surrounding the apparatus for reducing the heat loss by radiation and convection.

The path of the wire passing through the pressure die unit is as follows. It enters the melt chamber through a hole

from the chamber. The melt chamber holds of the molten polymer. From the melt chamber it passes through a 2 mm bore passage which, if necessary, can allow multiple strands of fine wire to pass through. From here the wire passes through an insert holder then passes through a die insert. The holes in the die inserts can be used to test the variations in the coating thickness of the wire. The wire then passes through a bottom cover and subsequently to the bull block. This is the original state of the assembly whose drawing is shown in Figure 44.

4.2.2 Modifications of the Pressure Chamber Unit

The new pressure die unit assembly is shown in Figure 45. It consists of a melt chamber, a pressure die chamber, two heater bands, a upper and a bottom cover, an insert holder, a die insert and a sleeve. Comparing with the previous system, a sleeve has been added to the unit, which makes it possible to adjust the length of the insert holder. The inner structure of the pressure die chamber is modified to make the insertion of the wire easier.

In order to facilitate easier passage of the wire through the unit, a new pressure die chamber (see Figure 46) has been designed which replaces the previous one (see Figure 47). Using the new one the wire can pass through the unit without having to dismantle the whole unit. To change a die or make a new wire pass through the unit, one simply

needs to open the bottom cover. In the previous system one had to remove the melt chamber from the pressure chamber to complete this task. It is to be noted that in the previous design the long 2 mm bore passage produced greater resistance for the wire passing through the unit, thus causing fracture of the wire.

In the new arrangement a sleeve (see Figure 49) has been used so that the insert holder can be made shorter to obtain variable coating thickness. In the previous system it could not be done. The previous and new insert holders are shown in Figure 48 and Figure 50 respectively.

There are several sizes of die inserts (see Figure 51) so that one can obtain wider range of coating thickness than that obtainable using the previous system(see Figure 52). The upper cover and the melt chamber(see Figure 53 and Figure 54) in the existing unit have been manufactured according to the modification. A general view of the pressure die unit is shown in Photo 2.

4.3 The Electrical Installation

4.3.1 Electrical Wiring Arrangement

The drawing bench is connected by a 3 phase plug to the mains and all electrical system on the bench are isolated from other devices by means of a 3 phase isolating switch and

a fuse bow system. From the fuse box, electricity is fed to the motor controller, heater bands and the associated controllers.

From the fuse box the 3 phases are brought to the KEB Combivert 56 frequency inverter. The 3 kW motor is then connected from this inverter by means of shielded cable.

The frequency inverter is normally operated from the remote control unit which is mounted on the bench. From this remote control unit one can run the motor forward or reverse, start or stop the motor, adjust the speed of the motor and also monitor the frequency at which the motor is being run.

4.3.2 Heater Bands

The heater bands chosen are IHNE-TESCH high capacity ceramic insulated cylindrical heater bands with an internal diameter of 80 mm by 36 mm high. The basic control unit can control up to 12 heater bands, controlling up to 6 heater bands at any one time. The original two heater controllers are west 3300 PID controllers. With these controllers it is possible to adjust the proportional, integral and differential control; to set the maximum control temperature and also the period of sensing; and to set the maximum time that power can be supplied to the heater band relay in percentage terms. The heater bands are controlled using a relay switch which is activated by the controllers. With these controllers it is

possible to tune each required heater band system so that the temperature fluctuated no more than ±1°C around the set point.

4.3.3 Temperature Controllers

Each controller operates a relay switch which in turn powers a heater band. The temperature of the heater bands is then monitored by the controller through a thermocouple (Type J). All 6 controllers are powered from a single phase supply but in order to try to keep a balanced load on the phases it is decided that each phase would supply two of the relays for the heater bands. Shielded cable is used for the power cable to the heater bands. The power and thermocouple cables are aligned so that they would not run along the same path.

In order to ensure the safe operation of the heater bands a device is used to interlock the heater band power supply and thermocouple sensors together when being connected to the controllers. In this way it is possible to operate one set of 6 heater bands safely at any one time and then the other set of 6 heater bands at a different time. A view of the complete installation can be seen in Photo 3. Each heater band is connected to the relay power supply by means of a 3-pin plug. In this configuration each heater band plug and its associated socket which leads to the controllers are labelled so as to prevent wrong connection. The plug and socket system is the weak link in the interlock system.

4.4 The Drawing Bench

The drawing bench is to support all the electrical equipments and ensure that the drive train is rigid. Its flat surface is used to mount the experimental units.

The drawing bench can facilitate drawing of wire from more than one experimental source with very little modification. Its basic frame is made out of 50x50x2 mm angle bar. The electrical equipment and a plate for the mounting of experimental units are then fixed to the frame. The support stand is used as a support for the pressure die unit and a wire feed mechanism. The wire can be pulled off the reel along its longitudinal axis. For fine wire, the wire spool can be held by a bold and nut unit. This stand can be attached to the plate in up to 4 positions so that the pressure die unit is always in a vertical line with the drawing surface of the bull block in its 4 possible bull block and locations. The overall view of the drawing bench can be seen in Photo 4.

Photo 5 (see page 99) shows a 0.4 mm stainless steel wire before and after the coating is applied. The die diameter used for coating is 0.46 mm and the polymer is Escorene which is a low density polyethylene.

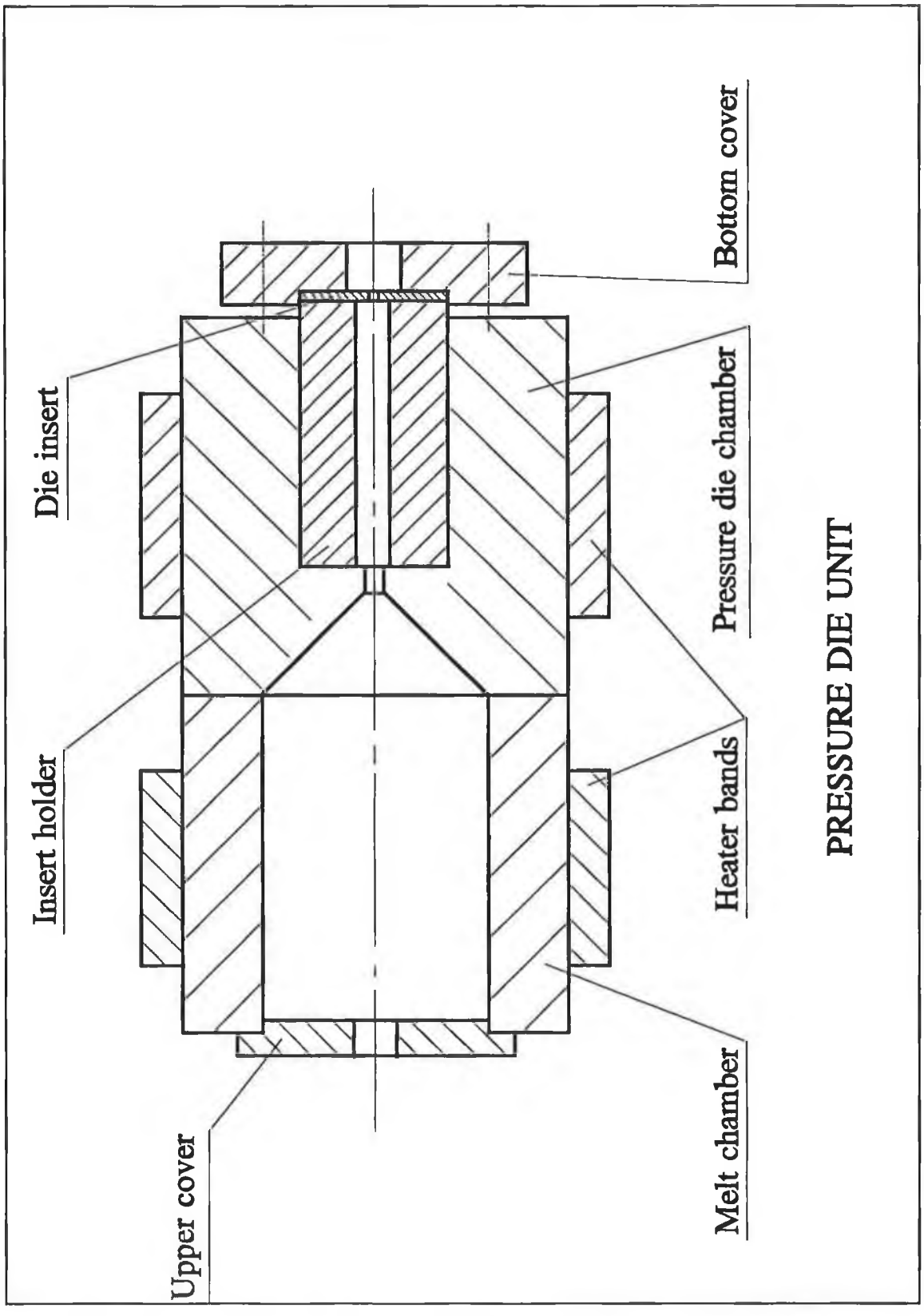

Figure 44 *The previous pressure die unit.*

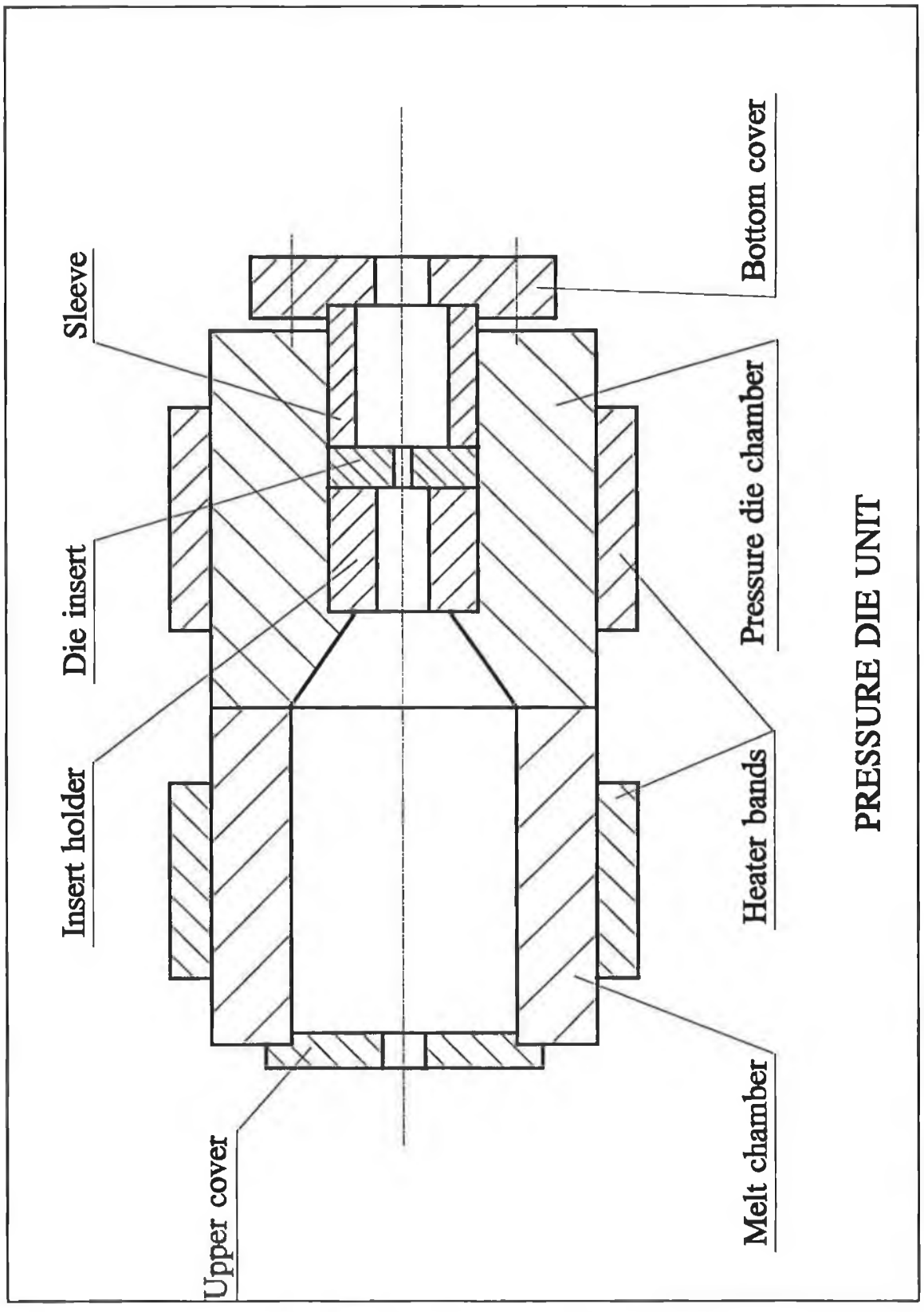

Figure 45 *The new pressure die unit.*

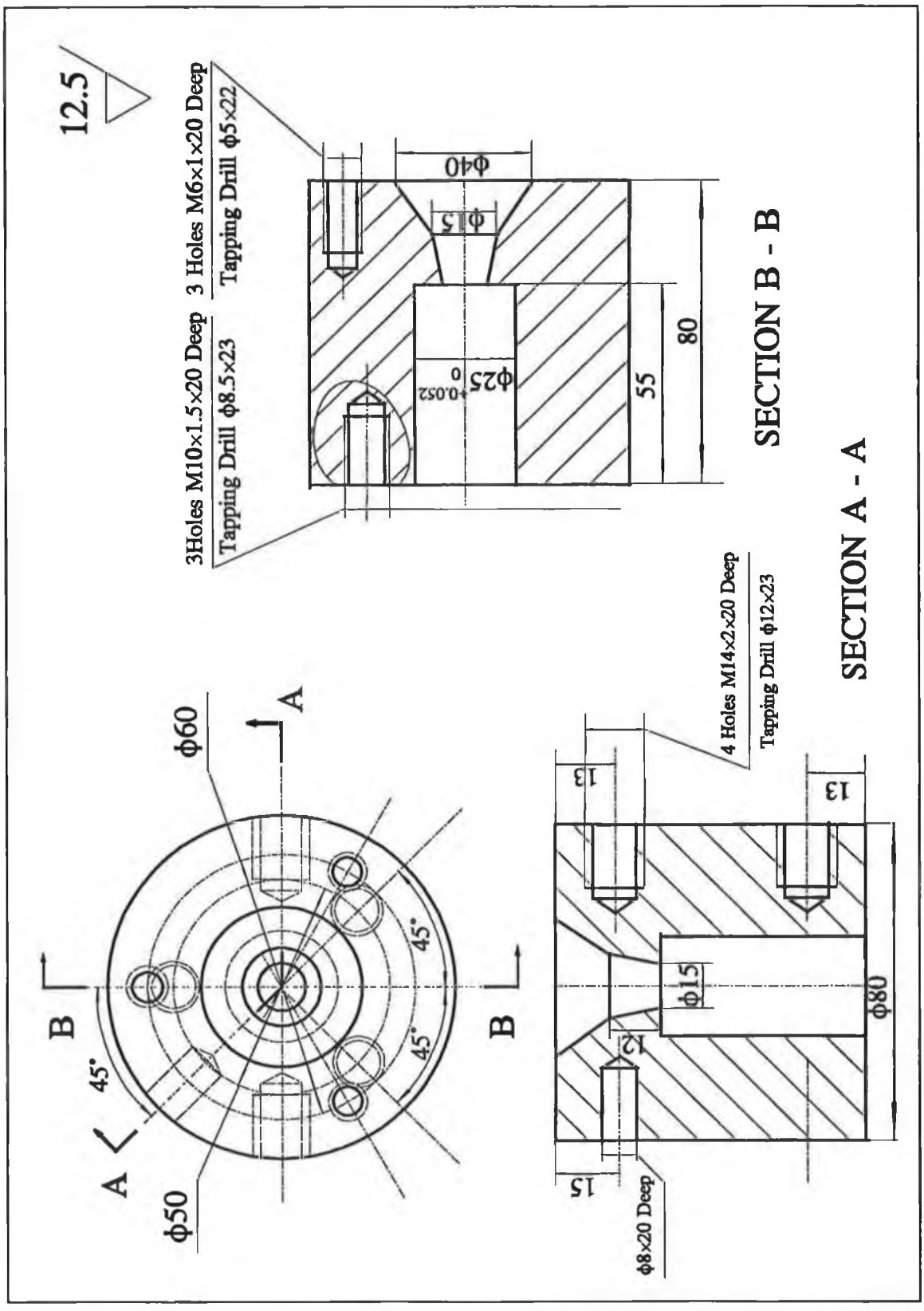

Figure 46 *The new pressure die chamber.*

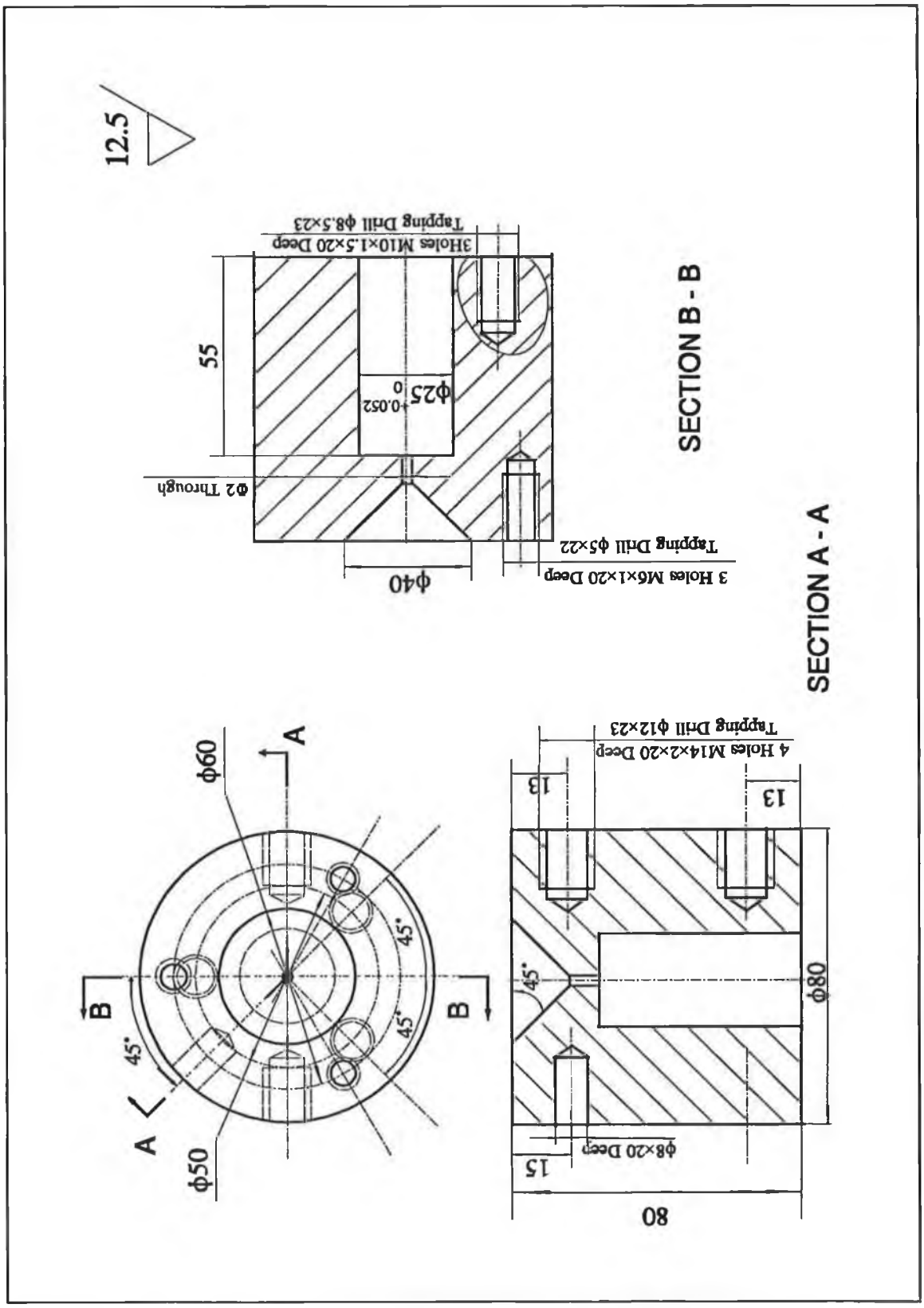

Figure 47 *The previous pressure die chamber.*

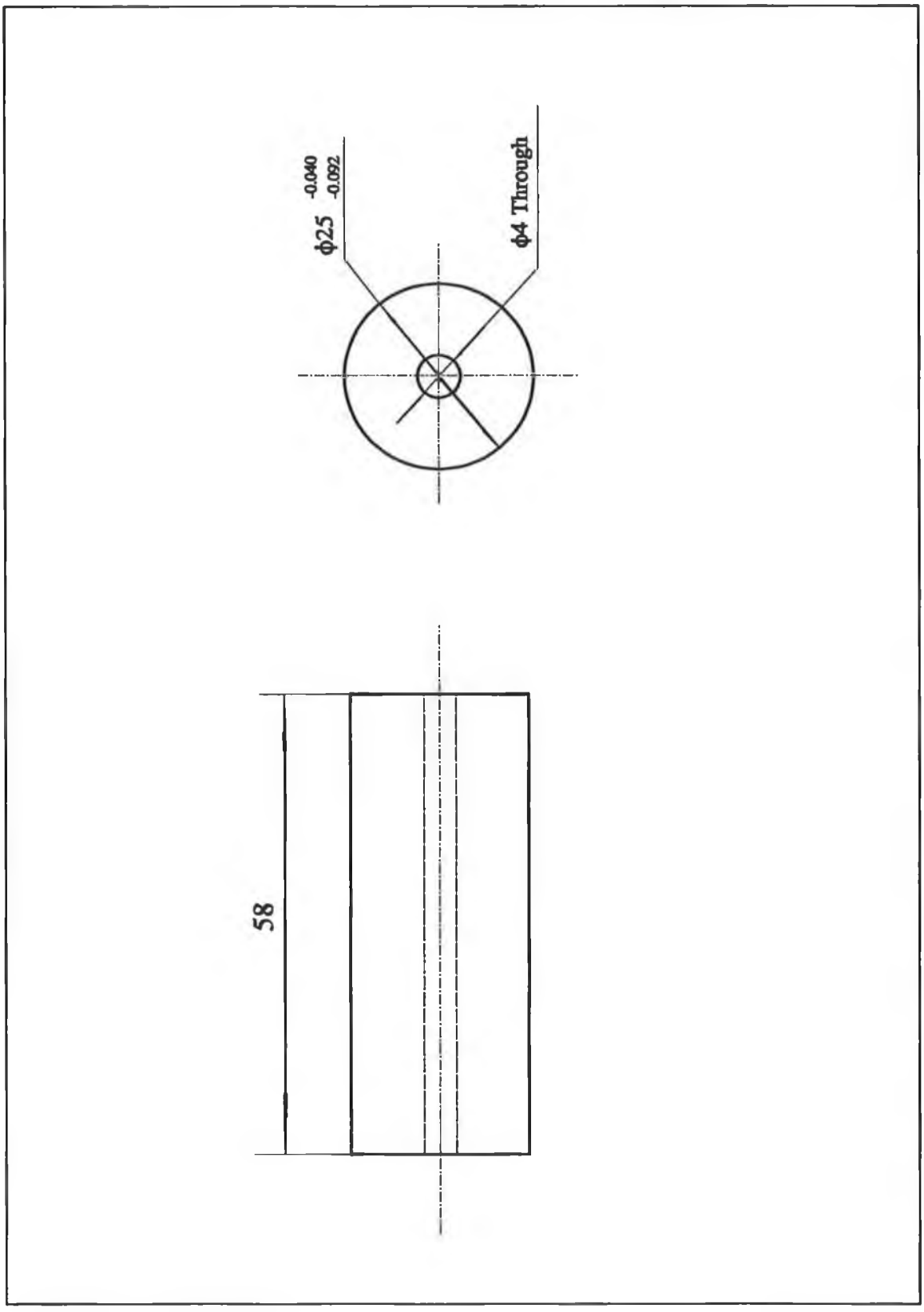

Figure 48 *The previous insert holder.*

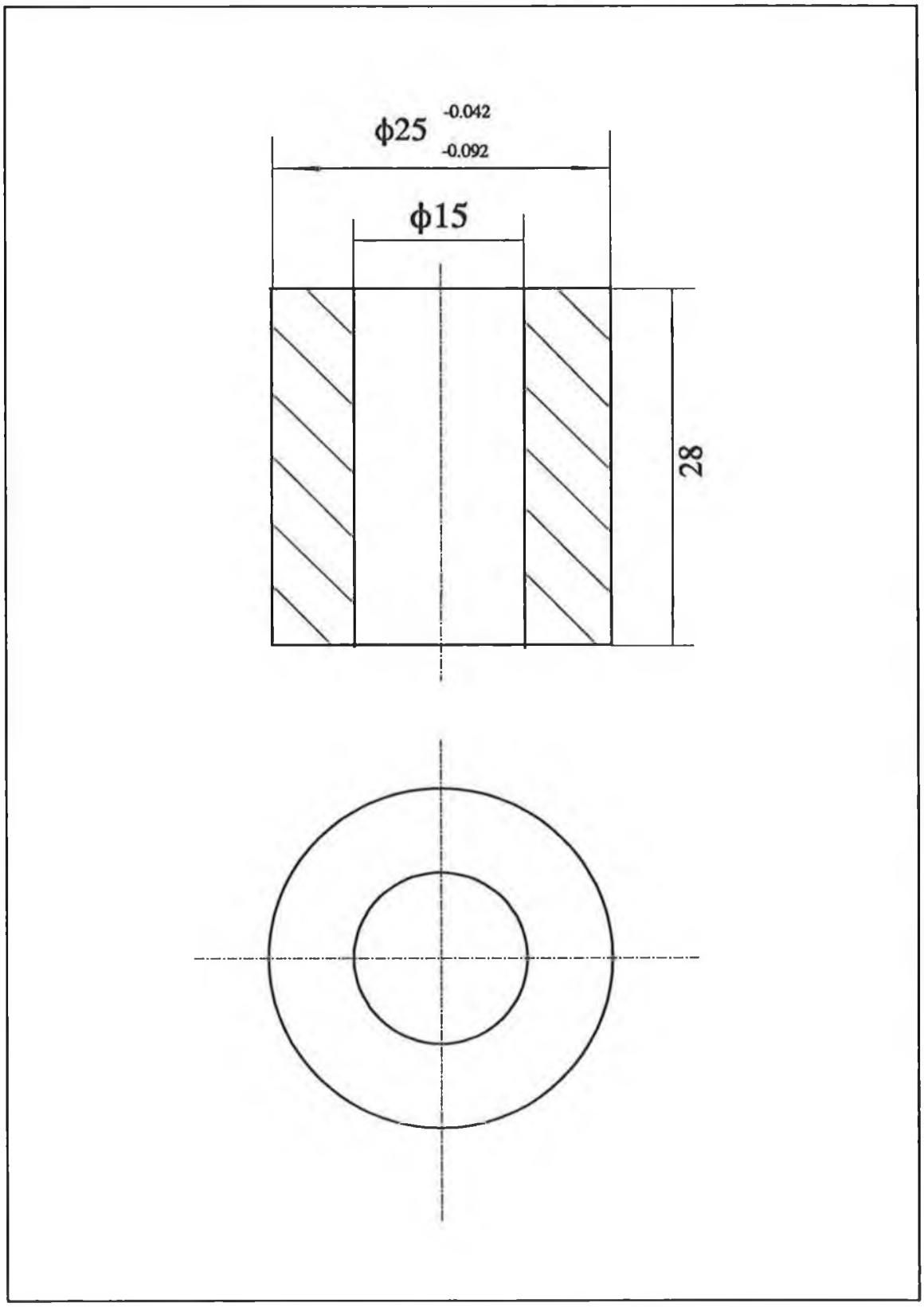

Figure 49 *The sleeve.*

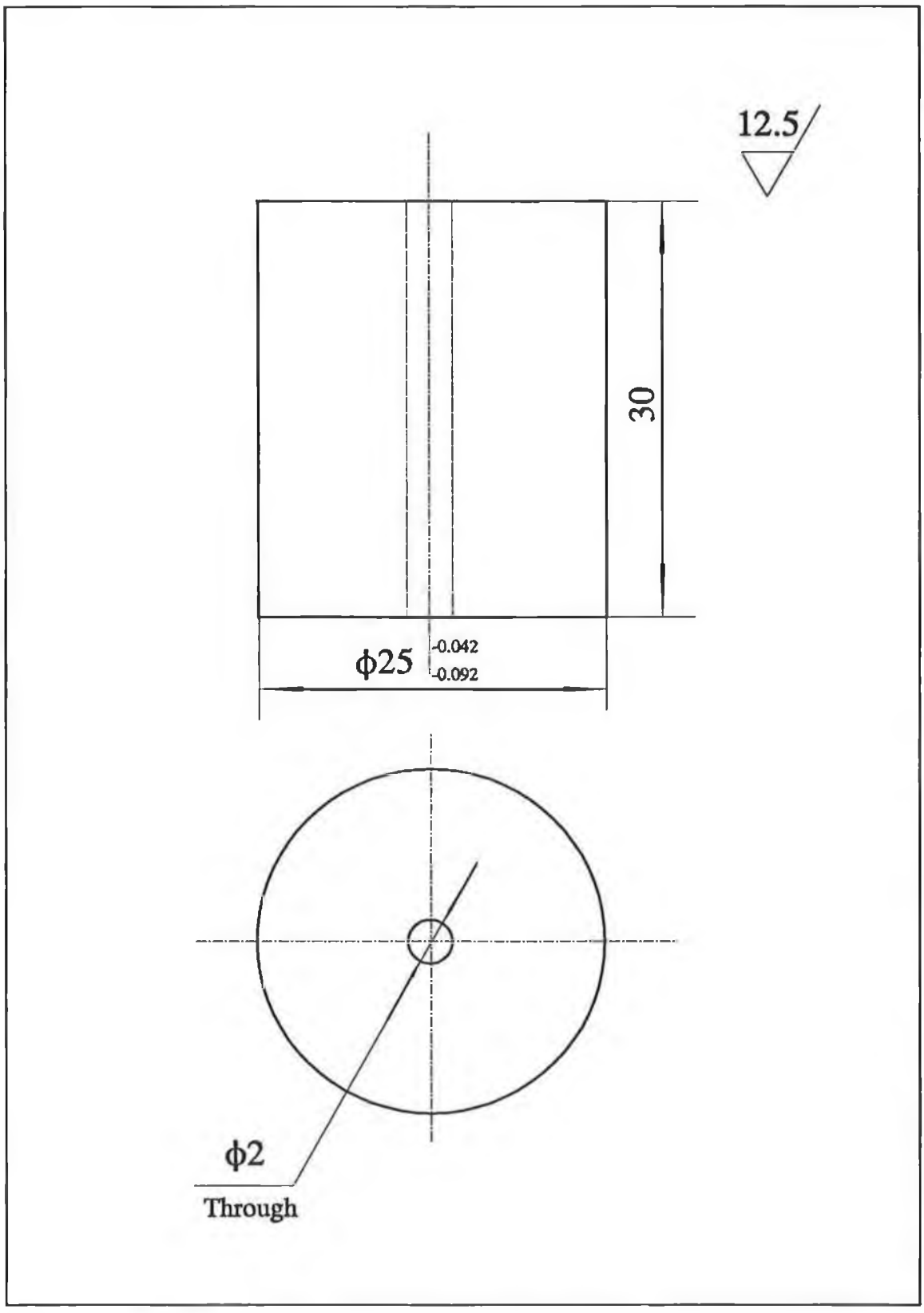

Figure 50 *The new insert holder.*

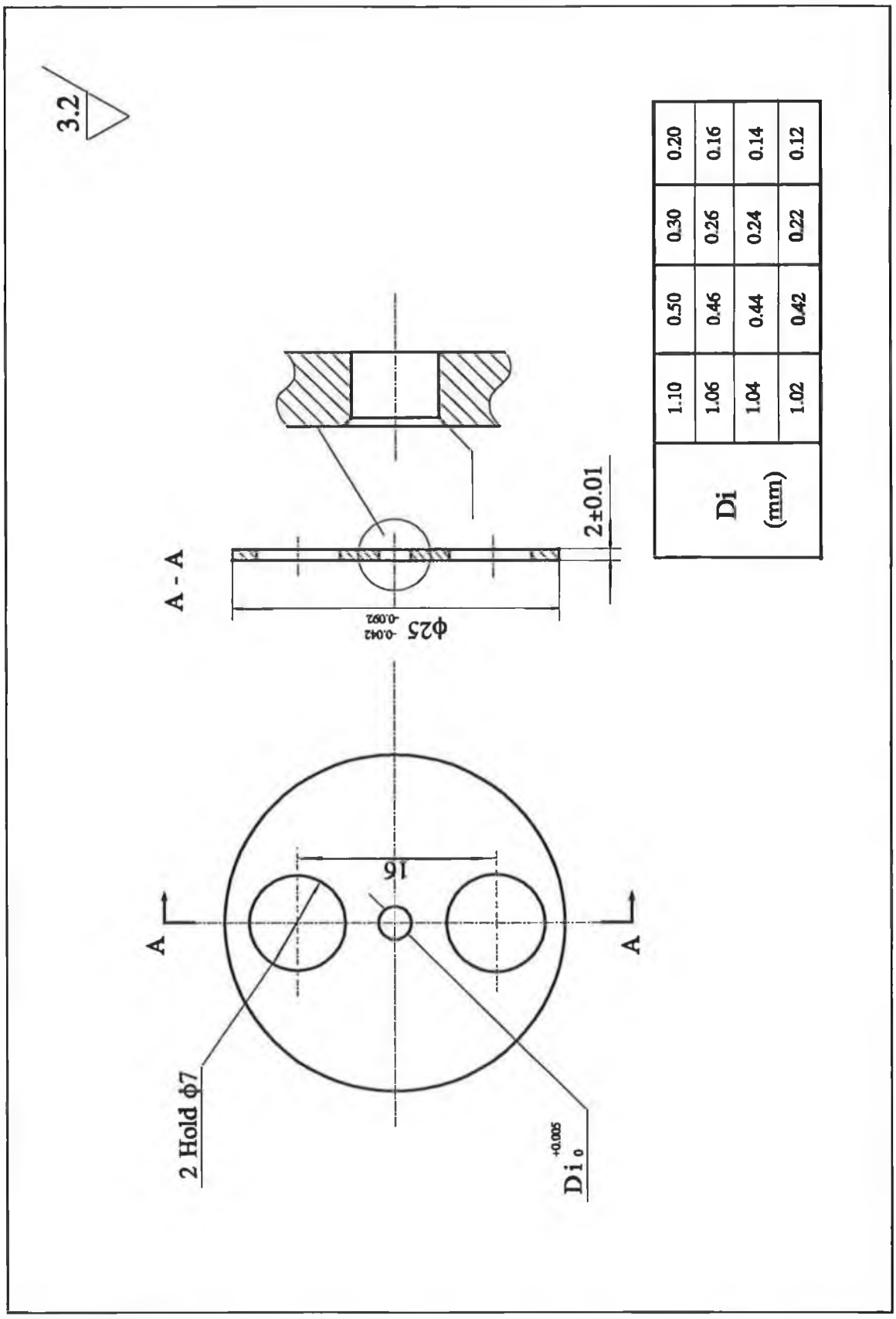

Figure 51 *The new die inserts.*

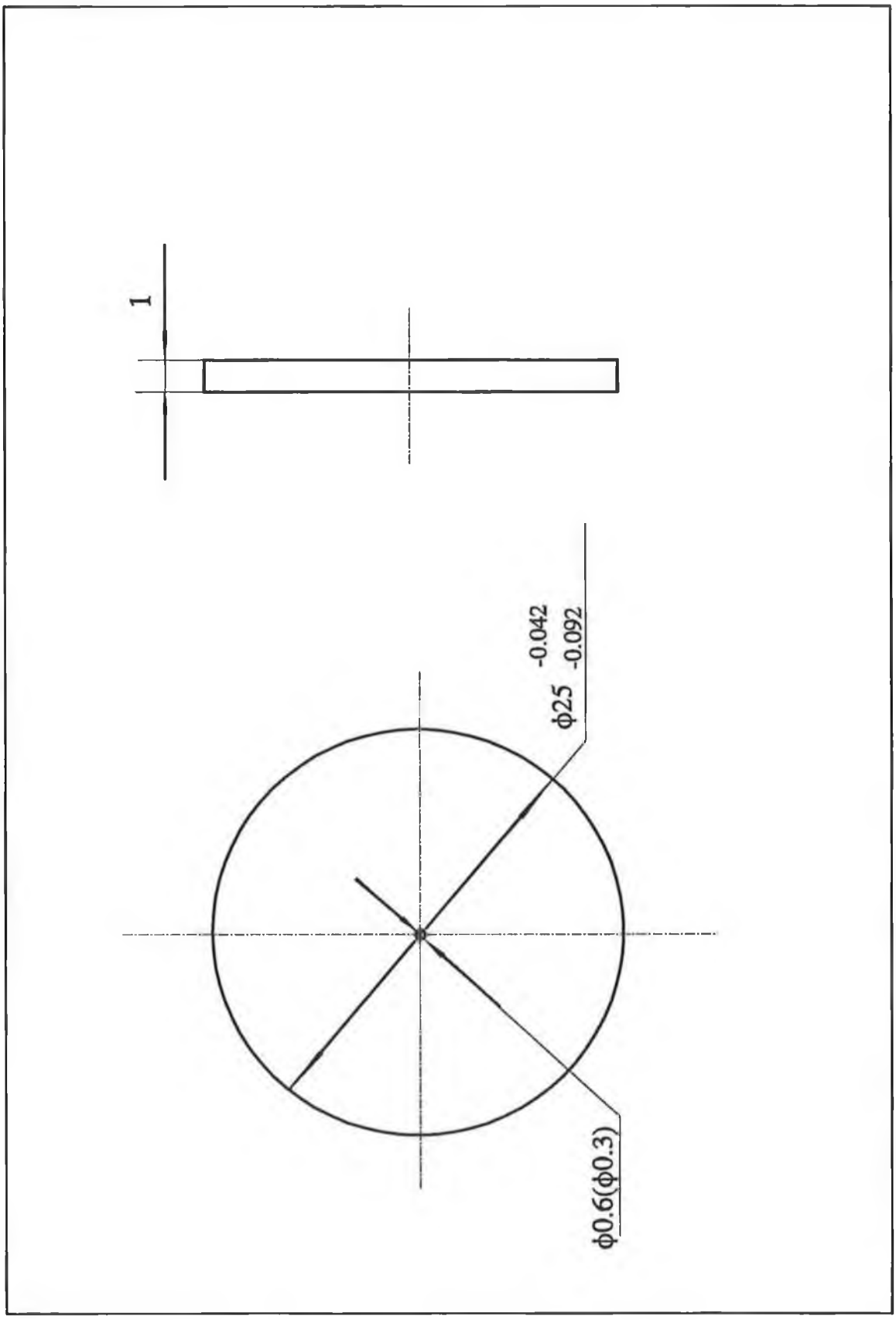

Figure 52 *The previous die inserts.*

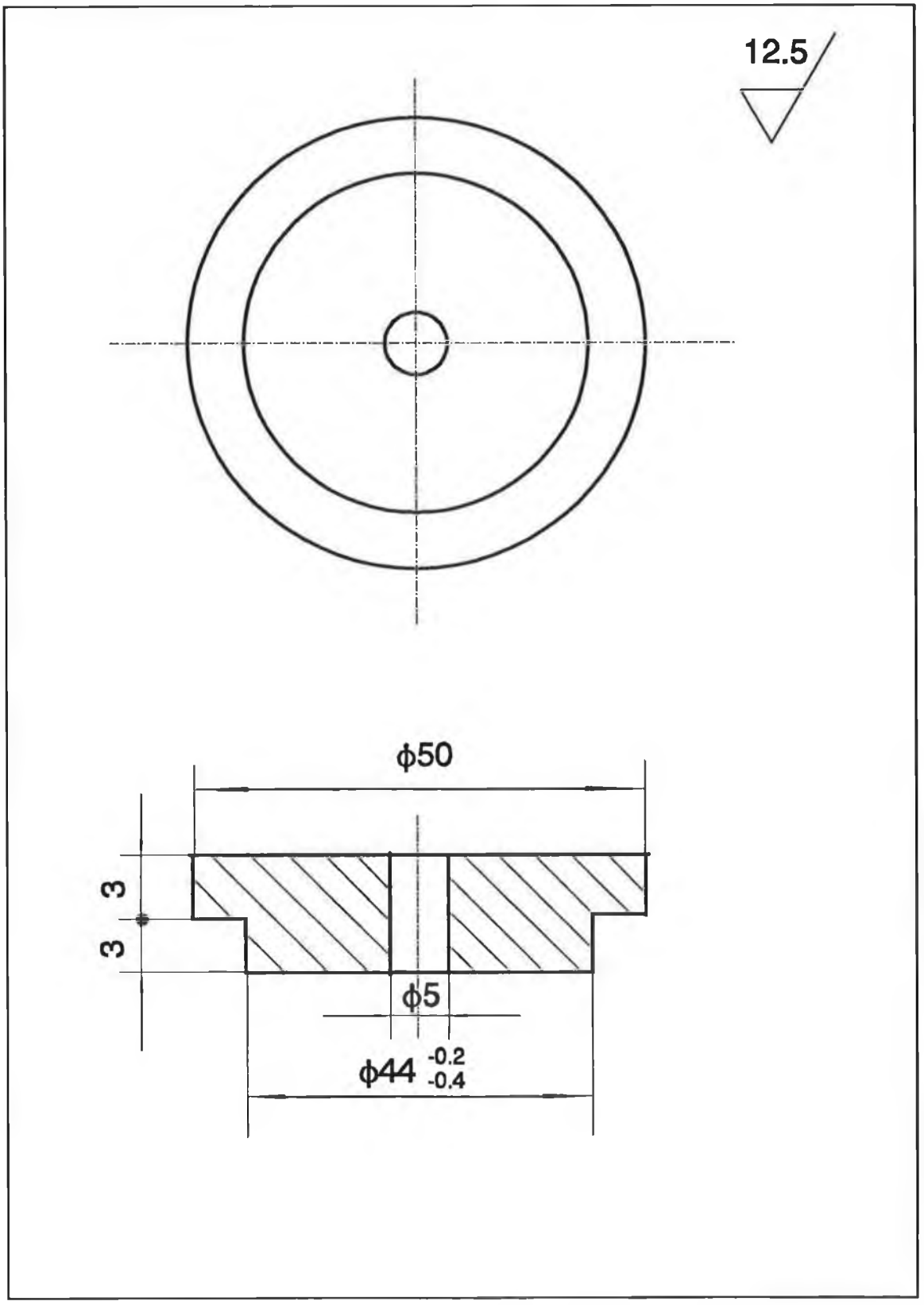

Figure 53 *The upper cover.*

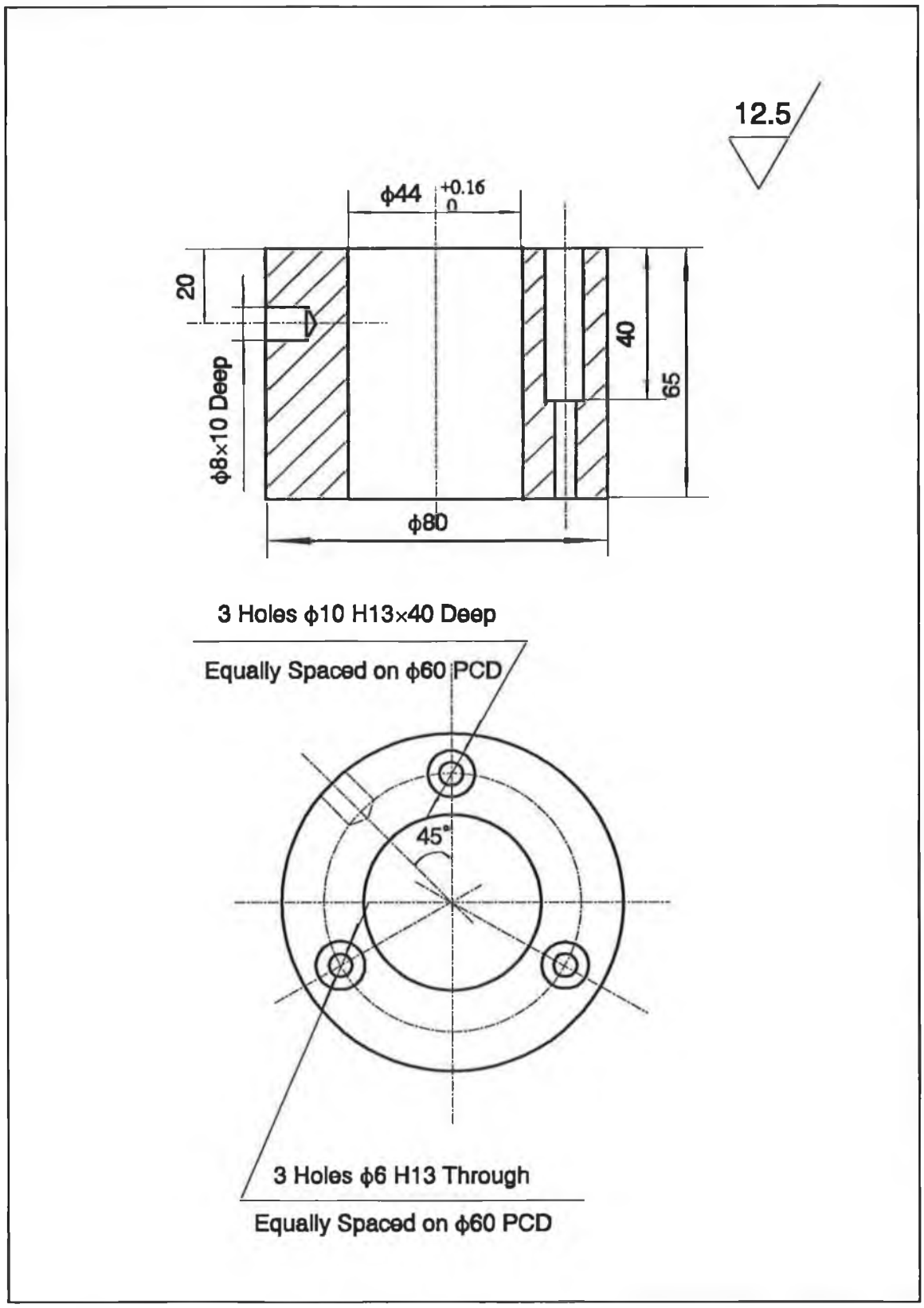

Figure 54 *The melt chamber.*

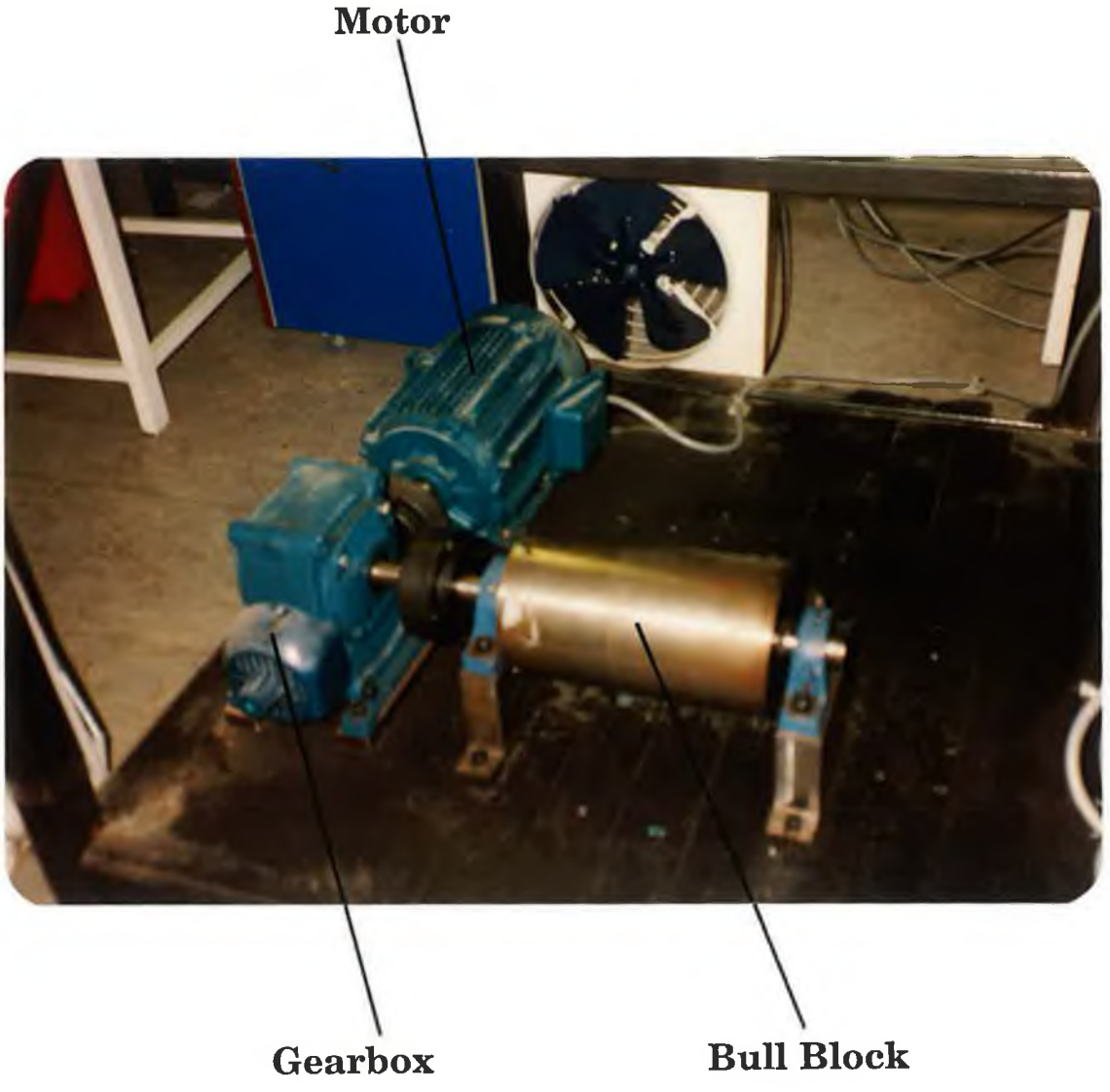

Photo 1 *The view of the drive train.*

Photo 2 *The pressure die unit.*

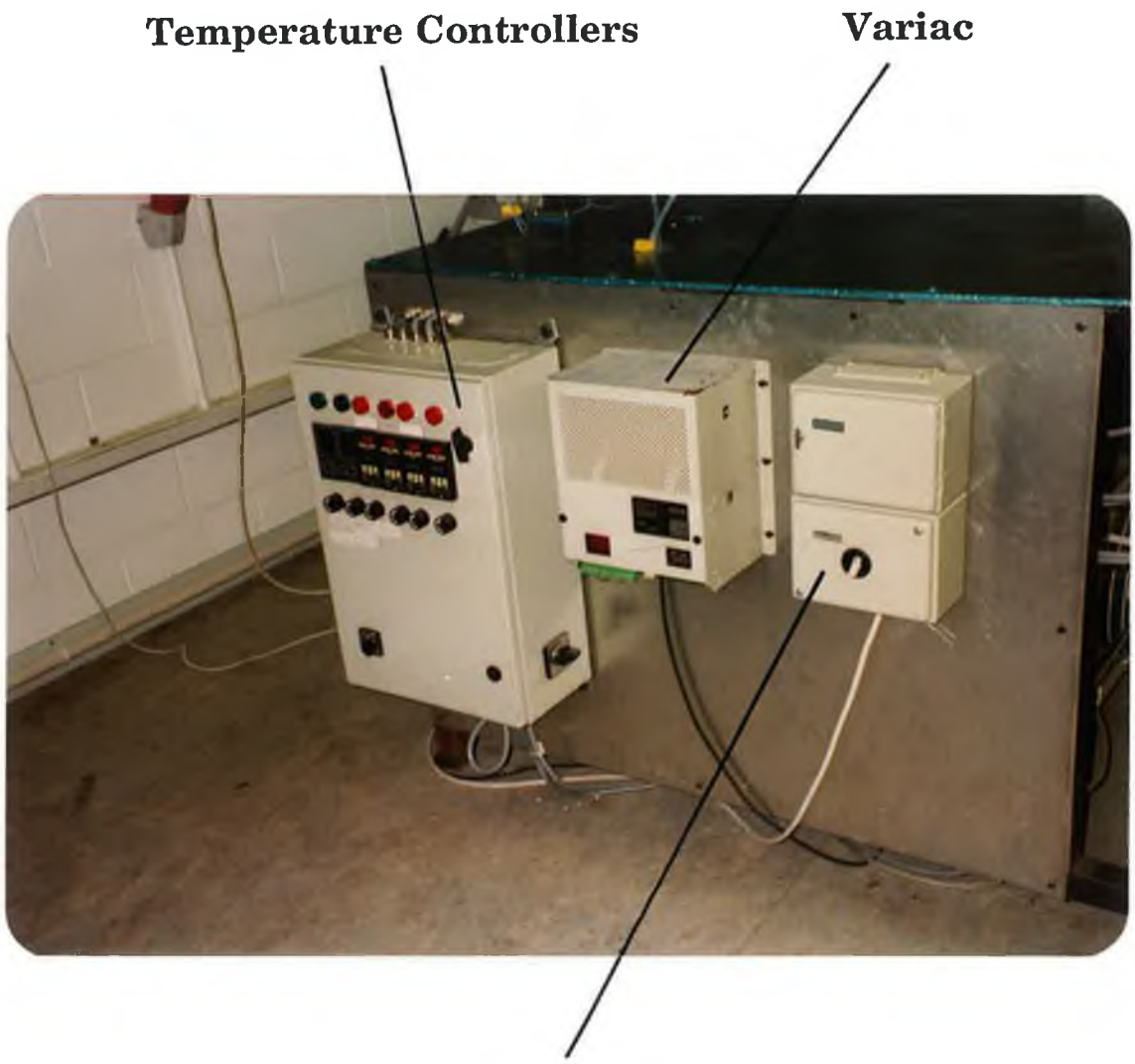

Photo 3 *The view of the complete installation.*

Photo 4 *The overall view of the drawing bench.*

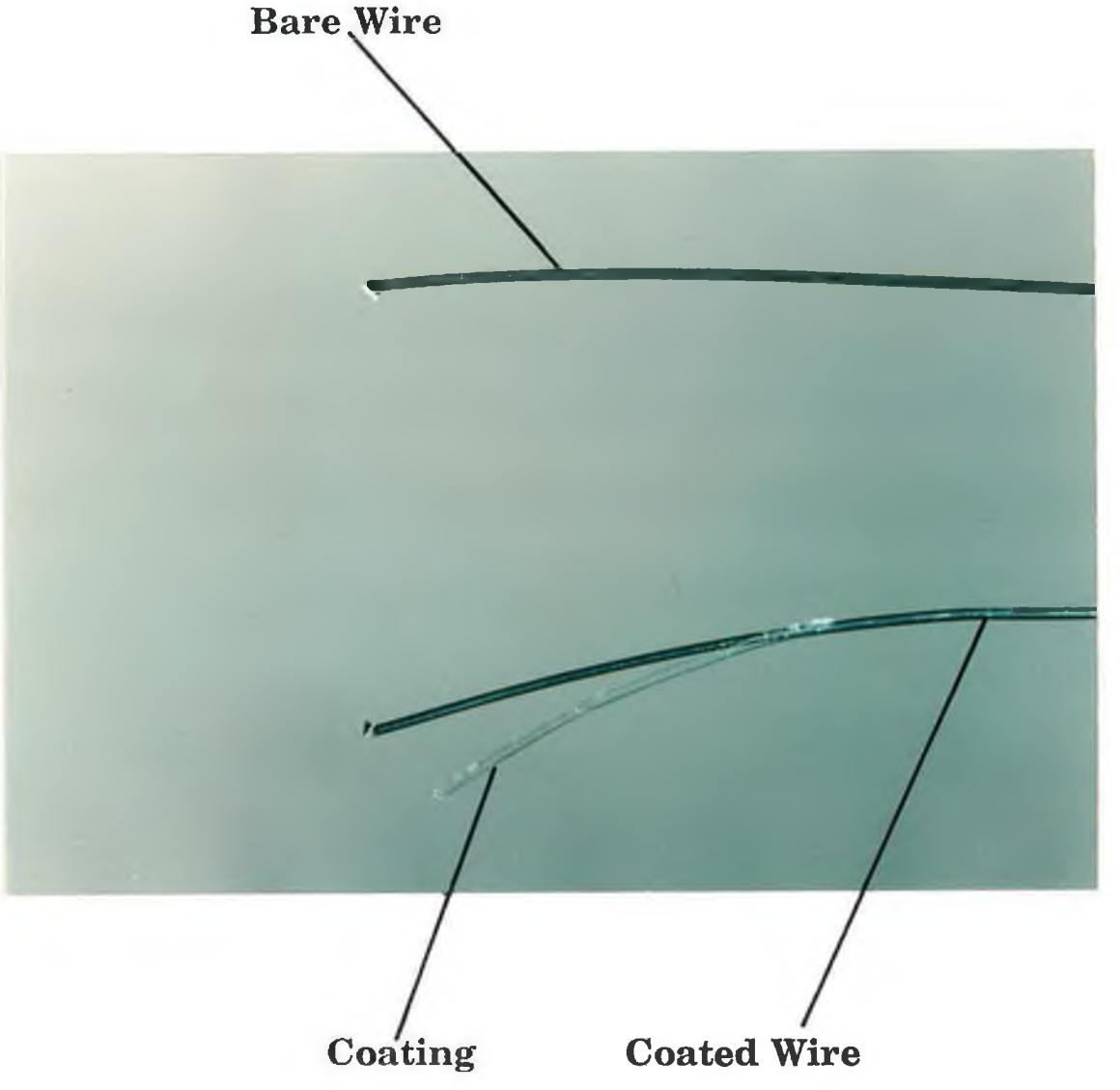

Photo 5 *The samples of the bare wire and coated wire.*

Chapter 5 Experimental Work and Results

5.1 Apparatus Shakedown

The experimental apparatus includes two sets of electrical systems. One is the wire driving system (drive-train) and the other is heating system. Before starting the experiment, the drawing bench is checked. It should be ensured that all the switches are in off position. The motor/gearbox/bull block is also checked to see if it is in a configuration which will give the range of drawing speeds required for the experiment. If not, the drive-train configuration is arranged again accordingly. At the beginning, the power to the drawing bench is turned on and the drive-train is run up to full speed in small steps using the remote speed controller to turn the motor on and vary the motor speed. This is to ensure that the wire driving system is running correctly.

Following the set up of the drive-train, the main switch of the heating system which supplies the electric sources to both the heater bands and the thermocouple is turned on. When the main switch is turned on, the thermocouple begins to work. Then the two single-phase power switches on the

controlling board are turned on which controls two heater bands respectively. It should be ensured that each heater band and its associated thermocouple are linked to the respective controllers which are going to be used. The following procedure is taken

1) Set the "Set Point" of the controller to 10°C above the ambient temperature.

2) Observe the temperature on the controller's display. This should start to rise within one minute after the single-phase switches are turned on.

3) If the temperature does not start to rise within this time, turn off the power to the heater bands and check to see which heater band is "on" and which thermocouple is monitoring. Make any necessary alterations.

The power to the heater band controllers is turned off after testing the heating system. The wire is threaded through the experimental apparatus and attached to the bull block. Then the melt chamber is filled with the desired polymer to be used and the heater band controllers are turned on again. The "set point" of the controllers are set to the temperature that is required for the experiment. A suitable time should be allowed for the heater band temperatures to stabilise.

Drawing of wire may then commence for the coating experiment at roughly the desired speed by adjusting the variac frequency using the remote control module. The direction of motor can also be altered with the remote control module. If further motor parameters are to be altered, (*i.e.* acceleration, deceleration, *etc.*) the KEB Combivert 56 manual should be consulted. To monitor the motor's running speed the Shimpo DT205 needs to be turned on and the remote tachometer needs to be pointed towards the motor coupling which is marked with a piece of reflective tape. It will give a reading of the motor's RPM within three seconds. The linear drawing speed depends on the motor/gearbox/bull block configuration. The RPM to drawing velocity conversion for each bull block set up is done as below:

Motor/gearbox/small bull block (ϕ 0.06 m)

Drawing velocity = RPM $\times$ 324.88 $\times$ 10^{-6} m/s

Motor/gearbox/large bull block (ϕ 0.15 m)

Drawing velocity = RPM $\times$ 812.2 $\times$ 10^{-6} m/s

Motor/small bull block (ϕ 0.06 m)

Drawing velocity = RPM $\times$ 3.142 $\times$ 10^{-3} m/s

Motor/large bull block (ϕ 0.15 m)

Drawing velocity = RPM $\times$ 7.854 $\times$ 10^{-3} m/s

When a series of experiments have been completed:

1) Turn the power off to the heater bands.

2) Set the "set point" of temperature controllers to 0°c (this is to ensure that the controllers are in a safe operating mode when the bench is not used).

3) Turn off the individual heater band controllers.

4) Turn off all power to the heater band's control panel.

5) Turn off the power to the bench after samples have been unwound off the bull block.

5.2 Experimental Procedure

The wire on which the coating experiments are carried out is threaded through the melt chamber and the pressure die chamber. In the pressure die chamber, the wire goes through the insert holder, a die insert and then the bottom cover. Then it is attached to the bull block with wrapping the leading end of the wire on a nut which has been fixed on the block. This is found by experiment to be the simplest and quickest way of attaching the wire to the bull block. The polymer is poured in the melt chamber, then the heater bands are turned on and when they reach their "set point" allow 15 minutes before the experiment starts.

Considering that in wire coating, the polymer is not completely solidified by the time it reaches the bull block. This causes the individual strands to become stuck together

and the polymer coating gets deformed. Therefore, the sample of the wire is taken from that part which lies between the bottom cover and the bull block. The sample is removed carefully and labelled. The untested wire is then drawn through the pressure die unit and attached to the bull block for the next test.

At the end of each experiment the remaining polymer is removed from the melt chamber and the pressure die chamber. Having turned off the power supply and disconnected the thermocouple, the melt chamber, is cleaned out mechanically using a spoon or similar tool. Using a high tensile strength-steel wire a hole is "drilled" in the insert holder and the die inserts. Once a hole is made, the wire may be threaded through the insert and the polymer will melt when heated again.

It should be noted that the unit has to be cleaned before the parts cool down. It is found that it is a great deal simpler to clean the experimental apparatus, when the polymer is molten than when the polymer is cold and has solidified.

After the experimental apparatus is cleaned the diameter of the coated wire is measured. Each sample is measured in 6 different positions along its length. At each position measurement is taken twice along two diameters at 90° rotation by a micrometer (resolution 0.001 mm) and the

average diameter of the coated wire in this position is written down. When measuring the coated wire diameter, the micrometer is turned slowly until its internal overload protection system slipped a ratchet.

5.3 Experimental Results and Discussion

In analyzing the data which are obtained from the experiments, the following assumptions are made:

1) No deformation took place of the bare wire.
2) The micrometer does not deform the polymer coating.

The thickness of the polymer coating on the wire may be obtained by subtracting the diameter of the bare wire from that of coated wire. The method to establish the diameters for both a bare and coated wire is to measure its diameters along its length at regular intervals for 6-12 times by a micrometer and to calculate its average values and standard square deviation. The formula used to calculate the mean value of the diameters is

$$\overline{x}=\sum_{i=1}^{n}\frac{x_i}{n}$$

where n is the times of measurement, x_i is the value of the measurement each time and $\overline{x}$ is the mean value of the measured diameter. The error of the diameter can be calculated from its standard deviation from the following equation,

$$S_n = z_{\alpha/2} \frac{\sigma_{n-1}}{\sqrt{n}}$$

where $z_{\alpha/2}$ is a coefficient with respect to a degree of certainty and

$$\sigma_{n-1} = \sqrt{\frac{(x_i - \bar{x})}{(n-1)}}$$

The number of measurement for the bare wires is 12, but that of the coated samples is 6. In these cases when the degree of certainty is 95%, for the bare wire: $z_{\alpha/2}=2.201$ and for the sample: $z_{\alpha/2}=2.571$.[1]

The results of an experiment may be summarized in the form

$$X = \bar{x} \pm S_n .$$

The mean value δ of the coating thickness of the samples is obtained by

$$\delta = \frac{D - \bar{D}_0}{2}$$

where D and $\bar{D}_0$ are the mean diameters of the coated and bare wires respectively. The error of the coating thickness is given by

$$S_\delta = \sqrt{S_D^2 + S_d^2} .$$

where S_D *and* S_d are the errors of the coated and bare wires respectively.

Because of the great deal of experimental results, some typical results are only mapped. All the experimental results are listed in Appendix VI.

The coating thickness of Escoren at 130°C and 150°C temperature on stainless steel wire with a nominal diameter of 0.4 mm is shown in Figure 55. The die used has a 0.5 mm hole and the melt chamber is fully filled. From the graph it can be seen that the coating thickness decreases gradually as the drawing speed increases.

The coating thickness of Escoren at 135°C, 140°C and 150°C temperature on the stainless steel wire with a nominal diameter of 0.4 mm is shown in Figure 56 . The hole on the die used is 0.46 mm. From the graph it can be seen that the coating thickness decreases gradually as the drawing speed increases.

The coating thickness of Escoreen at 145°C temperature on stainless steel wire with nominal diameter 0.1 mm is shown in Figure 57. The die insert has a 0.42 mm diameter hole. From the graph it can be seen that at the speed below 18cm/s, the coating thickness increases with drawing speed, but at the speed of above 18 cm/s, the coating thickness decreases with the drawing speed.

The coating thickness of Escoren at 135°C, 145°C and 155°C temperature on stainless steel wire with nominal diameter 0.2mm is shown in Figure 58. There is a 0.3mm hole on the die insert. From the graph it can been seen that at the speed below 40 cm/s, the coating thickness is constant with drawing speed, but at the speed above 40cm/s, the coating thickness decreases with drawing speed.

From above four graphs it can be seen that generally the coating thickness decreases with the increase of drawing speed. As the drawing speed gets higher, the tendency of the slide between the layers of polymer, and the polymer and the wire surface increase. This possibly causes the reduction of the coating thickness. When the drawing speed exceeds some limit, the slide will appear between the polymer and the wire.

Figure 59 shows the relationship between the gap and the coating thickness of Escoren at 145°C temperature on the stainless steel wire of 0.1mm nominal diameter and at 0.33 m/s drawing speed, when the diameter of the die inserts is respectively 0.42mm, 0.26mm, 0.20mm. Here the gap is the clearance between the die insert and the wire. From the graph it can be seen that the coating thickness increases with the gap. The same conclusion can also be seen in Figure 60, which shows the coating thickness of Escoren at the 135°C and 150°C temperature on a stainless steel wire of 0.4mm nominal diameter in the condition that the drawing speed is 0.20m/s

and the diameters of the die inserts are respectively 0.50mm, 0.46mm, 0.44mm, 0.42mm.

The theoretical coating thickness is equal to the size of the gap, but the experimental results are smaller than the theoretical results. This can be explained by the fact that the coating layer between the wire and outlet die surfaces is under tensile and shear stress which increase with the drawing speed giving less thickness than the gap at the outlet point. Also the temperature at the outlet of the unit is lower than that inside. The polymer coating attached on the wire at the outlet end has quite high temperature, which will finally cool down to the room temperature so that it will contract because of the loss of temperature.

From the experimental results, another phenomenon is also observed, the larger the gap, relatively closer to the theoretical value the coating thickness of the experimental results are. However, there is still substantial difference between the theoretical and experimental coating thickness.

Figure 61 shows the relationship between the diameter of the wire and the coating thickness of Escoren at 145°C temperature under the identical gap and drawing speed on stainless steel wire of 0.4mm, 0.2mm and 0.1mm nominal diameters. The drawing speed is 0.1m/s and the gap is 0.05mm. The diameters of the die inserts are respectively 0.50mm, 0.30mm, 0.20mm. From the graph it can see that the coating

thickness increases with the diameter of the wire. This perhaps due to the fact that with larger diameter wire the surface area of bonding is greater and hence a larger tensile pull can be applied to the soft layer of polymer at the exit end of the pressure unit. Also for larger diameter wire, the gap is relatively smaller will cause greater hydrodynamic pressure which could give higher coating thickness.

Figure 62 shows the relationship between the diameters of the wires and the maximum permissible drawing speed for the coating thickness of Escoren at 145°C temperature under 0.05mm identical gap on stainless steel wire of 0.4mm, 0.2mm and 0.1mm nominal diameters. The maximum permissible drawing speed is that limit which permits continuous coating thickness. From the graph it can be seen that the permissible drawing speed decreases with the increase of diameter of the wire. This can be explained as that for the thinner wire its area of surface is smaller, the amount of the polymer required by the wire coating is relative less than that for the larger diameter wire. Furthermore, for the larger diameter wire the pressure in the unit reduces because of the increase of the size of the die, which makes insufficient supply of the polymer in the unit.

Figure 63 shows the relationships between the gaps and the maximum permissible drawing speed for the coating thickness of Escoren at 145°C temperature on stainless steel wire of 0.1mm nominal diameter. From Figure 63 it can be seen

that the maximum drawing speed decreases with the increase of the gap. According to the calculation in Chapter 3, the maximum pressure in unit decreases with the diameter of the die insert. In the larger gap the more polymer is required, but corresponding pressure reduces because of the increase of die insert, therefore, the permissible drawing speed will decrease with the increase of the gap.

In overview, the thickness of the wire coating is affected by the drawing speed, the gap, the diameter of the wire, and temperature of polymer melt the main factors being the drawing speed and the gap. The coating thickness decreases with the increase of the drawing speed. The larger the gap, the closer to the gap the coating thickness is. The effect of temperature on the coating thickness has not been observed, but the quality of the coating is affected in the condition of higher or lower temperature. From the results, the optimum temperature is 145°C.

The permissible drawing speed is basically limited by the diameter of the wire and the gap. The higher permissible drawing speed can be achieved for the smaller diameter of the wire. Generally, to obtain the best quality of coating, the choice of the various parameters should be comprehensively considered.

The further improvement of the experimental apparatus is suggested. With the present apparatus, there exists some

instability for the drive system at lower range of drawing speed. Therefore, in order to suit the coating of thinner wire, a drive system which has a smaller inertia is recommended.

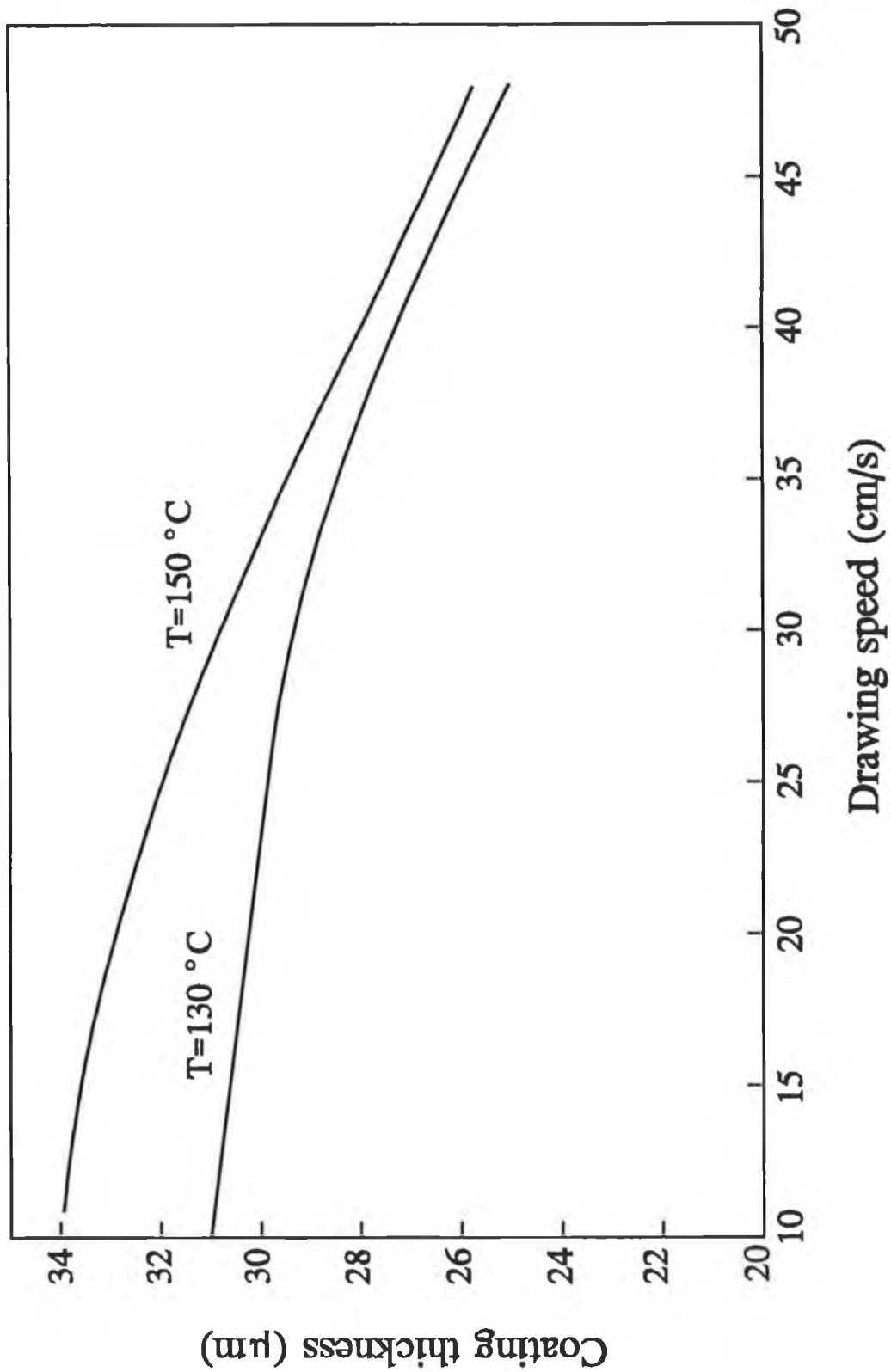

Figure 55 Coating thickness on stainless steel wire. The wire diameter: 0.4mm, die diameter: 0.5mm, polymer: Escoren.

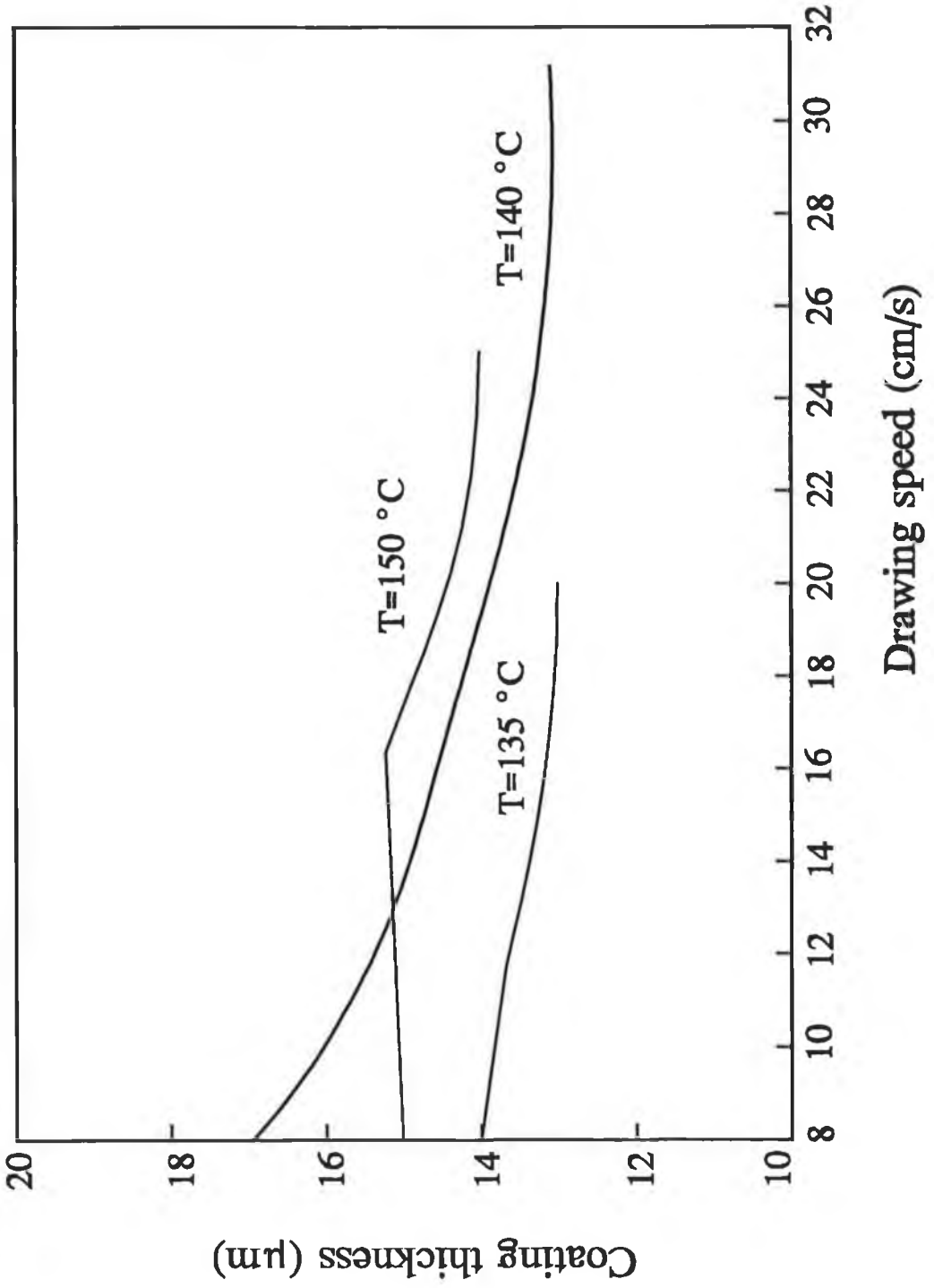

Figure 56 Coating thickness on stainless steel wire. The wire diameter: 0.4mm, die diameter: 0.46mm, polymer: Escoren.

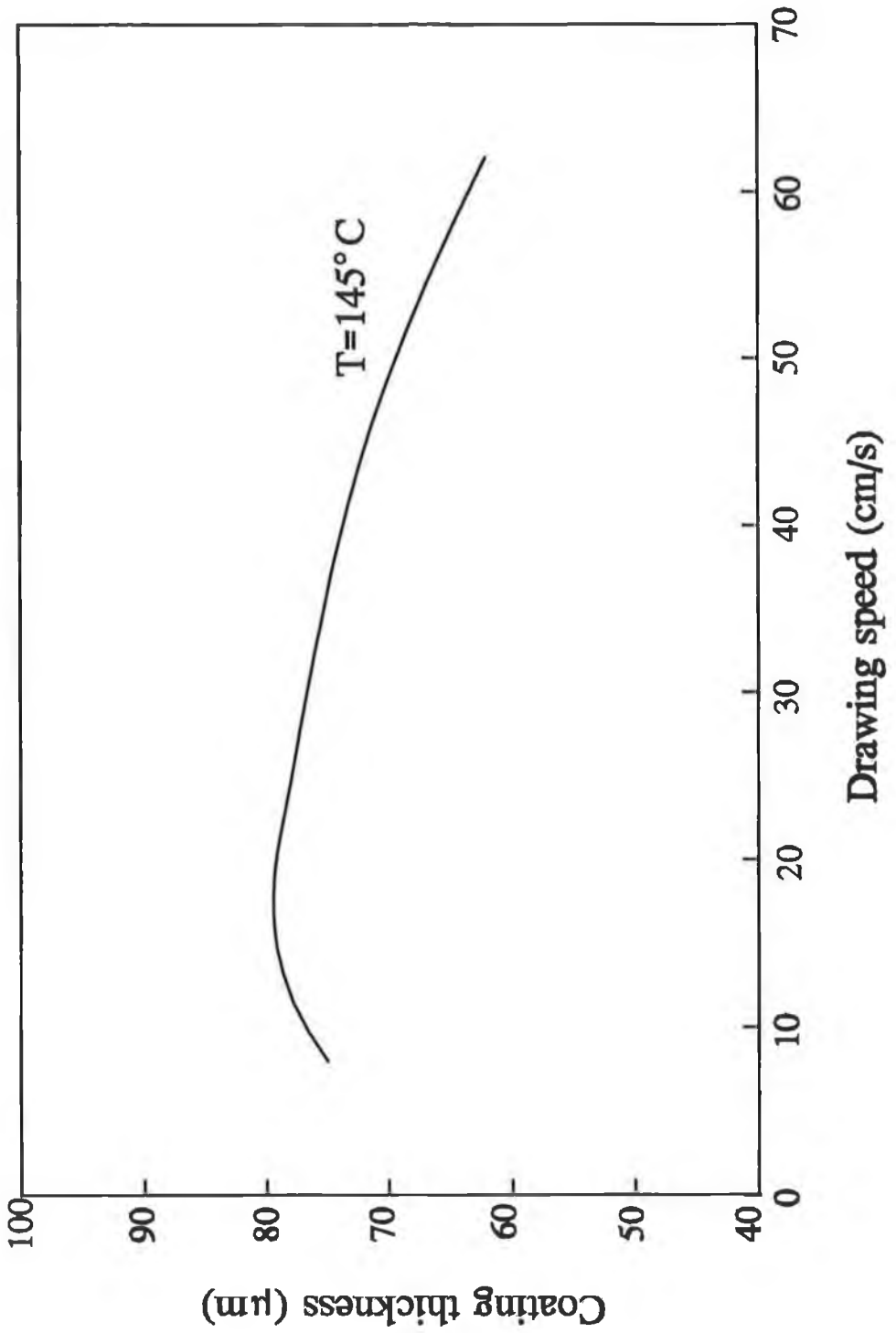

Figure 57 Coating thickness on stainless steel wire. The wire diameter: 0.1mm, die diameter: 0.42mm, polymer: Escoren.

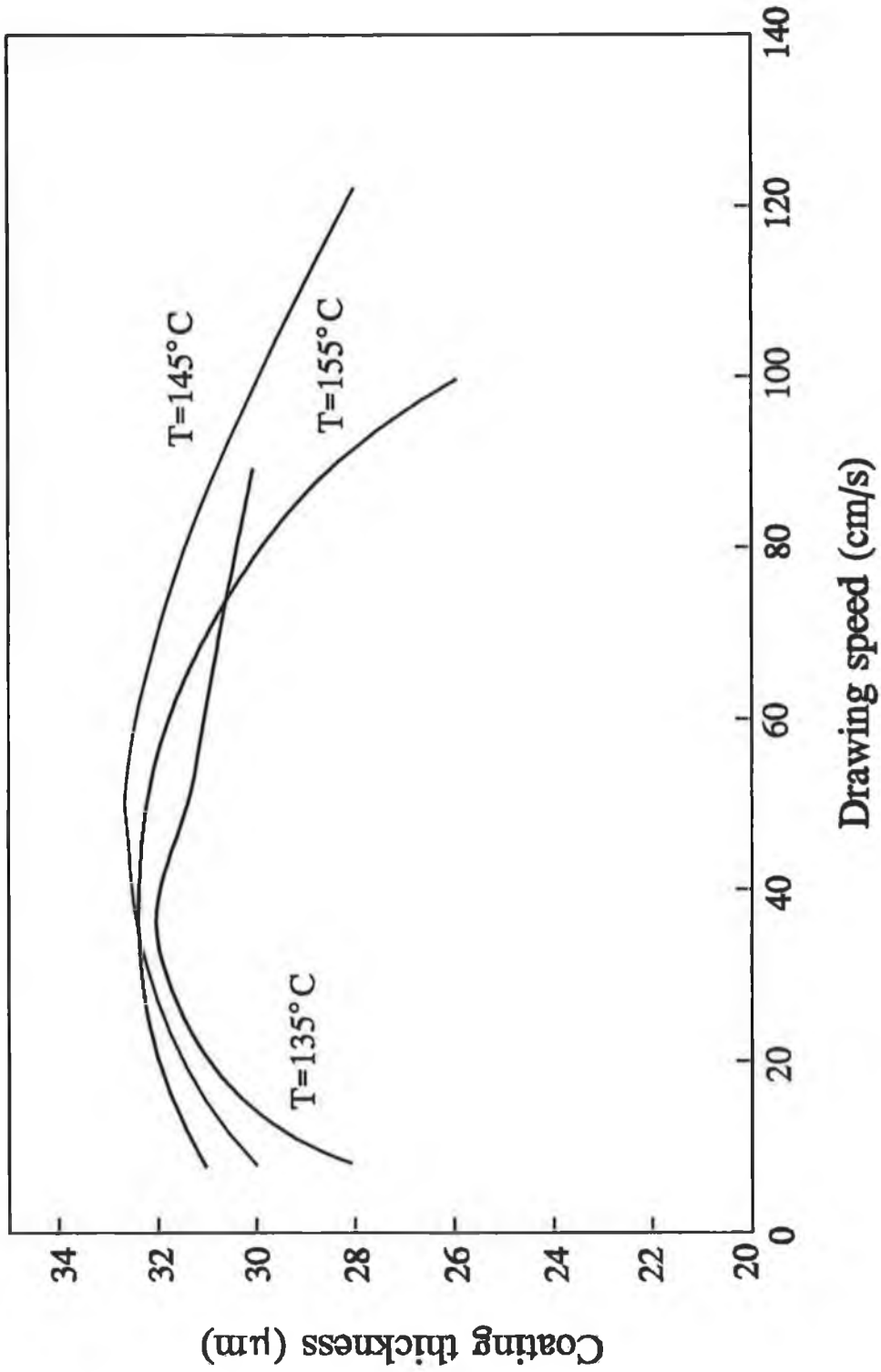

Figure 58 Coating thickness on stainless steel wire. The wire diameter: 0.2mm, die diameter: 0.30mm, polymer: Escoren.

Figure 59 Coating thickness on stainless steel wire. The wire diameter: 0.1mm, the drawing speed: 0.33m/s, polymer: Escoren.

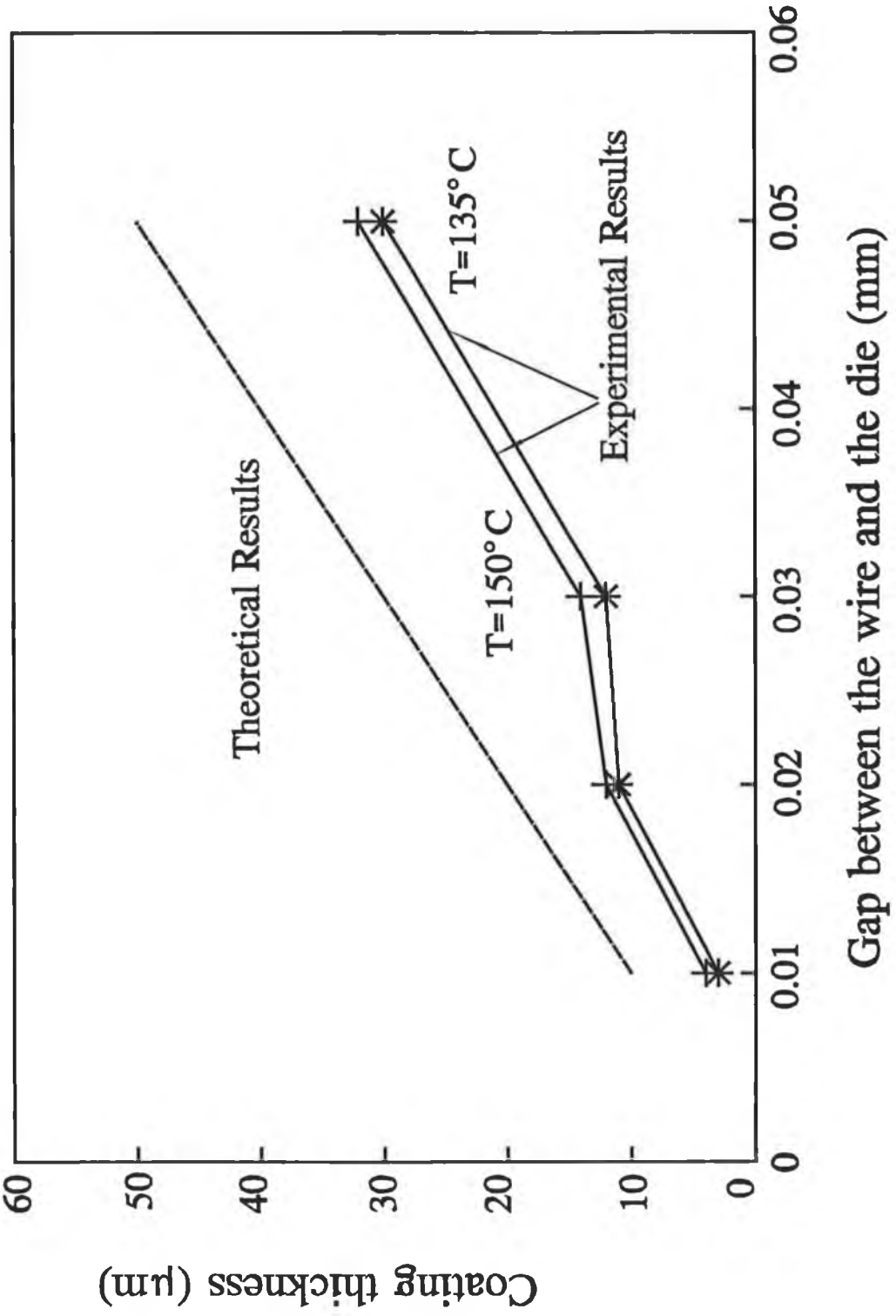

Figure 60 Coating thickness on stainless steel wire. The wire diameter: 0.4mm, the drawing speed: 0.20m/s, polymer: Escoren.

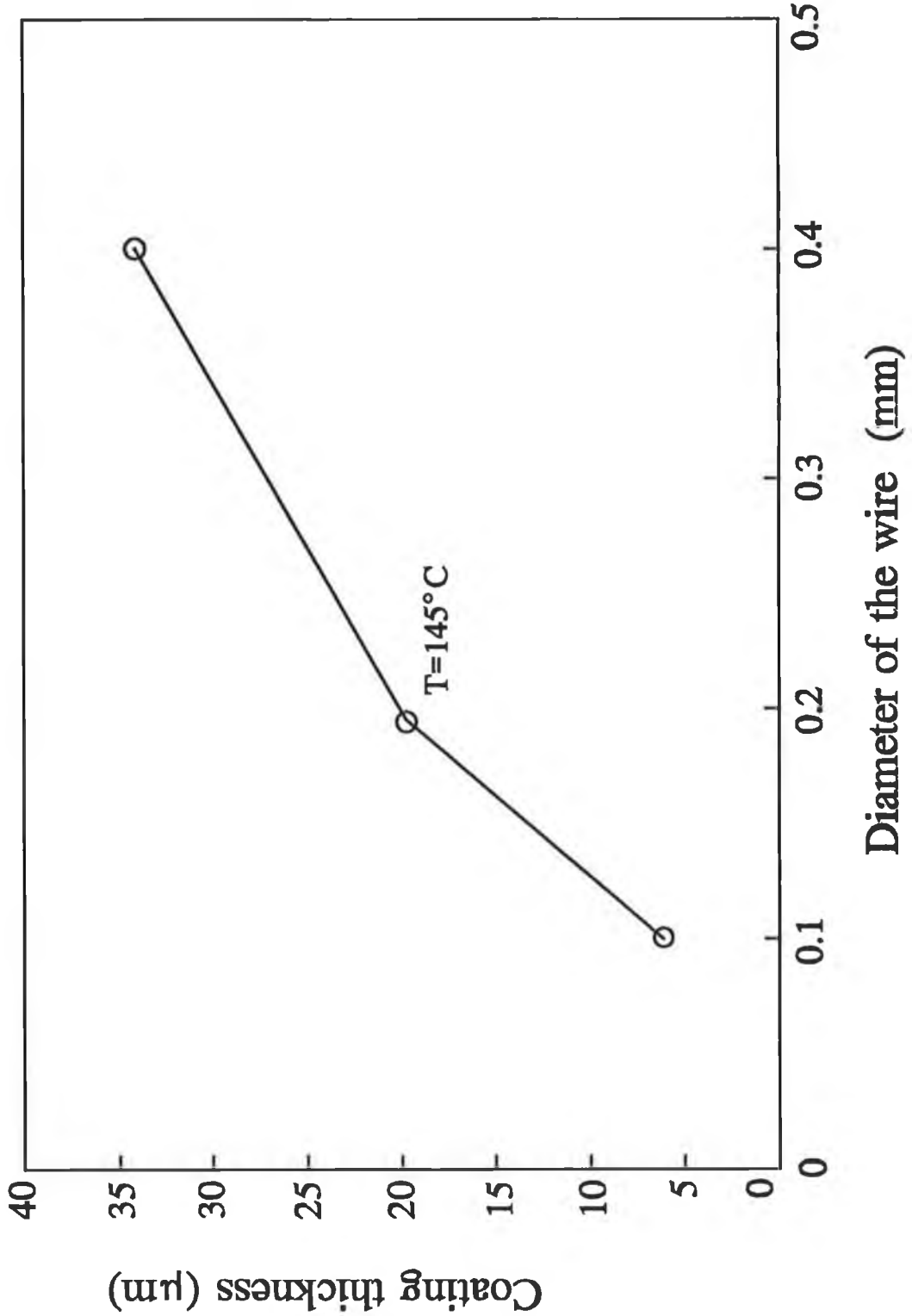

Figure 61 Coating thickness on stainless steel wire. The drawing speed: 0.10m/s, polymer: Escoren, the gap:0.05mm.

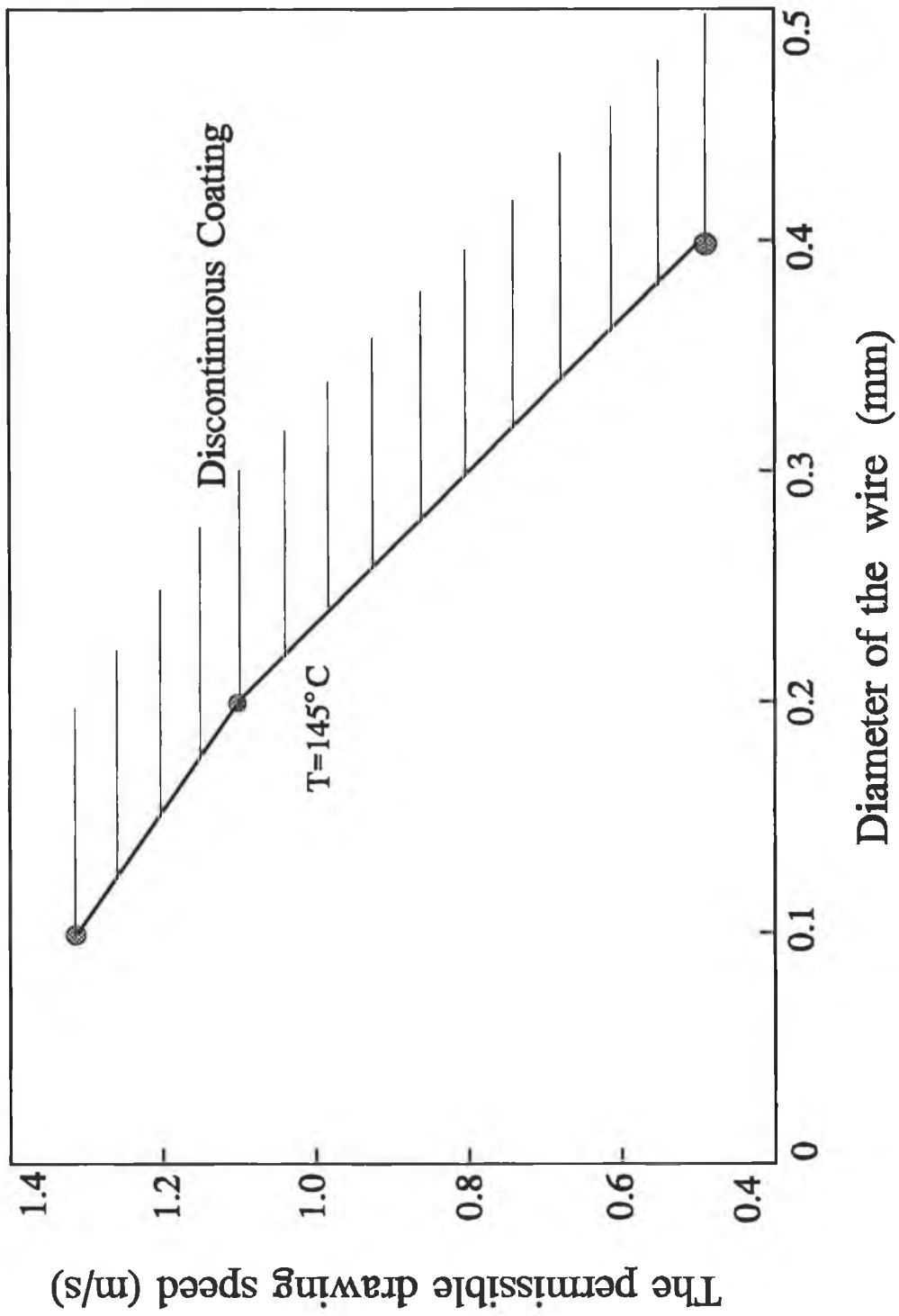

Figure 62 The relationship between the permissible drawing speed and the diameter of the wire. Polymer: Escoren, the gap: 0.05mm.

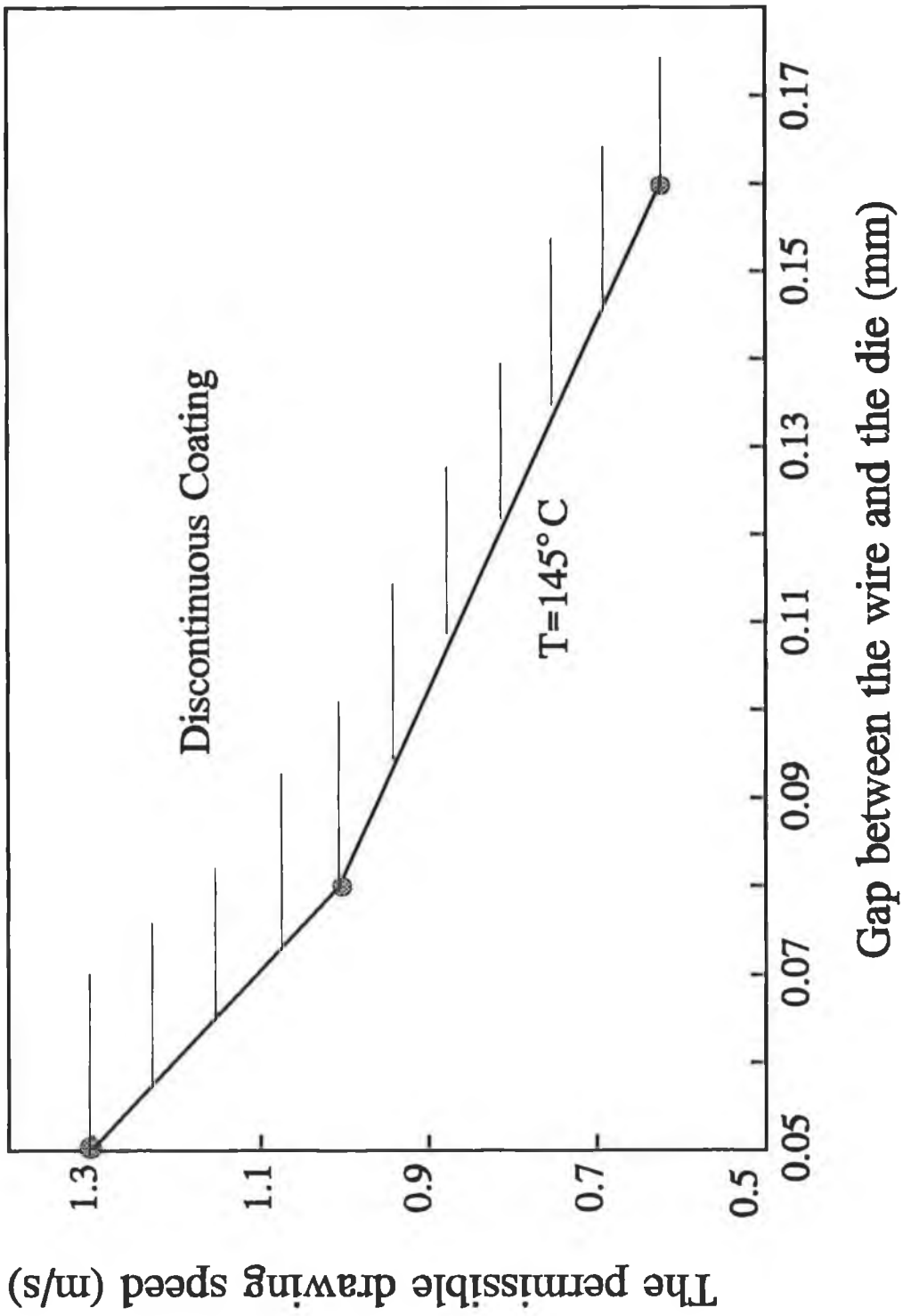

Figure 63 The relationship between the permissible drawing speed and the gap. Polymer: Escoren, temperature: 145°C, the diameter of the wire: 0.1mm.

Chapter 6

Conclusions and Suggestions Future Work

6.1 Conclusions

From the results of theoretical analyses, it can be stated that for Newtonian fluid, the maximum pressure P_m, the pulling force F and the equivalent stress σ_e change linearly with drawing speed for different magnitudes of the inlet length L_1, the outlet length L_2, the outlet radius R_2 and the viscosity of the polymer μ. However, for non-Newtonian fluid, P_m, F and σ_e change non-linearly with drawing speed. The predicted results based on non-Newtonian model are relatively smaller than those based on Newtonian model. For Newtonian fluid, the results obtained under cylindrical coordinate system are relatively smaller than those under Cartesian coordinate system.

A melt chamber and a die unit have been designed and used. The experiments have been carried out with fine wire of diameters ranging from 0.1 mm to 0.4 mm using a number of different dies under different temperature of the polymer melt.

It has been observed from the experimental results that the quality of the coating and the coating thickness of wires depend on a number of parameters including the drawing speed, the diameter of the wire being coated, the gap between the wire and the die and the temperature of the polymer melt, the main factors being the drawing speed and the gap. The bonding quality of the coating with the finer wire is better than the thicker one. The bonding quality is so good that it is not easy to scratch off by sharp edged tool.

6.2 Suggestions for Future Work

The further improvement of the experimental apparatus is suggested. With the present apparatus there exists some instability for the drive system at lower range of the drawing speed. Therefore, in order to suit the coating of thinner wire, a new drive system which will have a smaller inertia is recommended.

The pre-heating system of the wire before it passes through the polymer is suggested to be used. In order to achieve a better quality of coating at higher speeds it may be necessary to supply external air pressure to the polymer melt.

Optical or laser technique for measuring the coated diameter and thus the coating thickness would be desirable in any future work. Qualitative tests by scratching of the

coating by sharp edged tool proved good adhesion. However, quantitative assessment of the bond between the coating and the wire should be carried out. Experiments should be carried out with other polymeric coating materials such as polyester, Nylon etc. and other wire materials, copper, aluminium etc.

References

1. Wistreich J.G "The fundamentals of wire drawing"; Metallurgical Review, 1958, Vol. 3, No 10. p. 97-142.

2. Wistreich J.G. "ABC of Better Lubrication and Cooling in Steel Wire Drawing"; Wire, 1959, Nov. p. 1486

3. Christopherson D.G. & Naylor P.B. "Promotion of Fluid Lubrication in Wire Drawing"; Proceedings of the Institution of Mechanical Engineers, (1955) p. 643.

4. Wistreich J. G. "Lubrication in Wire Drawing" Wear, March 1967, p. 501-511.

5. Sturgen G.M. & Tattersall G.H. "Thick film Lubrication in Wire Drawing."; Wire Industry, (1959) Vol. 26, p. 1183.

6. Tattersall G.H. "Hydrodynamic Lubrication in Wire Drawing"; J. Mech. Eng. Sci., Vol.3, No.4, p. 378.

7. Middlemiss A. "Hydrodynamic Lubrication for Drawing Steel Wire." Tribology in Iron and Steel Works. ISI. Publication p. 125.

8. Orlov S.I., Kolmogorov V.L. Ural Skii. Stukalov V.T. "Integrated Development and Introduction of New High-speed Mills and Hydrodynamic Lubrication Systems for Drawing Wire."; Steel in the U.S.S.R., (1974), October p. 844.

9. Kolmogorov V.L. Selishchev K.P. "Cold Drawing Tubes with Improved Lubrication" Stall in English. 1962. p.830.

10. Bloor M., Dowson D and Parson B. "An Elasto-plasto-hydrodynamic Analysis of The Plane Strain Drawing Process" J.Mech.Sci., Vol.12, No.3, 1970.

11. Kudo H, Tsubouchi M, Takadha H and Okamura K, "An Investigation Into Plasto-hydrodynamic Lubrication with a Cold Sheet Drawing Test", Annals of CIRP, Vol 31/1. p. 175-180, 1974

12. Thompson P.J.& Symmons G.R. " A Plasto-Hydrodynamic Analysis of the Lubrication and Coating of Wire Using Polymer Melt During Drawing." Proc. Instn. Mech. Engrs., Vol. 191, 13/77, 1977.

13. Stevens A.J. " A Plasto-Hydrodynamic Investigation of the Lubrication and Coating of Wire Using a Polymer Melt During Drawing." M.Phil Thesis, Sheffield City Polytechnic. 1979.

14. Crampton R. "Hydrodynamic Lubrication and Coating of Wire Using a Polymer Melt During Drawing Process" PhD. Thesis Sheffield City Polytechnic, 1980

15. Hashmi M.S.J., Symmons G.R. and Parvinmehr H., " A Novel Technique of Wire Drawing" J. Mech. Eng. Sci., Vol 24, p. 1-4, 1982.

16. Symmons G.R., Hashmi M.S.J. and Parvinmehr H., "plasto-hydrodynamic Die-less Wire Drawing: Theoretical Treatment and Experimental Results", Proc. Int. Conf. on Developments in Drawing of Metals, Metal Society, London, p. 54-61, 1983.

17. Parvinmehr H., "Optimisation of Plasto-hydrodynamic System of Wire Drawing Using Polymer Melts", PhD Thesis, Sheffield City Polytechnic,1983.

18. Roger E. Lamb, Plasto-Hydrodynamic Polymer Coating of Fine Wires, M. Phil Thesis, Dublin City University, 1989.

19. Rabinowitsch B, *Uber Eie Viskostat Und Elastizitat Von Solen*, Z. Phys Chem, A145, 1929, pp.141.

20. Edward R. Dougherty, Probability and Statistics for the Engineering, Computing and Physical Sciences, Prentice-Hall International, Inc. 1990.

Appendix I. Program for Calculating Newtonian Analysis (I)

```
C THE PROGRAM IS USED TO FORM GRAPHIC DATA OF u-Pm , u-Force and u-Stress
C IN THE CASE OF VARIABLE L1
C*********************************************************************
C       ***   CALCULATING PROGRAM OF NEWTONIAN FLUID (I)    ***
C*********************************************************************
      IMPLICIT DOUBLE PRECISION (A-H,O-Z)
      DIMENSION V(6),C1(4)
      CHARACTER FILE_N*6,FILE_D*20,FILE_R*10,FILE_P1*20,FILE_P2*20
      CHARACTER FILE_P3*20,FILE_F1*20,FILE_F2*20,FILE_F3*20
      CHARACTER FILE_P4*20,FILE_F4*20
      CHARACTER FILE_S1*20,FILE_S2*20,FILE_S3*20,FILE_S4*20
      WRITE(6,10)
      READ(*,'(A6)') FILE_N
      PI=3.1415926
  10  FORMAT(' The Name of File =')
      FILE_D(1:5)='DATA\'
      FILE_D(6:11)=FILE_N
      FILE_D(12:15)='.DAT'
      FILE_R=FILE_N
      FILE_R(7:10)='.RES'
      FILE_P1(1:8)='CURVE\PL'
      FILE_P1(9:12)=FILE_N(3:6)
      FILE_P1(13:16)='.DT1'
      FILE_P2(1:8)='CURVE\PL'
      FILE_P2(9:12)=FILE_N(3:6)
      FILE_P2(13:16)='.DT2'
      FILE_P3(1:8)='CURVE\PL'
      FILE_P3(9:12)=FILE_N(3:6)
      FILE_P3(13:16)='.DT3'
      FILE_P4(1:8)='CURVE\PL'
      FILE_P4(9:12)=FILE_N(3:6)
      FILE_P4(13:16)='.DT4'
      FILE_F1(1:8)='CURVE\FL'
      FILE_F1(9:12)=FILE_N(3:6)
      FILE_F1(13:16)='.DT1'
      FILE_F2(1:8)='CURVE\FL'
      FILE_F2(9:12)=FILE_N(3:6)
      FILE_F2(13:16)='.DT2'
      FILE_F3(1:8)='CURVE\FL'
      FILE_F3(9:12)=FILE_N(3:6)
      FILE_F3(13:16)='.DT3'
      FILE_F4(1:8)='CURVE\FL'
      FILE_F4(9:12)=FILE_N(3:6)
      FILE_F4(13:16)='.DT4'
      FILE_S1(1:8)='CURVE\SL'
      FILE_S1(9:12)=FILE_N(3:6)
      FILE_S1(13:16)='.DT1'
      FILE_S2(1:8)='CURVE\SL'
```

```
      FILE_S2(9:12)=FILE_N(3:6)
      FILE_S2(13:16)='.DT2'
      FILE_S3(1:8)='CURVE\SL'
      FILE_S3(9:12)=FILE_N(3:6)
      FILE_S3(13:16)='.DT3'
      FILE_S4(1:8)='CURVE\SL'
      FILE_S4(9:12)=FILE_N(3:6)
      FILE_S4(13:16)='.DT4'
      OPEN (5,FILE=FILE_D,STATUS='OLD')
      OPEN (6,FILE=FILE_R)
      OPEN (1,FILE=FILE_P1)
      OPEN (2,FILE=FILE_P2)
      OPEN (3,FILE=FILE_P3)
      OPEN (4,FILE=FILE_P4)
      OPEN (7,FILE=FILE_F1)
      OPEN (8,FILE=FILE_F2)
      OPEN (9,FILE=FILE_F3)
      OPEN (10,FILE=FILE_F4)
      OPEN (11,FILE=FILE_S1)
      OPEN (12,FILE=FILE_S2)
      OPEN (13,FILE=FILE_S3)
      OPEN (14,FILE=FILE_S4)
      READ(5,*) U,R1,C2
      READ(5,*) R0,R2
      READ(5,*) (C1(I),I=1,4)
      READ(5,*) (V(I),I=1,6)
      WRITE(6,20) U,R1,C2
 20   FORMAT('Viscosity Coefficient =',E8.3,/
     . 'Inlet Radius R1 =',E8.3,'(mm)'/
     . 'Outlet die length L2 =',E8.3,'(mm)')
      WRITE(6,30) R0,R2
 30   FORMAT('The radius of wire R0 =',E8.3,'(mm)'/
     . 'Outlet Radius R2 =',E8.3,'(mm)')
      DO 50 IC1=1,4
      WRITE(6,201) IC1,C1(IC1)
 201  FORMAT(/'  *** C1(',I1,')=',E8.3,' (mm) ***')
      DO 50 IV=1,6
      WRITE (6,101) IV,V(IV)
 101  FORMAT(/'*  V(',I1,')=',E8.3,' (m/s) *')
      PM1=(R1**2-R0**2)*(R1-R0)**2/C1(IC1)
      PM2=(R2**2-R0**2)*(R2-R0)**2/C2
      PM0=4.*U*V(IV)*(R1-R2)*(R1+R2+R0)/1000.
      PM=PM0/(PM1+PM2)
      TAO1=(R1-R0)/2*PM/C1(IC1)+U*V(IV)/(R1-R0)/1000
      TAO2=-(R2-R0)/2*PM/C2+U*V(IV)/(R2-R0)/1000
      FORCE=2*PI*R0*(TAO1*C1(IC1)+TAO2*C2)
      SIGMAX=FORCE/PI/R0/R0
      SIGMAJ1=SQRT((SIGMAX+PM)**2+.5*TAO1**2)
      SIGMAJ2=SQRT((SIGMAX+PM)**2+.5*TAO2**2)
      WRITE(6,401) PM
      WRITE(6,402) FORCE
      WRITE(6,406) SIGMAX
      WRITE(6,404) SIGMAJ1
C     WRITE(6,405) SIGMAJ2
      WRITE(IC1,403) V(IV),PM
      WRITE(6+IC1,403) V(IV),FORCE
```

```
      WRITE(10+IC1,403) V(IV),SIGMAJ1
401   FORMAT(' Pm= ',E10.4,' (MPa)')
402   FORMAT(' Force= ',E10.4,' (N)')
403   FORMAT(2E14.4)
404   FORMAT('THE STRESS OF CALCULATION',E10.4,'(MPa)')
405   FORMAT('THE STRESS-II OF CALCULATION',E10.4,'(MPa)')
406   FORMAT('THE PULLING STRESS',E10.4,'(MPa)')
50    CONTINUE
      CLOSE(1)
      CLOSE(2)
      CLOSE(3)
      CLOSE(4)
      CLOSE(5)
      CLOSE(6)
      CLOSE(7)
      CLOSE(8)
      CLOSE(9)
      CLOSE(10)
      CLOSE(11)
      CLOSE(12)
      CLOSE(13)
      CLOSE(14)
      STOP
      END
```

Appendix II. Program for Calculating Newtonian Analysis (II)

```
C THE PROGRAM IS USED TO FORM GRAPHIC DATA OF u-Pm , u-Force and u-Stress
C IN THE CASE OF VARIABLE L2
C*****************************************************************
C        *** CALCULATING PROGRAM OF NEWTONIAN FLUID (II)    ***
C*****************************************************************
      IMPLICIT DOUBLE PRECISION (A-H,O-Z)
      DIMENSION V(6),C2(3)
      CHARACTER FILE_N*6,FILE_D*20,FILE_R*10,FILE_P1*20,FILE_P2*20
      CHARACTER FILE_P3*20,FILE_F1*20,FILE_F2*20,FILE_F3*20
      CHARACTER FILE_S1*20,FILE_S2*20,FILE_S3*20
      WRITE(6,10)
      READ(*,'(A6)') FILE_N
      PI=3.1415926
  10  FORMAT(' The Name of File =')
      FILE_D(1:5)='DATA\'
      FILE_D(6:11)=FILE_N
      FILE_D(12:15)='.DAT'
      FILE_R=FILE_N
      FILE_R(7:10)='.RES'
      FILE_P1(1:8)='CURVE\PC'
      FILE_P1(9:12)=FILE_N(3:6)
      FILE_P1(13:16)='.DT1'
      FILE_P2(1:8)='CURVE\PC'
      FILE_P2(9:12)=FILE_N(3:6)
      FILE_P2(13:16)='.DT2'
      FILE_P3(1:8)='CURVE\PC'
      FILE_P3(9:12)=FILE_N(3:6)
      FILE_P3(13:16)='.DT3'
      FILE_F1(1:8)='CURVE\FC'
      FILE_F1(9:12)=FILE_N(3:6)
      FILE_F1(13:16)='.DT1'
      FILE_F2(1:8)='CURVE\FC'
      FILE_F2(9:12)=FILE_N(3:6)
      FILE_F2(13:16)='.DT2'
      FILE_F3(1:8)='CURVE\FC'
      FILE_F3(9:12)=FILE_N(3:6)
      FILE_F3(13:16)='.DT3'
      FILE_S1(1:8)='CURVE\SC'
      FILE_S1(9:12)=FILE_N(3:6)
      FILE_S1(13:16)='.DT1'
      FILE_S2(1:8)='CURVE\SC'
      FILE_S2(9:12)=FILE_N(3:6)
      FILE_S2(13:16)='.DT2'
      FILE_S3(1:8)='CURVE\SC'
      FILE_S3(9:12)=FILE_N(3:6)
      FILE_S3(13:16)='.DT3'
      OPEN (5,FILE=FILE_D,STATUS='OLD')
      OPEN (6,FILE=FILE_R)
```

```
      OPEN (1,FILE=FILE_P1)
      OPEN (2,FILE=FILE_P2)
      OPEN (3,FILE=FILE_P3)
      OPEN (7,FILE=FILE_F1)
      OPEN (8,FILE=FILE_F2)
      OPEN (9,FILE=FILE_F3)
      OPEN (10,FILE=FILE_S1)
      OPEN (11,FILE=FILE_S2)
      OPEN (12,FILE=FILE_S3)
      READ(5,*) U,R1
      READ(5,*) R0,R2,C1
      READ(5,*) (C2(I),I=1,3)
      READ(5,*) (V(I),I=1,6)
      WRITE(6,20) U,R1,C1
   20 FORMAT('Viscosity Coefficient =',E8.3,'Ns/m²'/
     . 'Inlet Radius R1 =',E8.3,'(mm)'/
     . 'Inlet die length L1 =',E8.3,'(mm)')
      WRITE(6,30) R0,R2
   30 FORMAT('The radius of wire R0 =',E8.3,'(mm)'/
     . 'Outlet Radius R2 =',E8.3,'(mm)')
      DO 50 IC2=1,3
      WRITE(6,201) IC2,C2(IC2)
  201 FORMAT(/'  *** C2(',I1,')=',E8.3,' (mm) ***')
      DO 50 IV=1,6
      WRITE (6,101) IV,V(IV)
  101 FORMAT(/'*  V(',I1,')=',E8.3,' (m/s) *')
C ** The unit of mu U is Ns/m² AND that of Pm is MPa.
      PM1=(R1**2-R0**2)*(R1-R0)**2/C1
      PM2=(R2**2-R0**2)*(R2-R0)**2/C2(IC2)
      PM0=4.*U*V(IV)*(R1-R2)*(R1+R2+R0)
      PM=PM0/(PM1+PM2)/1000.
      CC1=(R0+R1)*PM/C1/2.+U*V(IV)/(R1-R0)/1000.
      CC2=R0*R1/2./U*PM/C1*1000.+R1*V(IV)/(R1-R0)
      TAO1=(R1-R0)/2*PM/C1+U*V(IV)/(R1-R0)/1000.
      TAO2=-(R2-R0)/2*PM/C2(IC2)+U*V(IV)/(R2-R0)/1000.
      FORCE=2*PI*R0*(TAO1*C1+TAO2*C2(IC2))
      SIGMAX=FORCE/PI/R0/R0
      SIGMAJ1=SQRT((SIGMAX+PM)**2+.5*TAO1**2)
      SIGMAJ2=SQRT((SIGMAX+PM)**2+.5*TAO2**2)
      WRITE(6,401) PM
      WRITE(6,402) FORCE
      WRITE(6,406) SIGMAX
      WRITE(6,404) SIGMAJ1
C     WRITE(6,405) SIGMAJ2
      WRITE(IC2,403) V(IV),PM
      WRITE(6+IC2,403) V(IV),FORCE
      WRITE(9+IC2,403) V(IV),SIGMAJ1
  401 FORMAT(' Pm= ',E10.4,' (MPa)')
  402 FORMAT(' Force= ',E10.4,' (N)')
  403 FORMAT(2E14.4)
  404 FORMAT('THE STRESS OF CALCULATION',E10.4,'(MPa)')
  405 FORMAT('THE STRESS-II OF CALCULATION',E10.4,'(MPa)')
  406 FORMAT('THE PULLING STRESS',E10.4,'(MPa)')
   50 CONTINUE
      CLOSE(1)
      CLOSE(2)
```

```
CLOSE(3)
CLOSE(5)
CLOSE(6)
CLOSE(7)
CLOSE(8)
CLOSE(9)
CLOSE(10)
CLOSE(11)
CLOSE(12)
STOP
END
```

Appendix III. Program for Calculating Newtonian Analysis (III)

```
C THE PROGRAM IS USED TO DRAW GRAPHIC DATA OF u-Pm, u-Force and u-Stress
C IN THE CASE OF VARIABLE R2
C*****************************************************************
C          ***   CALCULATING PROGRAM OF NEWTONIAN FLUID   ***
C*****************************************************************
      IMPLICIT DOUBLE PRECISION (A-H,O-Z)
      DIMENSION V(6),R2(4)
      CHARACTER FILE_N*6,FILE_D*20,FILE_R*20,FILE_P1*20,FILE_P2*20
      CHARACTER FILE_P3*20,FILE_F1*20,FILE_F2*20,FILE_F3*20
      CHARACTER FILE_P4*20,FILE_F4*20
      CHARACTER FILE_S1*20,FILE_S2*20,FILE_S3*20,FILE_S4*20
      WRITE(6,10)
      READ(*,'(A6)') FILE_N
      PI=3.1415926
  10  FORMAT(' The Name of File =')
      FILE_D(1:5)='DATA\'
      FILE_D(6:11)=FILE_N
      FILE_D(12:15)='.DAT'
      FILE_R=FILE_N
      FILE_R(7:10)='.RES'
      FILE_P1(1:8)='CURVE\PR'
      FILE_P1(9:12)=FILE_N(3:6)
      FILE_P1(13:16)='.DT1'
      FILE_P2(1:8)='CURVE\PR'
      FILE_P2(9:12)=FILE_N(3:6)
      FILE_P2(13:16)='.DT2'
      FILE_P3(1:8)='CURVE\PR'
      FILE_P3(9:12)=FILE_N(3:6)
      FILE_P3(13:16)='.DT3'
      FILE_P4(1:8)='CURVE\PR'
      FILE_P4(9:12)=FILE_N(3:6)
      FILE_P4(13:16)='.DT4'
      FILE_F1(1:8)='CURVE\FR'
      FILE_F1(9:12)=FILE_N(3:6)
      FILE_F1(13:16)='.DT1'
      FILE_F2(1:8)='CURVE\FR'
      FILE_F2(9:12)=FILE_N(3:6)
      FILE_F2(13:16)='.DT2'
      FILE_F3(1:8)='CURVE\FR'
      FILE_F3(9:12)=FILE_N(3:6)
      FILE_F3(13:16)='.DT3'
      FILE_F4(1:8)='CURVE\FR'
      FILE_F4(9:12)=FILE_N(3:6)
      FILE_F4(13:16)='.DT4'
      FILE_S1(1:8)='CURVE\SR'
      FILE_S1(9:12)=FILE_N(3:6)
      FILE_S1(13:16)='.DT1'
      FILE_S2(1:8)='CURVE\SR'
```

```
      FILE_S2(9:12)=FILE_N(3:6)
      FILE_S2(13:16)='.DT2'
      FILE_S3(1:8)='CURVE\SR'
      FILE_S3(9:12)=FILE_N(3:6)
      FILE_S3(13:16)='.DT3'
      FILE_S4(1:8)='CURVE\SR'
      FILE_S4(9:12)=FILE_N(3:6)
      FILE_S4(13:16)='.DT4'
      OPEN (5,FILE=FILE_D,STATUS='OLD')
      OPEN (6,FILE=FILE_R)
      OPEN (1,FILE=FILE_P1)
      OPEN (2,FILE=FILE_P2)
      OPEN (3,FILE=FILE_P3)
      OPEN (4,FILE=FILE_P4)
      OPEN (7,FILE=FILE_F1)
      OPEN (8,FILE=FILE_F2)
      OPEN (9,FILE=FILE_F3)
      OPEN (10,FILE=FILE_F4)
      OPEN (11,FILE=FILE_S1)
      OPEN (12,FILE=FILE_S2)
      OPEN (13,FILE=FILE_S3)
      OPEN (14,FILE=FILE_S4)
      READ(5,*) U,R1,C2
      READ(5,*) R0,C1
      READ(5,*) (R2(I),I=1,4)
      READ(5,*) (V(I),I=1,6)
      WRITE(6,20) U,R1,C2
 20   FORMAT('Viscosity Coefficient =',E8.3,/
     . 'Inlet Radius R1 =',E8.3,'(mm)'/
     . 'Outlet die length L2 =',E8.3,'(mm)')
      WRITE(6,30) R0,C1
30    FORMAT('The radius of wire R0 =',E8.3,'(mm)'/
     . 'Inlet die length L1 =',E8.3,'(mm)')
      DO 50 IR2=1,4
      WRITE(6,201) IR2,R2(IR2)
201   FORMAT(/'  *** R2(',I1,')=',E8.3,' (mm) ***')
      DO 50 IV=1,6
      WRITE (6,101) IV,V(IV)
101   FORMAT(/'*  V(',I1,')=',E8.3,' (m/s) *')
      PM1=(R1**2-R0**2)*(R1-R0)**2/C1
      PM2=(R2(IR2)**2-R0**2)*(R2(IR2)-R0)**2/C2
      PM0=4.*U*V(IV)*(R1-R2(IR2))*(R1+R2(IR2)+R0)/1000.
      PM=PM0/(PM1+PM2)
      TAO1=(R1-R0)/2*PM/C1+U*V(IV)/(R1-R0)/1000.
      TAO2=-(R2(IR2)-R0)/2*PM/C2+U*V(IV)/(R2(IR2)-R0)/1000.
      FORCE=2*PI*R0*(TAO1*C1+TAO2*C2)
      SIGMAX=FORCE/PI/R0/R0
      SIGMAJ1=SQRT((SIGMAX+PM)**2+.5*TAO1**2)
      SIGMAJ2=SQRT((SIGMAX+PM)**2+.5*TAO2**2)
      WRITE(6,401) PM
      WRITE(6,402) FORCE
      WRITE(6,406) SIGMAX
      WRITE(6,404) SIGMAJ1
      WRITE(IR2,403) V(IV),PM
      WRITE(6+IR2,403) V(IV),FORCE
      WRITE(10+IR2,403) V(IV),SIGMAJ1
```

```
401   FORMAT(' Pm= ',E10.4,' (MPa)')
402   FORMAT(' Force= ',E10.4,' (N)')
403   FORMAT(2E10.4)
404   FORMAT('THE STRESS OF CALCULATION',E10.4,'(MPa)')
406   FORMAT('THE PULLING STRESS',E10.4,'(MPa)')
50    CONTINUE
      CLOSE(1)
      CLOSE(2)
      CLOSE(3)
      CLOSE(4)
      CLOSE(5)
      CLOSE(6)
      CLOSE(7)
      CLOSE(8)
      CLOSE(9)
      CLOSE(10)
      CLOSE(11)
      CLOSE(12)
      CLOSE(13)
      CLOSE(14)
      STOP
      END
```

Appendix IV. Program for Calculating Newtonian Analysis (IV)

```
C THE PROGRAM IS USED TO FORM GRAPHIC DATA OF u-Pm , u-Force and u-Stress
C IN THE CASE OF VARIABLE μ
C*****************************************************************
C          ***   CALCULATING PROGRAM OF NEWTONIAN FLUID   ***
C*****************************************************************
      IMPLICIT DOUBLE PRECISION (A-H,O-Z)
      DIMENSION V(6),U(3)
      CHARACTER FILE_N*6,FILE_D*20,FILE_R*10,FILE_P1*20,FILE_P2*20
      CHARACTER FILE_P3*20,FILE_F1*20,FILE_F2*20,FILE_F3*20
      CHARACTER FILE_S1*20,FILE_S2*20,FILE_S3*20
      WRITE(6,10)
      READ(*,'(A6)') FILE_N
      PI=3.1415926
  10  FORMAT(' The Name of File =')
      FILE_D(1:5)='DATA\'
      FILE_D(6:11)=FILE_N
      FILE_D(12:15)='.DAT'
      FILE_R=FILE_N
      FILE_R(7:10)='.RES'
      FILE_P1(1:8)='CURVE\PU'
      FILE_P1(9:12)=FILE_N(3:6)
      FILE_P1(13:16)='.DT1'
      FILE_P2(1:8)='CURVE\PU'
      FILE_P2(9:12)=FILE_N(3:6)
      FILE_P2(13:16)='.DT2'
      FILE_P3(1:8)='CURVE\PU'
      FILE_P3(9:12)=FILE_N(3:6)
      FILE_P3(13:16)='.DT3'
      FILE_F1(1:8)='CURVE\FU'
      FILE_F1(9:12)=FILE_N(3:6)
      FILE_F1(13:16)='.DT1'
      FILE_F2(1:8)='CURVE\FU'
      FILE_F2(9:12)=FILE_N(3:6)
      FILE_F2(13:16)='.DT2'
      FILE_F3(1:8)='CURVE\FU'
      FILE_F3(9:12)=FILE_N(3:6)
      FILE_F3(13:16)='.DT3'
      FILE_S1(1:8)='CURVE\SU'
      FILE_S1(9:12)=FILE_N(3:6)
      FILE_S1(13:16)='.DT1'
      FILE_S2(1:8)='CURVE\SU'
      FILE_S2(9:12)=FILE_N(3:6)
      FILE_S2(13:16)='.DT2'
      FILE_S3(1:8)='CURVE\SU'
      FILE_S3(9:12)=FILE_N(3:6)
      FILE_S3(13:16)='.DT3'
      OPEN (5,FILE=FILE_D,STATUS='OLD')
      OPEN (6,FILE=FILE_R)
```

```
      OPEN (1,FILE=FILE_P1)
      OPEN (2,FILE=FILE_P2)
      OPEN (3,FILE=FILE_P3)
      OPEN (7,FILE=FILE_F1)
      OPEN (8,FILE=FILE_F2)
      OPEN (9,FILE=FILE_F3)
      OPEN (10,FILE=FILE_S1)
      OPEN (11,FILE=FILE_S2)
      OPEN (12,FILE=FILE_S3)
      READ(5,*) R1,C2,C1
      READ(5,*) R0,R2
      READ(5,*) (U(I),I=1,3)
      READ(5,*) (V(I),I=1,6)
      WRITE(6,20) R1,C1,C2
   20 FORMAT('Inlet Radius R1 =',E8.3,'(mm)'/
     . 'Inlet die length L1 =',E8.3,'(mm)'/
     . 'Outlet die length L2 =',E8.3,'(mm)')
      WRITE(6,30) R0,R2
   30 FORMAT('The radius of wire R0 =',E8.3,'(mm)'/
     . 'Outlet Radius R2 =',E8.3,'(mm)')
      DO 50 IU=1,3
      WRITE(6,201) IU,U(IU)
  201 FORMAT('  *** U(',I1,')=',E8.3,' (mm) ***')
      DO 50 IV=1,6
      WRITE (6,101) IV,V(IV)
  101 FORMAT('*  V(',I1,')=',E8.3,' (m/s) *')
      PM1=(R1**2-R0**2)*(R1-R0)**2/C1
      PM2=(R2**2-R0**2)*(R2-R0)**2/C2
      PM0=4.*U(IU)*V(IV)*(R1-R2)*(R1+R2+R0)/1000.
      PM=PM0/(PM1+PM2)
      TAO1=(R1-R0)/2*PM/C1+U(IU)*V(IV)/(R1-R0)/1000
      TAO2=-(R2-R0)/2*PM/C2+U(IU)*V(IV)/(R2-R0)/1000
      FORCE=2*PI*R0*(TAO1*C1+TAO2*C2)
      SIGMAX=FORCE/PI/R0/R0
      SIGMAJ1=SQRT((SIGMAX+PM)**2+.5*TAO1**2)
      SIGMAJ2=SQRT((SIGMAX+PM)**2+.5*TAO2**2)
      WRITE(6,401) PM
      WRITE(6,402) FORCE
      WRITE(6,406) SIGMAX
      WRITE(6,404) SIGMAJ1
C     WRITE(6,405) SIGMAJ2
      WRITE(IU,403) V(IV),PM
      WRITE(6+IU,403) V(IV),FORCE
      WRITE(9+IU,403) V(IV),SIGMAJ1
  401 FORMAT(' Pm= ',E10.4,' (MPa)')
  402 FORMAT(' Force= ',E10.4,' (N)')
  403 FORMAT(2E14.4)
  404 FORMAT('THE STRESS OF CALCULATION',E10.4,'(MPa)')
  405 FORMAT('THE STRESS-II OF CALCULATION',E10.4,'(MPa)')
  406 FORMAT('THE PULLING STRESS',E10.4,'(MPa)')
   50 CONTINUE
      CLOSE(1)
      CLOSE(2)
      CLOSE(3)
      CLOSE(5)
      CLOSE(6)
```

```
CLOSE(7)
CLOSE(8)
CLOSE(9)
CLOSE(10)
CLOSE(11)
CLOSE(12)
STOP
END
```

Appendix V. Program for Calculating Non-Newtonian Analysis

```
C*********************************************************************
C       ***   CALCULATING PROGRAM OF NON-NEWTONIAN FLUID   ***
C*********************************************************************
      IMPLICIT DOUBLE PRECISION (A-H,O-Z)
      COMMON PK,PMU,R0,R(2),CL(2),CC(4),V,PMS,DX,U(4)
C     DIMENSION V(6),R0(4),R2(4,4),C1(3)
      CALL INPUT
      WRITE(6,201)
      PK0=PK
      DPK=PK0/10.
      PK=0.
  10  CALL EQU0(PM)
      PK=PK+DPK
      IF (PK .LE. PK0) GOTO 10
      CLOSE(6)
 201  FORMAT('        k        Pm(MPa)      Force(N)'
     .'      Stress(MPa)       u0        u1')
      STOP
      END


      SUBROUTINE EQU0(PM)
C*********************************************************************
C            *** CALCULATION OF THE MEAN PRESSURE Pm   ***
C*********************************************************************
      IMPLICIT DOUBLE PRECISION (A-H,O-Z)
      COMMON PK,PMU,R0,R(2),CL(2),CC(4),V,PMS,DX,U(4)
      PI=3.1415926
      EPS=.000001
      X1=PMS
      CALL FUNX(X1,FUN)
      F1=FUN
      IF(F1 .EQ. 0.) THEN
      PM=X1
      GOTO 20
      ENDIF
      X2=X1+DX
      CALL FUNX(X2,FUN)
      F2=FUN
      IF (F2 .EQ. 0.) THEN
      PM=X2
      GOTO 20
      ENDIF
  10  FORMAT(2F12.7)
   5  A=X1-F1*(X2-X1)/(F2-F1)
      CALL FUNX(A,FUN)
      FA=FUN
      IF (FA .EQ. 0.) THEN
      PM=A
```

```
      GOTO 20
      ENDIF
      X1=X2
      F1=F2
      X2=A
      F2=FA
      IF (ABS(X1-X2) .GT. EPS) GOTO 5
      PM=X2
  20  TAO10=CC(1)-PM*R0/CL(1)
      TAO20=CC(3)-PM*R0/CL(2)
      TAO11=CC(1)-PM*R(1)/CL(1)
      TAO22=CC(3)-PM*R(2)/CL(2)
      FORCE=2*PI*R0*(TAO10*CL(1)-TAO20*CL(2))
      SIGMAX=FORCE/PI/R0/R0
      SIGMAJ1=SQRT((SIGMAX+PM)**2+.5*TAO10**2)
      SIGMAJ2=SQRT((SIGMAX+PM)**2+.5*TAO20**2)
      DO 35 I=1,2
      TEM1=PM/CL(I)
      TEM2=TEM1*R0
      U(2*I-1)=R0*((TEM2*TEM2*PK+2.)*TEM2/4.-CC(2*I-1)*((TEM2*
     . TEM2*PK+1.)-CC(2*I-1)*PK*(1.5*TEM2-CC(2*I-1))))+CC(2*I)
      U(2*I-1)=U(2*I-1)/PMU
      TEM3=TEM1*R(I)
      U(2*I)=R(I)*((TEM3*TEM3*PK+2.)*TEM3/4.-CC(2*I-1)*(((TEM3*
     . TEM3*PK+1.)-CC(2*I-1)*PK*(1.5*TEM3-CC(2*I-1)))))+CC(2*I)
      U(2*I)=U(2*I)/PMU
  35  CONTINUE
      WRITE(6,25) PK,PM,FORCE,SIGMAJ1
   25 FORMAT(3X(4E12.5))
      RETURN
      END

      SUBROUTINE INPUT
C*********************************************************************
C                  ***   INPUT OF INITIAL DATA   ***
C*********************************************************************
      IMPLICIT DOUBLE PRECISION (A-H,O-Z)
      COMMON PK,PMU,R0,R(2),CL(2),CC(4),V,PMS,DX,U(4)
      OPEN (5,FILE='NON.DAT',STATUS='OLD')
      OPEN (6,FILE='NON.RES')
C
C**  PARAMETERS OF FLUID PROPERTIES
C
      READ(5,*) PK,PMU
C
C**  PARAMETERS OF DIMENSIONS OF DIE AND WIRE
C
      READ(5,*) R0,R(1),R(2),CL(1),CL2
      CL(2)=-CL2
      READ(5,*) V,PMS,DX
      WRITE (6,101) R0,R(1),R(2)
  101 FORMAT('R0=',F8.3,' (mm),',3X,'R1=',F8.3,' (mm),',3X,
     . 'R2=',F8.3,' (mm)')
      WRITE(6,102) PMU,V
  102 FORMAT('Coefficient of Viscosity=',E10.4,'(Ns/mm^2)'/
     . 'Pulling velocity=', F8.3,'(mm/s)'/)
```

```
      RETURN
      END

      SUBROUTINE FUNX(X,FUN)
C**********************************************************************
C                 ***   CALCULATION OF Q(1)-Q(2)    ***
C**********************************************************************
      IMPLICIT DOUBLE PRECISION (A-H,O-Z)
      COMMON PK,PMU,R0,R(2),CL(2),CC(4),V,PMS,DX,U(4)
      DIMENSION Q(2)
C***  Calculation of Coefficients of equations to solve C1 and C3
      DO 50 I=1,2
      CF0=PMU*V-(R0*R0-R(I)*R(I))/4.*X/CL(I)*(2+PK*(R0*R0+R(I)*R(I))
     .*X*X/CL(I)/CL(I))
      CF1=(R0-R(I))*(1+PK*(R0*R0+R0*R(I)+R(I)*R(I))*X*X/CL(I)/CL(I))
      CF2=-3*PK/2.*X/CL(I)*(R0*R0-R(I)*R(I))
      CF3=PK*(R0-R(I))
      CALL EQU2(CF0,CF1,CF2,CF3,CC(2*I-1))
C***   Calculating C2 and C4
      C20=V*PMU-R0*R0/4.*X/CL(I)*(2+PK*R0*R0*X*X/CL(I)/CL(I))
      C21=R0*(1+PK*R0*R0*X*X/CL(I)/CL(I))
      C22=-3*PK/2.*X/CL(I)*R0*R0
      C23=PK*R0
      CC(2*I)=(C21*CC(2*I-1)+C22*CC(2*I-1)*CC(2*
     . (I-1)+1)+C23*CC(2*I-1)*CC(2*I-1)*CC(2*I-1)+C20)
C***  Calculation of Coefficients Q
      PI=4*ATAN(1D0)
      TEM1=X/CL(I)
      Q(I)=(PK*TEM1**3*(R(I)**6-R0**6)/12.-0.4*PK*
     . CC(2*I-1)*TEM1*TEM1*(R(I)**5-R0**5)+(3*PK*
     . CC(2*I-1)*CC(2*I-1)+1)/4*TEM1*(R(I)**4-R0**4)-
     . 2./3.*(R(I)**3-R0**3)*(CC(2*I-1)+CC(2*I-1)**3*PK)+
     . CC(2*I)*(R(I)*R(I)-R0*R0))
  50  CONTINUE
      FUN=Q(1)-Q(2)
      RETURN
      END


      SUBROUTINE EQU2(CF0,CF1,CF2,CF3,X2)
C**********************************************************************
C   ***  CALCULATION OF COEFFICIENTS Cs USING NUMERICAL METHOD    ***
C**********************************************************************
C**
C** This is used to solve a third-order-power-function equation,
C** cf0+cf1*x+cf2*x*x+cf3*x*x*x=0, which is called twice to obtain
C** C1 and C3 respectively.
C**
      IMPLICIT DOUBLE PRECISION (A-H,O-Z)
      COMMON PK,PMU,R0,R(2),CL(2),CC(4),V,PMS,DX,U(4)
      XS=PMS
      DS=DX
      EPS=.0000001
      X1=XS
      F1=CF0+CF1*X1+CF2*X1*X1+CF3*X1**3
      IF(F1) 1,2,1
```

```
 1  X2=X1+DX
    F2=CF0+CF1*X2+CF2*X2*X2+CF3*X2**3
    IF (F2) 90,7,90
90  IF (ABS(X1-X2)-EPS) 7,7,8
 8  A=X1-F1*(X2-X1)/(F2-F1)
    FA=CF0+CF1*A+CF2*A*A+CF3*A**3
    IF (FA) 9,3,9
 9  X1=X2
    F1=F2
    X2=A
    F2=FA
    GOTO 90
 2  X2=X1
 3  X2=A
 7  RETURN
    END
```

Appendix VI. Experimental Results

This Appendix contains the experimental results of this research project.

n: The motor's running speed;

u_0: The drawing speed;

D_0 The nominal diameter of the bare wire;

$\bar{D}_0$: The mean diameter of the bare wire;

D: The mean diameter of the coated wire;

δ: The coating thickness, $\delta=(D-\bar{d})/2$;

D_2: The diameter of the die;

T: The temperature of the polymer melt;

S_d: The error of the bare wire;

S_D: The error of the coated wire;

S_δ: The error of the coating thickness, i.e. $S_\delta=(S_D^2+S_d^2)^{1/2}$;

D.C.: Discontinuous coating.

A. Measurements of the Diameters of Bare Wires

1. Stainless Steel Wire with a Nominal Diameter of 0.1 mm

   a. Measured Diameter (mm).

0.099	0.099	0.099	0.099	0.099	0.099
0.100	0.100	0.100	0.100	0.099	0.100

   b. Mean Diameter: $\bar{D}_0=0.099$ mm;

   c. The error: $S_d=0.0003$ mm.

2. Stainless Steel Wire with a Nominal Diameter of 0.2 mm

   a. Measured Diameter (mm)

0.399	0.400	0.399	0.401	0.400	0.399
0.399	0.400	0.400	0.399	0.400	0.400

b. Mean Diameter: $\overline{D}_0$=0.400 mm;

c. The error: S_d=0.0004 mm.

3. Stainless Steel Wire with a Nominal Diameter of 0.4 mm

a. Measured Diameter (mm)

0.192	0.193	0.193	0.192	0.192	0.193
0.192	0.193	0.193	0.192	0.192	0.192

b. Mean Diameter: $\overline{D}_0$=0.192 mm;

c. The error: S_d=0.0003 mm.

B. Measurements of the Coated Wires

1. D_0=0.4mm, D_2=0.50mm, T=130°C.

n(rpm)	120	240	350	480	600
u_o(m/s)	0.10	0.20	0.28	0.39	0.49
1	0.464	0.457	0.456	0.452	D.C.
2	0.458	0.455	0.463	0.448	
3	0.465	0.459	0.460	0.446	
4	0.460	0.464	0.462	0.454	
5	0.462	0.457	0.455	0.442	
6	0.461	0.463	0.454	0.458	
D	0.462	0.459	0.458	0.450	
S_D	0.003	0.004	0.004	0.006	
$\delta \pm S_\delta$	0.031 ±0.003	0.030 ±0.004	0.029 ±0.004	0.025 ±0.006	

2. D_0=0.4mm, D_2=0.50mm, T=150°C.

n(rpm)	140	260	380	500	600	700
u_o(m/s)	0.11	0.21	0.31	0.41	0.49	0.57
1	0.468	0.469	0.468	0.463	0.460	D.C.
2	0.469	0.468	0.447	0.451	0.451	
3	0.468	0.456	0.459	0.456	0.455	
4	0.466	0.468	0.463	0.454	0.452	
5	0.465	0.465	0.466	0.464	0.460	
6	0.467	0.466	0.469	0.450	0.448	
D	0.467	0.465	0.462	0.456	0.454	
S_D	0.002	0.005	0.008	0.006	0.005	
$\delta \pm S_\delta$	0.034 ±0.002	0.033 ±0.005	0.031 ±0.008	0.028 ±0.006	0.027 ±0.005	

3. D_0=0.4mm, D_2=0.50mm, T=120°C.

n(rpm)	100	150	196
u_o(m/s)	0.08	0.12	0.16
1	0.445	0.447	D.C.
2	0.443	0.446	
3	0.438	0.445	
4	0.450	0.443	
5	0.448	0.442	
6	0.447	0.449	
D	0.445	0.445	
S_D	0.004	0.003	
$\delta \pm S_\delta$	0.023 ±0.004	0.023 ±0.003	

4. D_0=0.4mm, D_2=0.46mm, T=150°C.

n(rpm)	102	195	250	306	455
u_o(m/s)	0.08	0.16	0.20	0.25	0.37
1	0.430	0.430	0.428	0.430	D.C.
2	0.428	0.431	0.429	0.428	
3	0.429	0.432	0.429	0.430	
4	0.429	0.431	0.426	0.426	
5	0.429	0.432	0.428	0.429	
6	0.429	0.430	0.427	0.426	
D	0.429	0.431	0.428	0.428	
S_D	0.001	0.001	0.001	0.002	
$\delta \pm S_\delta$	0.015 ±0.001	0.016 ±0.001	0.014 ±0.001	0.014 ±0.002	

5. D_0=0.4mm, D_2=0.46mm, T=135°C.

n(rpm)	102	127	195	251	365
u_o(m/s)	0.08	0.10	0.16	0.20	0.30
1	0.427	0.426	0.427	0.425	D.C.
2	0.428	0.429	0.428	0.426	
3	0.428	0.427	0.425	0.427	
4	0.428	0.429	0.427	0.426	
5	0.430	0.427	0.426	0.427	
6	0.428	0.427	0.424	0.427	
D	0.428	0.428	0.426	0.426	
S_D	0.001	0.001	0.002	0.001	
$\delta \pm S_\delta$	0.014 ±0.001	0.014 ±0.001	0.013 ±0.002	0.013 ±0.001	

6. D_0=0.4mm, D_2=0.46mm, T=140°C.

n(rpm)	102	126	195	228	284	376	477
u_o(m/s)	0.08	0.10	0.16	0.19	0.23	0.31	0.39
1	0.433	0.435	0.424	0.431	0.424	0.427	D.C.
2	0.432	0.434	0.433	0.426	0.428	0.426	
3	0.432	0.432	0.429	0.430	0.428	0.428	
4	0.432	0.433	0.429	0.427	0.426	0.426	
5	0.434	0.429	0.426	0.428	0.417	0.425	
6	0.432	0.430	0.429	0.431	0.428	0.423	
D	0.433	0.432	0.428	0.429	0.425	0.426	
S_D	0.001	0.002	0.003	0.002	0.005	0.002	
$\delta \pm S_\delta$	0.017 ±0.001	0.016 ±0.002	0.014 ±0.003	0.015 ±0.002	0.013 ±0.005	0.013 ±0.002	

7. D_0=0.4mm, diediameter D_2=0.44mm, T=145°C.

n(rpm)	102	185	252	296	386	460
u_o(m/s)	0.08	0.15	0.21	0.24	0.31	0.37
1	0.425	0.423	0.427	0.423	0.410	D.C.
2	0.425	0.421	0.425	0.424	0.421	
3	0.425	0.426	0.426	0.418	0.415	
4	0.424	0.426	0.425	0.426	0.417	
5	0.425	0.426	0.423	0.417	0.425	
6	0.424	0.426	0.420	0.419	0.420	
D	0.425	0.425	0.424	0.421	0.418	
S_D	0.001	0.002	0.003	0.004	0.006	
$\delta \pm S_\delta$	0.013 ±0.001	0.013 ±0.002	0.012 ±0.003	0.011 ±0.004	0.009 ±0.006	

8. D_0=0.4mm, D_2=0.44mm, T=150°C.

n(rpm)	102	173	240	295	367
u_o(m/s)	0.08	0.14	0.20	0.24	0.30
1	0.422	0.424	0.423	0.425	D.C.
2	0.417	0.426	0.424	0.425	
3	0.421	0.417	0.425	0.423	
4	0.421	0.425	0.424	0.420	
5	0.415	0.425	0.423	0.424	
6	0.416	0.423	0.425	0.425	
D	0.419	0.423	0.424	0.424	
S_D	0.003	0.003	0.001	0.002	
$\delta \pm S_\delta$	0.010 ±0.003	0.012 ±0.003	0.012 ±0.001	0.012 ±0.002	

9. D_0=0.4mm, D_2=0.44mm, T=135°C.

n(rpm)	102	172	251	328	411
u_o(m/s)	0.08	0.14	0.20	0.27	0.33
1	0.427	0.421	0.420	0.418	D.C.
2	0.426	0.423	0.423	0.422	
3	0.426	0.422	0.419	0.421	
4	0.425	0.420	0.423	0.418	
5	0.426	0.424	0.423	0.418	
6	0.425	0.424	0.420	0.418	
D	0.426	0.422	0.421	0.419	
S_D	0.001	0.002	0.002	0.002	
$\delta \pm S_\delta$	0.013 ±0.001	0.011 ±0.002	0.011 ±0.002	0.010 ±0.002	

10. D_0=0.4mm, D_2=0.42mm, T=135°C.

n(rpm)	102	185	251	295	372	451
u_o(m/s)	0.08	0.15	0.20	0.24	0.30	0.37
1	0.406	0.406	0.406	0.403	0.403	D.C.
2	0.407	0.405	0.406	0.404	0.402	
3	0.403	0.405	0.405	0.403	0.402	
4	0.406	0.407	0.406	0.404	0.402	
5	0.406	0.405	0.407	0.405	0.403	
6	0.405	0.406	0.404	0.403	0.402	
D	0.406	0.406	0.406	0.404	0.402	
S_D	0.002	0.001	0.001	0.001	0.001	
$\delta \pm S_\delta$	0.003 ±0.002	0.003 ±0.001	0.003 ±0.001	0.002 ±0.001	0.001 ±0.001	

11. D_0=0.4mm, D_2=0.42mm, T=145°C.

n(rpm)	102	184	250	295	378	454
u_o(m/s)	0.08	0.15	0.20	0.24	0.31	0.37
1	0.406	0.405	0.406	0.403	0.404	D.C.
2	0.406	0.405	0.405	0.403	0.404	
3	0.407	0.407	0.405	0.404	0.404	
4	0.407	0.406	0.404	0.403	0.403	
5	0.405	0.405	0.404	0.405	0.401	
6	0.404	0.406	0.405	0.403	0.402	
D	0.406	0.406	0.405	0.404	0.403	
S_D	0.001	0.001	0.001	0.001	0.001	
$\delta \pm S_\delta$	0.003 ±0.001	0.003 ±0.001	0.003 ±0.001	0.002 ±0.001	0.002 ±0.001	

12. D_0=0.4mm, D_2=0.42mm, T=155°C.

n(rpm)	102	172	250	295	434	496
u_o(m/s)	0.08	0.14	0.20	0.24	0.35	0.37
1	0.408	0.408	0.408	0.405	0.406	D.C.
2	0.408	0.407	0.406	0.406	0.407	
3	0.405	0.407	0.408	0.404	0.403	
4	0.405	0.407	0.406	0.405	0.403	
5	0.408	0.407	0.405	0.406	0.405	
6	0.405	0.405	0.407	0.404	0.404	
D	0.407	0.407	0.407	0.405	0.405	
S_D	0.002	0.001	0.001	0.001	0.002	
$\delta \pm S_\delta$	0.004 ±0.002	0.004 ±0.001	0.004 ±0.001	0.003 ±0.001	0.003 ±0.002	

13. D_0=0.1mm, D_2=0.20mm, T=145°C.

n(rpm)	102	295	408	640	870	1079	1421	1610
u_o(m/s)	0.08	0.24	0.33	0.52	0.71	0.88	1.15	1.31
1	0.110	0.113	0.111	0.110	0.108	0.111	0.112	D.C.
2	0.112	0.111	0.111	0.110	0.103	0.109	0.107	
3	0.112	0.112	0.113	0.108	0.110	0.106	0.109	
4	0.112	0.109	0.115	0.110	0.110	0.108	0.103	
5	0.110	0.112	0.115	0.112	0.105	0.105	0.109	
6	0.110	0.110	0.112	0.112	0.105	0.105	0.110	
D	0.111	0.111	0.113	0.110	0.107	0.107	0.108	
S_D	0.001	0.002	0.002	0.002	0.003	0.003	0.003	
$\delta \pm S_\delta$	0.006 ±0.001	0.006 ±0.002	0.007 ±0.002	0.006 ±0.002	0.004 ±0.003	0.004 ±0.003	0.005 ±0.003	

14. D_0=0.1mm, D_2=0.26mm, T=145°C.

n(rpm)	92	150	230	422	630	789	924	1024
u_o(m/s)	0.08	0.12	0.19	0.34	0.51	0.64	0.75	0.83
1	0.139	0.148	0.145	0.145	0.135	0.123	0.130	D.C.
2	0.148	0.149	0.149	0.148	0.140	0.122	0.130	
3	0.139	0.149	0.147	0.145	0.139	0.121	0.120	
4	0.140	0.149	0.150	0.151	0.130	0.120	0.132	
5	0.151	0.145	0.141	0.148	0.135	0.128	0.123	
6	0.140	0.150	0.149	0.148	0.130	0.125	0.129	
D	0.143	0.148	0.147	0.148	0.135	0.123	0.127	
S_D	0.006	0.002	0.004	0.002	0.005	0.003	0.005	
$\delta \pm S_\delta$	0.022 ±0.006	0.025 ±0.002	0.024 ±0.004	0.025 ±0.002	0.018 ±0.005	0.012 ±0.003	0.014 ±0.005	

15. D_0=0.1mm, D_2=0.42mm, T=145°C.

n(rpm)	94	172	295	410	598	733
u_o(m/s)	0.08	0.14	0.24	0.33	0.49	0.60
1	0.257	0.261	0.255	0.249	0.241	D.C.
2	0.258	0.260	0.251	0.250	0.239	
3	0.259	0.262	0.258	0.251	0.241	
4	0.259	0.262	0.254	0.251	0.240	
5	0.258	0.260	0.252	0.251	0.240	
6	0.258	0.260	0.252	0.251	0.241	
D	0.258	0.261	0.254	0.251	0.240	
S_D	0.001	0.001	0.003	0.001	0.001	
$\delta \pm S_\delta$	0.080 ±0.001	0.081 ±0.001	0.078 ±0.003	0.076 ±0.001	0.071 ±0.001	

16. D_0=0.2mm, D_2=0.30mm, T=135°C.

n(rpm)	102	366	496	733	968	1101	1300
u_o(m/s)	0.08	0.30	0.40	0.60	0.79	0.89	1.06
1	0.243	0.256	0.253	0.255	0.258	0.248	D.C.
2	0.237	0.255	0.255	0.249	0.259	0.249	
3	0.240	0.258	0.254	0.251	0.259	0.247	
4	0.238	0.257	0.257	0.250	0.240	0.249	
5	0.248	0.257	0.253	0.251	0.253	0.262	
6	0.240	0.258	0.255	0.239	0.250	0.248	
D	0.241	0.257	0.255	0.249	0.253	0.251	
S_D	0.004	0.001	0.002	0.006	0.008	0.006	
$\delta \pm S_\delta$	0.025 ±0.004	0.033 ±0.001	0.032 ±0.002	0.029 ±0.006	0.031 ±0.008	0.030 ±0.006	

17. D_0=0.2mm, D_2=0.30mm, T=145°C.

n(rpm)	102	246	608	858	1101	1499	1600
u_o(m/s)	0.08	0.20	0.49	0.70	0.89	1.22	1.30
1	0.250	0.256	0.259	0.254	0.250	0.249	D.C.
2	0.251	0.254	0.250	0.254	0.257	0.252	
3	0.252	0.253	0.258	0.255	0.254	0.242	
4	0.252	0.255	0.257	0.255	0.254	0.250	
5	0.255	0.254	0.258	0.255	0.252	0.248	
6	0.252	0.255	0.260	0.254	0.257	0.248	
D	0.252	0.255	0.257	0.255	0.254	0.248	
S_D	0.002	0.001	0.004	0.001	0.003	0.004	
$\delta \pm S_\delta$	0.030 ±0.002	0.032 ±0.001	0.033 ±0.004	0.032 ±0.001	0.031 ±0.003	0.028 ±0.004	

18. D_0=0.2mm, D_2=0.30mm, T= 155°C.

n(rpm)	102	431	700	903	1201	1356
u_o(m/s)	0.08	0.35	0.57	0.73	0.98	1.10
1	0.253	0.259	0.258	0.260	0.235	D.C.
2	0.253	0.259	0.248	0.259	0.228	
3	0.252	0.258	0.250	0.260	0.245	
4	0.252	0.258	0.254	0.255	0.254	
5	0.253	0.257	0.252	0.235	0.252	
6	0.252	0.257	0.255	0.259	0.240	
D	0.253	0.258	0.253	0.255	0.242	
S_D	0.001	0.001	0.004	0.010	0.010	
$\delta \pm S_\delta$	0.031 ±0.001	0.033 ±0.001	0.031 ±0.004	0.032 ±0.010	0.025 ±0.010	